Provenance and depositional age of the Cryogenian 'grand conglomérat', host of the Kamoa Cu-deposit, Democratic Republic of Congo

By

Philippe Gerald Eric Trudel

A thesis submitted in partial fulfilment of the
Requirements for the degree of
Master of Science (MSc) in Geology

The Faculty of Graduate Studies
Laurentian University
Sudbury, Ontario, Canada

THESIS DEFENCE COMMITTEE/COMITÉ DE SOUTENANCE DE THÈSE
Laurentian Université/Université Laurentienne
Faculty of Graduate Studies/Faculté des études supérieures

Title of Thesis Titre de la thèse	Provenance and depositional age of the Cryogenian 'grand conglomérat', host of the Kamoa Cu-deposit, Democratic Republic of Congo
Name of Candidate Nom du candidat	Trudel, Philippe G.E.
Degree Diplôme	Master of Science Science
Department/Program Département/Programme	Geology
Date of Defence Date de la soutenance	October 11, 2019

APPROVED/APPROUVÉ

Thesis Examiners/Examinateurs de thèse:

Dr. Elizabeth C. Turner
(Supervisor/Directrice de thèse)

Dr. Alessandro Ielpi
(Committee member/Membre du comité)

Dr. David Broughton
(Committee member/Membre du comité)

Dr. Deanne van Rooyen
(External Examiner/Examinatrice externe)

Approved for the Faculty of Graduate Studies
Approuvé pour la Faculté des études supérieures
Dr. David Lesbarrères
Monsieur David Lesbarrères
Dean, Faculty of Graduate Studies
Doyen, Faculté des études supérieures

ACCESSIBILITY CLAUSE AND PERMISSION TO USE

Abstract

The Kamoa copper deposit (759 Mt, 2.67% Cu at 1% cut-off) is one of the largest copper deposits in the central African copperbelt. Mineralisation at Kamoa is hosted by the Cryogenian 'grand conglomérat', which was deposited in an intracratonic rift and its sub- basins associated with the break-up of Rodinia, and is equated to the 'Sturtian' glaciation, the oldest of the Neoproterozoic glacial events. Using detrital zircon geochronology, the provenance of syn-glacial and underlying pre-glacial units is compared, to evaluate the temporal dynamics of the sediment supply at Kamoa. The detrital zircon age distributions suggest that the 'grand conglomérat' was derived from locally exposed basement of the Mesoproterozoic Kibaran Supergroup and from significant recycling of underlying pre-glacial units, with minor contributions from distal, primary source areas. The stratigraphic differences in the distribution of zircon age populations of the strata at Kamoa may reflect changes in glacial dynamics or of rifting during deposition of the 'grand conglomérat'. A Neoproterozoic zircon age population ~700 Ma is probably derived from rift-related volcanic rocks and is significant because it repositions the timing of mid-Neoproterozoic rifting in the Katangan basin and the maximum depositional age of the 'grand conglomérat'. The new age constraints suggest that the mid-Neoproterozoic 'Sturtian' glaciation was globally diachronous.

Keywords: Detrital zircon, provenance, snowball Earth, Katangan basin

Co-Authorship Statement

Chapter 2 was co-authored with E.C. Turner. Fieldwork, major interpretations, and the first draft of the manuscript were done by the candidate. The co-author conceived the project and edited the manuscript, adding their experience and knowledge. Guidance and training was provided by the co-authors, but the main interpretations and conclusions were made by the candidate. The first drafts of both manuscripts were done by the candidate with editing done by the co-authors.

Acknowledgements

I would like to acknowledge the financial assistance of Ivanhoe Mines, NSERC, and the Goodman School of Mines for funding this project. I would also like to acknowledge logistical support while at the Kamoa camp from David Edwards, Franck Twite, and Dr. David Broughton. I would like to acknowledge Willard Desjardins for making the thin sections and for providing much-needed junk food during late nights with the Wilfley table. I would like to thank Dr. William Zhe for assisting me with use of the CL detector on the SEM for my zircon imaging. I would like to acknowledge the help of Dr. Joe Petrus for taking the time and patience to teach me how to use the LA-ICP-MS and for helping me out whenever it was behaving temperamentally. A big shout out to Dr. Elizabeth Turner for guiding me through this project and for assisting me whenever and wherever she may be and of course for teaching me a lot about the intricacies of the English language. I would of course like to thank my family and friends and especially Jacqueline Huggins for supporting me throughout this project no matter what.

TABLE OF CONTENTS

List of Tables

List of Figures

List of Appendices

1.0 Introduction

The central African copperbelt (CACB; northwestern Zambia and southeastern Democratic Republic of Congo) is the world's largest sedimentary-rock-hosted copper district and hosts ~9% of the world's copper resources (Mudd et al., 2013). The Neoproterozoic Katanga Supergroup contains numerous Cu-Co (± Zn-Pb-Ag) deposits, including the Kamoa Cu-deposit (Fig. 1). The Neoproterozoic Katanga Supergroup was deposited in intracratonic rift basins along the southern margin of the Congo-São Francisco craton during the break-up of Rodinia (Hitzman et al., 2012). The Katanga Supergroup consists of the Roan Group and the overlying Nguba and Kundelungu groups (Fig. 2; Cailteux, 1994; Batumike et al., 2007; Cailteux and De Putter, 2018). The Kamoa deposit is hosted by glacially influenced diamictite of the 'grand conglomérat' (Mwale Formation), which is associated with the 'Sturtian' glaciation, the oldest of the postulated mid-Neoproterozoic 'snowball Earth' glaciations.

Stratigraphy and lithofacies played a role in dictating the geographic and stratigraphic position of ore in the Kamoa-Kakula district. Ore is generally hosted by pyritic siltstone and "clast-poor" (<20% clasts >2 mm; Schmandt et al., 2013) diamictite near the base of the 'grand conglomérat', but the detailed internal stratigraphy of the 'grand conglomérat' and of the basal diamictite in particular are not regionally consistent, a reality that should be expected given deposition from sediment-gravity flows. Fundamentally, the influence of stratigraphy on the distribution of grade is known to be important even though the mechanism by which it acted remains obscure. Given the presence of a reliable sedimentological understanding of the 'grand conglomérat' at Kamoa (Kennedy et al., 2018), a more detailed investigation of sediment provenance and delivery

dynamics may identify subtle variations that could help understand and correlate the stratigraphy.

The ‘snowball Earth’ theory remains highly controversial ~20 years after it was first postulated. The original ‘snowball Earth’ theory suggested that two glaciations, the ‘Sturtian’ and the younger ‘Marinoan’, were each globally synchronous events during which glacial coverage expanded to low latitudes ~30° from the equator (Kirschvink, 1992; Hoffman et al., 1998; Hoffman and Schrag, 2002). The cause of the ‘snowball Earth’ glaciations was thought to be from an increase in continental weathering due to break-up of Rodinia, which decreased CO_2 levels until polar ice sheets caused a run-away albedo effect coating the surface of the Earth in ice (Goddéris et al., 2004); such a series of events had been predicted based on physical modelling (Budyko, 1940). Earth eventually returned to a normal greenhouse state because undiminished volcanic degassing increased atmospheric CO_2 and caused rapid deglaciation resulting in cap carbonates overlying interpreted glacial diamictite (Kirschvink, 1992; Hoffman et al., 1998).

Alternative theories that seek to explain the timing and extent of the ‘snowball Earth’ glaciations include the ‘slushball Earth’ and ‘zipper-rift’ theories. The ‘slushball Earth’ theory suggests that the glaciations were globally synchronous and that they occurred close to low latitudes, but that there was still a belt of open ocean along the Equator, which is based primarily on climate modeling (Hyde et al., 2000). The ‘zipper-rift’ theory suggests that ‘snowball Earth’ glaciations are similar to modern-day alpine glaciations, with regional, diachronous glacial coverage developing at variable times along the uplifted shoulders of rift-margins during break-up of Rodinia, and is based primarily on sedimentology and stratigraphy of glacial diamictite (Eyles and Januszczak, 2004; Fairchild and Kennedy, 2007; Allen and Etienne, 2008).

An important test that would help discern between the various theories and models for ‘snowball Earth’ is the geochronology of glacial deposits associated with the mid-Neoproterozoic low-latitude glaciations. Well-constrained depositional ages for ‘Sturtian’ diamictite from basins across the globe could indicate whether glaciations occurred diachronously or synchronously. The provenance of glacial diamictite is also a test of whether individual glacial episodes were locally or of broader provenance, shedding light on the extent of the ‘Sturtian’ glaciation.

Recent work at Kamoa suggests that there was only minor (if any) glacial influence on the deposition of the ‘grand conglomérat’ in the Kamoa sub-basin (Kennedy et al., 2018). The rarity of glacially striated clasts from outcrop near Kamoa and of ice-rafted dropstones, as well as the predominant composition of the clasts (i.e., quartzite from the nearby Nzilo promontory) suggests that the clasts were locally derived from conglomerate and breccia of the Mwashya and Dipeta subgroups (Kennedy et al., 2018). The local provenance of the clasts in the ‘grand conglomérat’, and lack of evidence of other glacial influence, led the authors to conclude that diamictite of the ‘grand conglomérat’ are debrites with no direct glacial influence, and that the principal control on sedimentation was tectonically driven rifting. The local fault-controlled deposition of diamictite suggests that sedimentation was diachronous throughout the Katangan basin and was temporally controlled by rifting in individual sub-basins. Uranium-Pb detrital zircon geochronology is a tool used to identify the provenance of clastic sedimentary rocks when compared to the ages of basement rocks that served as possible sediment source areas (Fedo et al., 2003; Gehrels, 2012). Probability density plots, which show the frequency of grains of an age population while also incorporating the error involved in each respective analysis, provide a useful method for displaying data and comparing age populations in a sample to those of source areas.

In this study, new U-Pb detrital zircon data from the syn-rift, glacially influenced ‘grand conglomérat’ and the underlying pre-glacial Dipeta and Mwashya subgroups at Kamoa are compared to zircon data from previous studies of strata from the Katanga Supergroup and nearby basement. Comparison of the detrital zircon age distributions of pre- and syn-glacial clastic units from this study to those of previous studies, along with comparisons of age populations to those of possible source areas, are used to determine the provenance of strata at Kamoa. The youngest detrital zircon population from the ‘grand conglomérat’ should indicate the maximum possible depositional age of the ‘Sturtian’ diamictite in central Africa. The results may hold important implications for the evolution of the Katangan basin, sedimentary dynamics and sediment provenance of intracontinental glacially influenced strata, maximum depositional age of the stratigraphic units, and the timing and extent of the ‘Sturtian’ glaciation during break-up of Rodinia.

2.0 Geologic Background

2.1 Katangan basin

The Katanga Supergroup unconformably overlies Paleoproterozoic basement of the Lufubu metamorphic complex (LMC; Rainaud et al., 2005b), a 2050-1850 Ma block that is inferred to underlie the CACB based on the unconformable relationship observed between metamorphic rocks of the LMC and sedimentary rocks of the Roan Group at the Kafue anticline. The Katangan basin is bounded by the Neoarchean Kasai block, the Paleoproterozoic Bangweulu block, and the Mesoproterozoic Kibaran and Irumide belts (Fig. 1; Rainaud et al., 2005b; De Waele et al., 2008).

Evolution of the Katangan basin began with rifting associated with the break-up of Rodinia, and is marked by deposition of syn-rift lower Roan Group strata [i.e., roches argilo-talcqueuses (RAT)], which were deposited during syndepositional basement faulting in fault-bounded half-grabens (Selley et al., 2018). The initial rift stage was followed by tectonic quiescence, which caused basin starvation throughout a thermal sag phase during which accommodation space was limited (Kennedy et al., 2018; Selley et al., 2018). The episode of sediment starvation was accompanied by development of sub- to supratidal evaporitic cycles in a marginal-marine setting, in which thick evaporite successions accumulated interbedded with minor carbonate strata of the upper Roan Group (Jackson et al., 2003; Bull et al., 2011). The 2nd stage of basin evolution began with deposition of the Mwashya Subgroup, which consists of arkosic sandstone, siltstone, and conglomerate, during an increase in accommodation space due to interconnection of normal faults and rapid subsidence in sub-basins (Kennedy et al., 2018). Tectonic activity during this time was accompanied by widespread bimodal volcanism related to intracratonic rifting (Kampunzu et al., 2000). Deposition of the ‘grand conglomérat’ also accompanied the tectonic activity associated with rifting in the Kamoa sub-basin (Kennedy et al., 2018). The ‘grand conglomérat’ marks the base of the Nguba Group and its thickness is highly variable from <100 m up to 1.8 km thick throughout the Katangan basin and is attributed to the Sturtian glaciation (the older of the Neoproterozoic ‘snowball Earth’ events). The third stage of basin evolution is described as consisting of slow thermal subsidence accompanied by a decrease in accommodation space because extensional rifting was no longer active; this phase is marked by deposition of the Kakontwe Formation (Kennedy et al., 2018), which some workers have referred to as a “cap carbonate”, because it is carbonate unit that directly overlies interpreted glacial diamictite. The base of the Kundelungu Group is marked by the ‘petit conglomérat’, a

thin (~25 m) diamictite that is attributed to the Marinoan glaciation (the younger of the Neoproterozoic ‘snowball Earth’ events). The ‘petit conglomérat’ is overlain by the ‘calcaire rose’, which is also referred to as a “cap carbonate” (Cailteux, 1994). The final stage of basin evolution consists of basin inversion and formation of a foreland basin during the Lufilian orogeny, which formed due to collision of the Kalahari and Congo cratons ~592-512 Ma during assembly of Gondwana (Rainaud et al., 2005a).

Selley et al. (2018) interpreted the configuration of the Katangan basin prior to Lufilian deformation to have a maximum depocentre in the central Congolese part of the CACB, with uplifted margins along the northern edge of the Katangan basin in DRC and the southern edge in Zambia, and the rift axis oriented approximately NE. Evidence for the orientation of the rift axis is based on isopach mapping of marker units such as the ‘grand conglomérat’. Using isopach maps to identify abrupt thickness variations in key stratigraphic units also allows for the identification of interpreted synsedimentary normal faults that trend NE. Bounding faults along basement inliers of the Kibaran belt in the DRC are subparallel to interpreted normal faults related to extension during Neoproterozoic rifting, which supports the interpreted northeast trend of the Katangan rift axis (Selley et al., 2018).

The Lufilian orogen forms a convex-northwards southeast-trending fold-and-thrust belt that is divided into 4 tectonic zones, from south to north: the Katangan high, the synclinorial belt, the ‘domes’ region, and the external fold-and-thrust belt (Selley et al., 2005). The external fold-and-thrust belt is characterised by thin-skinned deformation, whereas the ‘domes’ region was affected by thick-skinned deformation in which Katangan strata were deformed along with pre-Katangan basement (Selley et al., 2005). The boundary between these two tectonic zones is depicted by a

gradational change in structural style and a northward decrease in metamorphic grade from upper greenschist to prehnite-pumpellyite facies (Selley et al., 2005).

The ‘grand conglomérat’ has long been considered as a marker horizon in the Katangan basin useful for mapping and stratigraphic studies since the early 1900s. In the 1970s the ‘grand conglomérat’ was considered to represent a tillite from continental glaciation based on the presence of striated clasts and dropstones. More recently the ‘grand conglomérat’ has been associated with the ‘Sturtian’ glaciation, one of two Cryogenian glaciations alongside the ‘Marinoan’ glaciation, which the ‘petit conglomérat’ is associated with. Contemporary studies have examined the stratigraphy and sedimentology of the ‘grand conglomérat’ in several localities in the Katangan basin (Master et al., 2005; Batumike et al., 2006; Wendorff and Key, 2009; Master and Wendorff, 2011; Kennedy et al., 2018). Master and Wendorff (2011) summarise the observations of previous workers well: the ‘grand conglomérat’ consists of poorly sorted matrix supported conglomerate that is generally massive (i.e., a diamictite), but that does have crude bedding and reverse grading present in some localities. The diamictite is often intercalated with siltstone and sandstone beds often with dropstones present. Clasts range in size from cm-scale gravel to >1 m sized boulders and are generally subrounded to subangular with striated faces present in several locations. Clasts vary in composition dependent on the area in the basin with in the western portion of the basin the predominant clast population is quartzite derived from the Kibaran Supergroup, whereas in the NW area a wide variety of clasts: quartzite, granitic pegmatite, marble, quartz vein, chert, mafic intrusives. Microstructures present in diamictite matrix are also interpreted to be the result of glacial processes. The ‘grand conglomérat’ also has fluid-escape structures (e.g., flame structures) and evidence of soft-sediment deformation (e.g., slump folding) and was deposited in a tectonically active setting,

which is supported by syndepositional microfaulting. The dominant interpretation through the use of modern studies is that the ‘grand conglomérat’ records subaqueous debrites with intercalated sandstone and siltstone beds derived from muddy-sandy turbidite flows.

Wendorff and Key (2009) have also interpreted erosional intervals representing ~200 m of erosion to imply significant uplift of underlying blocks during extensional faulting, which supports the interpretation that the ‘grand conglomérat’ was deposited in a tectonically active intracratonic rift basin. Wendorff and Key (2009) have interpreted the southern margin of the Katangan basin to represent a steeply uplifted margin with a high topographic relief and that the northern margin consists of a relatively shallow gradient with low relief based on two main pieces of evidence: (1) clast size decreases in the diamictite moving NW to the SE away from the interpreted boundaries of the rift margin of the Katangan basin, and (2) non-glacial sedimentary beds (i.e., siltstone and sandstone beds) decrease in thickness going from NW to the SE as well supporting the interpretation of the sediments being derived from the margins of the basin inwards. Due to the differences in the interpreted topographic relief between the northern and southern margins of the Katangan basin, Wendorff and Key (2009) have suggested that the glaciation occurred simultaneously on both margins and that the glaciation is independent of topographic relief, unlike the ‘zipper-rift’ model for the ‘Sturtian’ glaciation (Eyles and Januszczak, 2004). However, presence of intercalated non-glaciogenic sediment indicates that the glaciation was not permafrozen and the hydrologic cycle was ongoing, which argues against a ‘hard snowball Earth’. Batumike et al. (2006) performed geochemistry on the ‘grand conglomérat’ and found that its geochemical signature can be constrained to continental arc characteristic and interpreted the Ubendian belt and the Bangweulu block as being the source of detritus for the with minor contribution from Mesoproterozoic and Archean source areas, but this

study was done without considering how sedimentary and glacial dynamics would account for detritus in the Northwest of the Katangan basin being sourced from sources far to the East.

2.2 Katanga Supergroup Stratigraphy

The Neoproterozoic Katanga Supergroup is a succession up to ~10 km thick that was deposited along the (present-day) southern margin of the Congo-São Francisco craton during the break-up of Rodinia (Hitzman et al., 2012). The Katanga Supergroup consists of the basal Roan Group and the overlying Nguba and Kundelungu groups (Fig. 2; Cailteux, 1994; Cailteux et al., 2007; Batumike et al., 2007; Cailteux and De Putter, 2018;). The maximum depositional age of the Katanga Supergroup is ~880 Ma, based on the age of the youngest known intrusion that predates the Katanga Supergroup (883 Ma Nchanga granite; Armstrong et al., 2005).

The Katangan basin was deformed and in places metamorphosed during basin inversion caused by the Lufilian orogeny, one of many Pan-African orogenies that took place during assembly of Gondwana (ca. 592-512 Ma; Rainaud et al., 2005a). It is difficult to undertake stratigraphic studies of the Roan Group in the DRC, because it is now mainly represented by large (hectometre- to kilometre-scale) blocks in tectonic ‘megabreccia’ that formed because of basin inversion during the Lufilian orogeny, and through salt tectonics (Jackson et al., 2003; Cailteux and De Putter, 2018).

The Roan Group in the Zambian copperbelt, where it remains stratigraphically intact, consists of the RAT, Mines, Dipeta, and Mwashya subgroups (Fig. 2; Cailteux, 1994). The RAT Subgroup consists of basal conglomerate overlain by stromatolitic dolostone, dolomitic siltstone, and dolomitic sandstone. The Mines Subgroup consists of dolostone, dolomitic siltstone, and shale. The Dipeta Subgroup consists of dolostone, dolomitic siltstone, and arkosic sandstone with rift-

related mafic intrusives locally present. The Mwashya Subgroup consists of carbonaceous shale, siltstone, arkosic sandstone, and conglomerate (Cailteux et al., 2007). In some areas the Mwashya Subgroup is intercalated with bimodal volcanic rocks and volcaniclastics (Key et al., 2001).

The Nguba Group conformably overlies the Roan Group and consists of glacially influenced diamictite of the ‘grand conglomérat’, which has been affiliated with the ‘Sturtian’ glaciation, and is thought to have been deposited between 765 and 735 Ma based on felsic volcanic rocks intercalated with the Mwashya Subgroup and by volcanic centres present in the Kakontwe Formation in Zambia (Key et al., 2001). Rooney et al. (2015) have an age of 727 ±3.9 Ma from a Re-Os age of black shale of the Mwashya Subgroup in the Katangan basin. The ‘grand conglomérat’ is overlain by limestone, dolostone, and dolomitic shale of overlying units, and in some areas is intercalated with mafic volcanic flows and sills (Kennedy et al., 2018; Cailteux and De Putter, 2018).

The Kundelungu Group consists of the ‘petit conglomérat’, a thin diamictite affiliated with the ca. 660-635 Ma ‘Marinoan’ glaciation (Prave et al., 2016). It is overlain by limestone, dolostone, carbonaceous shale, siltstone, and sandstone of the youngest Katangan units. The depositional age of the Kundelungu Group is not well constrained, and its best chronological constraint is correlation to ‘Marinoan’ diamictite from Namibia, which is dated 635 ±1.2 Ma (Hofmann et al., 2004). The Biano Group (upper Kundelungu Group) has a maximum depositional age of 573 Ma Ar^{40}/Ar^{39} from detrital muscovite, which suggests that it was deposited in the foreland basin of the Lufilian arc (Master et al., 2005).

2.3 Kamoa Area Geology

The Kamoa deposit is located ~25 km west of Kolwezi, DRC, on the periphery of the western foreland tectonic domain of the CACB (Fig. 3). The Kamoa deposit (759 Mt, 2.67% Cu at 1% cut-off; Gilchrist, 2019) was initially discovered in an exploration program in an area of the CACB that was once thought to be unprospective for sedimentary-rock-hosted copper deposits (Broughton and Rogers, 2010). The Kamoa deposit has since been the subject of several studies focussing on aspects of the mineralisation (Schmandt et al., 2013), detailed sedimentology of the host succession (Kennedy et al., 2018), and structural controls on mineralisation (Twite et al., 2019).

Rocks of the Roan, Nguba, and Kundelungu groups outcropping near Kamoa gently dip away from basement inlier 'domes' of the Mesoproterozoic Kibaran Supergroup, which consists of quartzite, phyllite, metaconglomerate, and minor metagabbro (Kokonyangi et al., 2007; Schmandt et al., 2013). The stratigraphic units of importance to this study are the uppermost units of the Roan Group (Dipeta and Mwashya subgroups) and the basal unit of the Nguba Group ('grand conglomérat', also known as the Mwale Formation). The Dipeta and Mwashya subgroups are subdivided into the lower, middle, and upper Dipeta and the lower and upper Mwashya, respectively (Fig. 4). The Dipeta and Mwashya subgroups consist of interbedded arkosic sandstone, siltstone, and pebbly conglomerate, which in the case of the Mwashya subgroup were deposited by subaqueous non-cohesive debris flows with coeval or successive deposition from high-density and high-concentration silty and sandy turbidity currents (Kennedy et al., 2018). There is a minor breccia facies that consists of angular clasts almost entirely of composed of quartzite (i.e., Kibaran Supergroup quartzite). The angularity and monomictic nature of clasts, and the presence of 'jig-saw' fit of clasts, suggests local derivation along fault scarps as talus slopes with very little transport. Otherwise, most clasts in the sandstone and

conglomerate are subrounded to rounded and composed of quartzite, with minor angular basalt clasts. The deposition of syn-rift Dipeta and Mwashya subgroups is interpreted to record initiation of rifting in the Kamoa sub-basin (Kennedy et al., 2018).

The ‘grand conglomérat’ is up to 1.8 km thick at Kamoa and consists of diamictite and siltstone intercalated with volcanic flows and sills. The unit has extreme thickness variation throughout the Kamoa sub-basin from only a few metres close to the margins of the basin up to 1.8 km in the depocentre (Kennedy et al., 2018). The ‘grand conglomérat’ is subdivided informally in the Kamoa area into the basal diamictite (Ng 1.1.1), lower Kamoa pyritic siltstone (Ng 1.1.2), the middle diamictite (Ng 1.1.3), the upper Kamoa pyritic siltstone (Ng 1.1.4), and the upper diamictite (Ng 1.1.5). The basal diamictite is further subdivided into the lower package diamictite (Ng 1.1.1.1), siltstone interbed (Ng 1.1.1.2), and upper package diamictite (Ng 1.1.1.3; Fig. 4).

‘Grand conglomérat’ diamictite in the Kamoa area was deposited in a deep-water subaqueous setting from cohesive debris flows, and its siltstone-dominated facies were deposited from low-density, low-concentration turbidity currents following diamictite deposition events (Kennedy et al., 2018). The dominant clast type in the diamictite is rounded clasts of Kibaran Supergroup quartzite; minor siltstone, granitoid, phyllite, gneiss, and basalt clasts are also present. The diamictite facies is interpreted to have been resedimented from cobbly to sandy sediment of the underlying Mwashya and Dipeta subgroups, based on the predominant clast composition in the diamictite, and mixed with silty matrix material during downslope transport of the mass flow, all recording local provenance (Kennedy et al., 2018). Mafic volcanic flows and sills are intercalated between the lower Kamoa pyritic siltstone (KPS) and the middle diamictite at Kamoa. The mafic volcanic rocks are thicker to the west of Kamoa and reach thicknesses up to

~300 m thick. The presence of peperite at the contacts of the mafic volcanic units and the sedimentary rocks, and the presence of sedimentary clasts in the mafic flows, indicates that extrusion of the mafic rocks was coeval with deposition of the subaqueous debrites. Pillow basalts with selvages are present in the mafic volcanic flows, which indicates subaqueous deposition, and supports the interpretation that the mafic flows were coeval with diamictite deposition. Angular clasts of mafic volcanic material are present in some of the diamictite units, which suggests that there were several episodes of alternating debrite deposition and mafic volcanism.

Kennedy et al. (2018) performed a very detailed sedimentological and stratigraphic study of the ‘grand conglomérat’ and of the underlying Mwashya Subgroup and ‘poudingue’ conglomerate through over 300 km of drill core in the Kamoa sub-basin and interpreted a three-stage basin evolution. (1) Segmented basement faulting during initial extension created isolated depocentres. (2) Connection of syndepositional normal faults and rapid subsidence created large volumes of accommodation space in the rapidly deepening sub-basin. (3) Tectonic activity waned, with only minor faulting and slow thermal subsidence leading to shallowing and diminished accommodation space. Facies associated with the first step of basin development at Kamoa are the breccia, conglomerate, and sandstone-dominated facies of the ‘poudingue’ and Mwashya Subgroup, interpreted as representing deposition on talus slopes along synsedimentary extensional faults followed by mass flows and turbidites deposited in a subaqueous fan-delta. Facies associated with the second step of basin development at Kamoa are the diamictite-dominated facies with minor siltstone, sandstone, and conglomerate of the ‘grand conglomérat’. Diamictite at Kamoa was deposited from debris flows that formed during slope failure, due to seismicity during active faulting, and were derived from the mixing of previously formed

muddy, gravelly, and cobbly sediment of the Mwashya Subgroup and ‘poudingue’ conglomerate. Homogeneity and thickness of the diamictite were interpreted to have been caused by the amalgamation of individual debris flows that reworked any finer-grained sediment that may have been deposited between them. Finer-grained facies in the ‘grand conglomérat’ (e.g., KPS) are interpreted as turbidites that were deposited following debris flows, but not reworked by subsequent debris flows. The lower KPS is a marker unit in the stratigraphy at Kamoa that marks the transition from oligomictic basal diamictite to polymictic middle diamictite, a transition that is also identifiable from a change in matrix composition from greyish-green matrix in the basal diamictite to dark greyish-black matrix in the middle diamictite. The third step in evolution of the Kamoa sub-basin is recorded by the transition from the ‘grand conglomérat’ to the overlying Kakontwe Formation, due to slower subsidence and thermal sag rather than tectonically driven extensional faulting (Kennedy et al., 2018).

The provenance of the Mwashya Subgroup shows that it is predominantly locally derived from Kibaran metasedimentary rocks locally exposed near the Kamoa sub-basin, with minor primary input of Kibaran intrusive rocks ~1380-1370 Ma. There is some debate as to whether the Mwashya Subgroup is fluvial and corresponds to the uppermost Roan Group or if it actually belongs to the lowermost Nguba Group and is possibly related to the ‘grand conglomérat’. Relying purely on detrital zircon geochronology, there is no way of distinguishing between the two, but the interpretation of Kennedy et al. (2018) , based on lithofacies of the Mwashya Subgroup and the ‘grand conglomérat’, indicate that the ‘Mwashya’ sandstones in the Kamoa region are part of the lower Nguba Group, deposited in subaqueous turbiditic fans presaging and related to the ‘grand conglomérat’.

The Kamoa sub-basin is bounded by NE-trending faults that form half-grabens, which are identifiable through isopach mapping, with faults identified by abrupt lateral thickness variations in the sedimentary packages (Kennedy et al., 2018). Twite et al. (2019) supports the orientation of basin-bounding faults through a detailed structural analysis of drill-core at Kamoa. The orientation of synsedimentary normal faults at Kamoa is sub-parallel to the approximate orientation of the rift axis for the Katangan basin, as interpreted by Selley et al. (2018).

2.4 Regional crustal blocks as sediment source areas

The Katangan basin is located in central Africa (DRC and Zambia), where it is surrounded by older crustal blocks and orogenic belts of the Congo craton, including the Neoarchean to Paleoproterozoic Kasai block, the Paleoproterozoic Bangweulu block, and the Mesoproterozoic Kibaran and Irumide belts (Fig. 1; De Waele et al., 2008). The Katangan Supergroup unconformably overlies the Paleoproterozoic basement of the Lufubu metamorphic complex (LMC; Rainaud et al., 2005b). These immediate crustal neighbours are surrounded regionally by other tectonic blocks (Fig. 5), each on a scale of hundreds of kilometres in present-day exposure and each with a suite of igneous and metasedimentary rocks characterised by reworked detrital zircon as well as variably metamorphosed intrusive bodies containing primary igneous zircon. The nature, age, and distribution of these blocks (Figs. 5, 6; Tables. 1, 2) are essential to deciphering the dynamics of sediment supply through the episodes of rifting, thermal subsidence, glaciation, and orogeny that took place in the mid- to late Neoproterozoic.

The Congo craton in central Africa consists of Archean cratonic blocks that collectively amalgamated throughout the Proterozoic (Figs. 1 and 5; DeWaele et al., 2008). The assembly of the Archean cratonic components occurred during the Paleoproterozoic ‘Eburnean’ (ca. 2.2-1.9

Ga) orogenic events (De Waele et al., 2008). The Congo craton underwent another episode of deformation and metamorphism during the Mesoproterozoic ‘Kibaran’ (ca. 1400-1000 Ma) orogenic events (De Waele et al., 2008). Widespread plutonism occurred during the ‘Eburnean’, and granitoid intrusions ~2.2-1.9 Ga commonly intrude older Paleoproterozoic and Archean crust (Key et al., 2001).

An obstacle to identifying the source of both original and reworked zircon in the Katangan basin is the existence of extensive Phanerozoic cover in the Congo basin, a broad area north and west of the Kibaran and Kasai blocks (Fig. 5).The nature of the basement under Phanerozoic cover in the Congo basin is unclear, because it is completely unexposed; its identity can only be inferred based on the identity of surrounding cratonic blocks and from detrital zircon studies of Congo basin strata (Linol et al., 2016). This problem is vexing, because the transport direction of the material investigated in this study, the ‘grand conglomérat’, was approximately from the northwest (Kennedy et al., 2018). Depending on the mode of transport, material from beyond the present-day exposure areas of the Kasai block and Kibaran belt may have been delivered to the northwestern part of the Katangan basin. Given the reality that most of the ‘grand conglomérat’ material at Kamoa consists of demonstrably locally derived detritus, the problem of more distal sources may be comparatively unimportant.

2.4.1 Archean Cratonic Blocks

The major Archean cratonic blocks of the Congo craton that are possible source areas for Katangan sediment include the Neoarchean Angola and Kasai blocks are, and the Neoarchean Tanzania craton (De Waele et al., 2008). The Kasai block is the most probable source of zircon because of its proximity to the Katangan basin (Fig. 1).

The Kasai block consists of Neoarchean granulite-facies granitic gneisses that have been dated ~2561-2538 Ma with Paleoproterozoic 'Eburnean' granitoid intrusions cross-cutting them that have been dated ~2058 Ma (Key et al., 2001). The geochronological work of Key et al. (2001) is the only U-Pb dating of crystalline basement rocks from the Kasai block. Older, less precise and less rigorous geochronological techniques (e.g., whole rock Rb-Sr, Pb-Pb errorchrons) were not included in this text. Batumike et al. (2009) analysed detrital zircon from modern river sediments that cross-cut the Kasai block in central DRC and identified two dominant Archean populations (~2890 Ma and 2620 Ma), three Paleoproterozoic populations (~2390 Ma, 2150 Ma, and 2070 Ma), and minor Mesoproterozoic grains, which suggests that the Kasai block is predominantly Archean, but was tectonically reworked in the Paleoproterozoic.

Rainaud et al. (2003) proposed the existence of an unexposed Mesoarchean terrane (the 'Likasi terrane') that underlies the Paleoproterozoic basement of the Katangan basin. This suggestion is based on xenocrystic Mesoarchean (~3.2 Ga) zircon from a lapilli tuff intercalated in the Mwashya Subgroup near Likasi, DRC, and on Mesoarchean detrital zircon from a quartzite in the Muva Supergroup (described below), where it outcrops in the Kafue anticline (Zambian copperbelt). There are no known exposures of Mesoarchean rocks of this age in the vicinity of the CACB.

2.4.2 Paleoproterozoic Cratonic Blocks

Paleoproterozoic cratonic components include the Bangweulu block, the Lufubu metamorphic complex (LMC), and basement inliers of the 'domes' region (Rainaud et al., 2005b; Debruyne et al., 2014). The Bangweulu block is a Paleoproterozoic craton that consists of schists intruded by granitoids that are interpreted to be related to overlying metavolcanics rocks (Debruyne et al.,

2014). Magmatic rocks of the Bangweulu block have been dated ~2050-1930 Ma (De Waele and Fitzsimons, 2007). A large proportion of the Bangweulu block (>50% of its surface area) is overlain by Paleoproterozoic metasedimentary rocks of the Muva Supergroup, which consists of the basal Mporokoso Group and the overlying Kasama Formation (De Waele and Fitzsimons, 2007). The Mporokoso Group has a maximum depositional age of <1829 Ma constrained by detrital zircon, whereas the Kasama Formation is considerably younger, with a maximum depositional age of <1434 Ma constrained by detrital zircon (De Waele and Fitzsimons, 2007). Detrital zircon of the Muva Supergroup have a unimodal detrital zircon age distribution ~2000-1800 Ma that is interpreted to be derived from underlying crystalline rocks of the Bangweulu block (De Waele and Fitzsimons, 2007).

Several basement inliers are exposed in the ‘domes’ region of Zambia. The basement inliers represent exhumation of basement rocks along faults during structural deformation and also the eroded cores of anticlines (Selley et al., 2018). The basement inliers consist of schist, gneiss, and metavolcanic and metasedimentary rocks that are intruded by (~50% of outcrop) voluminous granitoid intrusions (Rainaud et al., 2005b). Of particular interest is a basement inlier (the Kafue ‘anticline’) that is an extension of the Irumide belt in the southeastern part of the basin. The metamorphic and igneous units are widely exposed in the Kafue anticline, and are what Rainaud et al. (2005b) termed the Lufubu metamorphic complex (LMC), suggesting that the LMC is a Paleoproterozoic magmatic arc that underlies the CACB. Rainaud et al. (2005b) established the age of the LMC as ~2050-1850 Ma based on geochronology of gneiss and granitoids exposed in the Kafue anticline and in the Irumide belt; the gneiss that provided an age of ~2050 Ma may also be related to magmatism in the Usagaran belt and the Bangweulu block (De Waele et al., 2006b).

2.4.3 Paleoproterozoic Orogenic Belts

There are several Paleoproterozoic source areas, including the Usagaran, Ubendian, Rusizian, and Ruwenzori orogenic belts (Fig. 5), that were deformed during the ca. 2.2-1.9 Ga 'Eburnean' events (De Waele et al., 2008). The 'Eburnean' events may have deformed and reworked Archean crust to form the Paleoproterozoic Bangweulu block (De Waele, 2005).

The Ubendian belt is located between the Bangweulu block, the Tanzania block, and the Kibaran belt, and is dominated by granitoid gneisses, orthogneisses and other metasedimentary rocks, and eclogite-facies metamorphic rocks (De Waele et al., 2008; Boniface et al., 2012; Kazimoto et al., 2014). Metabasites and orthogneisses in the Ubendian belt are ~2713-2638 Ma, and were affected by granulite-facies metamorphism ~2020 Ma (Kazimoto et al., 2014). The metamorphic rocks of the Ubendian belt were intruded by volumetrically minor granitoids ~1990-1940 Ma (Kazimoto et al., 2014). Eclogites and metapelites in the Ubendian belt were also dated ~1886-1866 Ma with metamorphic rims recording a Mesoproterozoic metamorphic event ~1090 Ma (Boniface et al., 2012). Paragneisses in the Ubendian belt also contain metamorphic zircon that have been dated ~1950-1901 Ma (Boniface and Appel, 2018).Volcanic rocks in the Ubendian belt have also been dated at 1943 Ma and 1871 Ma (Tulibonywa et al., 2015). The Ubendian belt underwent granulite-facies metamorphism ~2100-2025 Ma based on metamorphic zircon from the gneisses, which were intruded by granitoids around 1860 Ma (Lenoir et al., 1994). Granitoids that intrude the Paleoproterozoic metamorphic rocks of the Ubendian belt have also been dated at ~1925-1890 Ma; there is a single Mesoproterozoic granitoid intrusion (Chimala granite) ~1407 Ma (Thomas et al., 2018). The Ubendian belt also contains a younger series of metasedimentary rocks that were deposited ~1166-1007 Ma in an isolated basin overlying Ubendian basement (Boniface et al., 2014). The Usagaran belt, adjacent to the Tanzania block and the Irumide belt

and considered to be the southern continuation of the Ubendian belt, consists of ortho- and paragneisses and eclogitic rocks that have been dated at ~1999 Ma, which were intruded by volumetrically minor granitoids that are ~1910-1817 Ma (Collins et al., 2004; Sommer et al., 2005). Reddy et al. (2003) dated granitic gneiss and post-tectonic granitoid intrusions in the Usagaran belt that are ~2705 Ma and 1877 Ma, respectively.

The Rusizian and Ruwenzori belts are considered to be the northern continuation of the Ubendian belt (Hanson, 2003) and thus similar ages can be expected from them; this cannot be confirmed because of a lack of geochronology and research in these belts compared to the Ubendian and Usagaran belts. One of the only reliable geochronological studies of the Ruwenzori basement dated gneisses that gave ages between 2637 and 2584 Ma (Link et al., 2010).

2.4.4 Mesoproterozoic Orogenic Belts

Mesoproterozoic orogenic belts include the Irumide and Kibaran belts, which flank the Katangan basin, as well as the Karagwe-Ankole belt in the more distant northeast (DeWaele et al., 2008; Tack et al., 2010).

The Kibaran belt consists of metasedimentary rocks that are intruded by bimodal igneous intrusions (Kokonyangi et al., 2007; Tack et al., 2010). The metasedimentary rocks of the Kibaran belt consist of the four subdivisions of the ~10-km-thick Kibaran Supergroup: the Kiaora, Nzilo, Hakanson, and Lubudi groups (Kokonyangi et al., 2007). The Kibaran Supergroup consists of quartzite, metaconglomerate, metapelite, and minor intercalated metavolcanics rocks. Abundant bimodal magmatic rocks ~1.38-1.37 Ga intrude the Kiaora Group, but do not intrude the overlying Nzilo Group. The bimodal intrusions that cross-cut the Kiaora Group are products

of the ca. 1380-1375 Ma extensional ‘Kibaran’ tectono-magmatic event, and occupy roughly 40% of the exposure area of the Kibaran Supergroup (Tack et al., 2010). Their deformation style, which is shared with only the enclosing Kiaora Group, together with their absence from the rest of the Kibaran Supergroup, indicates a disconformity lasting at least 50 m.y. after deposition, intrusion and metamorphism of the Kiaora Group and before deposition of the overlying Nzilo Group (Kokonyangi et al., 2006; Tack et al., 2010; Fernandez-Alonso et al., 2012). Several ‘post-Kibaran’ S-type, tin granitoids cross-cut the entirety of the Kibaran Supergroup and constrain its minimum possible age of deposition to >1080-950 Ma (Kokonyangi et al., 2004). The Nzilo Group, which is important in the Kamoa area, was derived from various sources, including recycling of the underlying Kiaora Group and its 1381.37 Ga orthogneisses and granites (Kokonyangi et al., 2004; Kokonyangi et al., 2007). The Nzilo Group and the two overlying, less well-known groups were subjected to deformation that did not affect the ~1 Ga intrusives. Collectively, these data limit the depositional age of the Kiaora Group to >1.38 Ga, and bracket the depositional age of the Nzilo Group and younger Kibaran Supergroup rocks to between 1.38 Ga and 1.08 Ga.

The Karakwe-Ankole belt (KAB) consists of metasedimentary and metavolcanic rocks that are separated into a western domain (WD) and an eastern domain (ED) by a structural boundary zone delineated by the Kabanga-Musongati (KM) mafic layered intrusion (Tack et al., 2010; Fernandez-Alonso et al., 2012). The WD consists of Mesoproterozoic metasedimentary and minor intercalated metavolcanic rocks of the Akanyaru Supergroup, which overlie Paleoproterozoic basement of the Ubendian-Ruwenzori belts and are intruded by granitoids and minor mafic intrusions (Fernandez-Alonso et al., 2012). The Akanyaru Supergroup is bracketed by ~1.43 Ga felsic volcanic rocks at the base of the Akanyaru Supergroup and <1.2 Ga from the

maximum depositional age of detrital zircon from the upper Akanyaru Supergroup (Fernandez-Alonso et al., 2012). The ED consists of Paleoproterozoic to Mesoproterozoic metasedimentary rocks of the Kagera Supergroup that are intruded by KM magmatic rocks and that overlie the Archean Tanzania craton (Fernandez-Alonso et al., 2012). The Kagera Supergroup is bracketed by a tuff from the base of the Kagera Supergroup ~1.78 Ga to ~1.37 Ga and by theca.1375 Ma KM magmatic rocks that intrude the Kagera Supergroup (Fernandez-Alonso et al., 2012). Together, the KAB and KIB record intracratonic sedimentation with widespread magmatic activity ~1380-1370 Ma, minor magmatic activity ~1205 Ma, and orogenesis occurring ~1080 Ma, based on metamorphic zircon. Post-kinematic granitoids ~1000-950 Ma are present throughout both the KIB and KAB (Kokonyangi et al., 2004, 2006, 2007; Tack et al., 2010; Fernandez-Alonso et al., 2012).

The Irumide belt consists of minor Paleoproterozoic orthogneisses (~2050-1920 Ma) and abundant Mesoproterozoic granitoid intrusions ~1050-1000 Ma associated with the ‘Irumide’ orogeny (De Waele, 2005; De Waele et al., 2006a, 2006b, 2009). The Irumide belt underwent metamorphism during the ‘Irumide’ orogeny ~1050-1000 Ma, as indicated by metamorphic zircon overgrowths, which was contemporaneous with ‘Irumide’-aged magmatism (De Waele et al., 2003, 2009). Minor anorogenic granitoids ~1650-1590 Ma also outcrop in the Irumide belt (De Waele et al., 2006b, 2009). A granitic gneiss that outcrops in the Irumide belt was dated ~2726 Ma and is the only known Neoarchean basement in the area (De Waele, 2005). Strongly deformed metasedimentary rocks of the Muva Supergroup outcrop along the Irumide belt (De Waele and Fitzsimons, 2007). It was recently suggested by Debruyne et al. (2014) that the basement inliers of the ‘domes’ region, the Irumide belt, and the Bangweulu block are related to one another and formed a mid-Paleoproterozoic magmatic arc terrane, which now forms the

basement of the CACB, an idea that expands upon the theory of the LMC of Rainaud et al. (2005b).

2.4.4 Neoproterozoic Source Areas

Neoproterozoic source areas for zircon that are 1000-800 Ma include several granitoid intrusions that post-date the pre-Katangan basement, such as the ~883 Ma Nchanga granite (Armstrong et al., 2005) and the ~977 Ma Mitwaba granites in the Kibaran belt (Kokonyangi et al., 2004) and granitoid intrusions ~950 Ma located in the Irumide belt (De Waele et al., 2009). Zircon that are <800 Ma are probably derived from rift-related mafic-intermediate volcanic and plutonic rocks that are present throughout the Katangan basin (Key et al., 2001; Barron, 2003).

2.5 Existing detrital zircon data from Katanga Supergroup

Geochronological studies of Precambrian basement and supracrustal rocks provide a framework for interpreting detrital age spectra by identifying possible original source areas and secondary sources of reworked zircon. Comparing the age populations of detrital zircon in the Kamoa sub-basin to the ages of possible Congolese cratonic and supracrustal rocks identifies their origin and illuminates the geological events that affected the Katangan basin and more specifically the Kamoa sub-basin (Fig. 6, 7).

Previous detrital zircon geochronology studies of the Katangan succession are few and focus predominantly on the Roan Group (Armstrong et al., 2005; Master et al., 2005; Halpin and Selley, 2010; Liu et al., 2019); only one previous study included detrital zircon work on the ‘grand conglomérat’ (Master et al., 2005). Collectively, the studies of Roan Group zircon

provenance span much of the basin. Given that the nature and age of nearby source terranes would have differed according to location, it should be expected that a given stratigraphic unit might contain a different suite of detrital zircon populations in different locations. The presence of a zone of Paleoproterozoic-cored basement highs (‘domes’) that spans the centre of the basin is of particular concern, because several of the previous studies collected at least some of their samples from the flanks of these structures (Fig. 1; Armstrong et al., 2005; Master et al., 2005; Halpin and Selley, 2010; Liu et al., 2019). Detrital zircon geochronological results for the Katanga Supergroup and other relevant geological units are summarised in Figs. 8 and 9.

Armstrong et al. (2005) analysed detrital zircon from the lower Roan Group from drill-core on the northern flank of the Kafue anticline, where Katanga Supergroup strata directly overlie the Nchanga granite. The combined results for both samples of the lower Roan Group show that it is dominated by a mid-Paleoproterozoic population ~1900 Ma that corresponds to locally exposed LMC of the Kafue anticline with minor Neoproterozoic grains ~900 Ma sourced from the underlying Nchanga granite, which intrudes the LMC (Armstrong et al., 2005).

Master et al. (2005) analysed the detrital zircon geochronology of the lower Roan Group and the ‘grand conglomérat’ in the southeasternmost part of the basin (Fig. 1). Detrital zircon from the three lower Roan Group samples are dominated by mid-Paleoproterozoic populations ~2000-1800 Ma, but contain two ~900 Ma grains. The Mwashya Subgroup sample has most grains ~2000 Ma and ~900 Ma. The sample from the ‘grand conglomérat’ has grains ~1945-1845 Ma, ~1000 Ma, and a discordant mid-Neoproterozoic grain with an age of 729±50 Ma. The dominant source areas are interpreted to be the Ubendian belt (mid-Paleoproterozoic population), the Kibaran belt (Mesoproterozoic population), and early Neoproterozoic granitoid intrusions (~900 Ma grains). Samples analysed in Master et al. (2005) are from the eastern part of the basin, near

both the Paleoproterozoic Bangweulu block and the Paleoproterozoic-cored Kafue anticline; the number of zircon analysed was low in all samples, and, especially when placed under a 5% discordance filter rather than the 10% discordance filter used in the paper, is statistically insufficient to make meaningful comparisons for provenance studies.

Halpin and Selley (2010) collected samples for detrital zircon geochronology from throughout the Katangan basin in the central and northwestern parts of the basin but focussed predominantly on the Roan Group. The dominant age populations in all samples of RAT, RGS, Mines, lower Roan Group, and upper Roan Group strata are mid-Paleoproterozoic, ranging from ~2000-1800 Ma, with secondary populations of Mesoproterozoic grains ~1400-1200 Ma and minor amounts of Archean grains. Rare early Neoproterozoic grains are present (~900 Ma) in some of the samples. The only sample in the study that does not have a dominant mid-Paleoproterozoic population is a sample of the ‘poudingue’ conglomerate from Kolwezi, which has a dominant Mesoproterozoic population. There were 91 grains analysed of the ‘poudingue’ conglomerate, which is an adequate number of grains.

Liu et al. (2019) collected samples from the Kitwe and Mindola formations on the western flank of the Kafue anticline (lower Roan Group in Zambia; Liu et al., 2019), stratigraphic equivalents of the Mines and RAT subgroups in the DRC), exclusively from the Chambishi ‘basin’ on the flank of the Kafue inlier (“anticline”) in the southeastern part of the basin. The material is dominated by mid-Paleoproterozoic grains (i.e., >90% of the total detrital zircon) that are ~2098-1744 Ma. The interpretation based on the dominance of the mid-Paleoproterozoic age population is that the strata of the lower Roan Group were derived from the LMC and Bangweulu block. There are some ~1850-1744 Ma grains in both samples that are ~100 m.y. younger than the LMC and Bangweulu block, but that do not have a known source area. The presence of this

population suggests that the lower Roan Group had other source areas apart from the LMC and Bangweulu block. Minor Archean grains are suggested to be derived from the Muva Supergroup, a Paleoproterozoic (> 1800 Ma) succession overlying Paleoproterozoic basement in the Bangweulu block, which inherited zircon originally from Archean terranes such as the Tanzania craton (De Waele and Fitzsimons, 2007). Minor Mesoproterozoic grains ~1500 Ma and ~1000 Ma are suggested to be derived from two separate granitoid suites in the Irumide belt.

The only detrital zircon samples of the Kibaran Supergroup are the four samples of the Nzilo Group from the Mitwaba area, DRC ~200 km north of Kamoa (Kokonyangi et al., 2007). All four samples were collected a few 100 metres from one another above the interpreted disconformity separating the Nzilo Group from the older Kiaora Group. A basal conglomerate, a metapelite, and two quartzite samples were collected from the Nzilo Group for the detrital zircon study; there are no significant differences in the detrital zircon age distributions between samples (Kokonyangi et al., 2007). The combined number of grains analysed with a 5% discordance filter is 105 grains, which is an adequate number of grains for the detrital zircon age spectra to be meaningful.

The main issue concerning the validity of the detrital zircon data from Kokonyangi et al. (2007) when comparing them to the results of the preset study is that the samples of Nzilo Group were from far enough away that there may be significant differences in the surrounding basement rocks of the Mitwaba area compared to the Kamoa area. Another possible issue is that the metasedimentary rocks of the Kibaran Supergroup in the Nzilo promontory in the Kamoa area are undifferentiated on maps and have no stratigraphic constraints, which means that the Kibaran metasedimentary rocks locally exposed near Kamoa could be from any one of the four stratigraphic units of the Kibaran Supergroup. Comparisons of the detrital zircon data of this

study to those of Kokonyangi et al. (2007) as a proxy for the Kibaran metasedimentary rocks located on the Nzilo promontory should be taken approached cautiously. Future work should include samples of basement rocks underlying the Katangan sedimentary rocks at Kamoa, which would be analysed to determine what its detrital zircon spectrum is. Kibaran basement samples analysed in the present study yielded too few zircon to be useful for detrital zircon geochronology.

Kibaran-aged intrusives (i.e., ~1380-1370 Ma) should be common in strata in the NW part of the basin adjacent to the Kibaran belt where Kibaran intrusives outcrop and are relatively abundant (~30-40% of map distribution; Kokonyangi et al., 2007). Detrital zircon samples from the NW part of the basin (Halpin and Selley, 2010; this study) have a more significant contribution of Mesoproterozoic grains in their detrital zircon age distributions than strata from elsewhere in the Katangan basin (Fig. 8).

Conversely, the Irumide belt contains relatively abundant ~1000 Ma intrusives (~30-50% of map area; De Waele and Fitzsimons, 2007), but detrital zircon samples in the SE part of the basin only have minor contributions of Mesoproterozoic grains ~1000 Ma (Fig. 8). The lack of a detrital zircon population ~1000 Ma is probably due to the fact that many of the detrital zircon samples analysed in previous studies in the area were based on too few grains to account for minor populations such as the Mesoproterozoic population ~1000 Ma. However, Liu et al. (2019) sampled a large number of grains and still the number of Mesoproterozoic grains in their detrital zircon age distributions are relatively small (Fig. 8). The lack of the ~1000 Ma population is probably because the Irumide-aged intrusions are relatively far away from where the samples were taken, and demonstrates that the Roan Group was predominantly sourcing locally exposed basement material rather than distal source areas.

3.0 Materials and Methods

3.1 Sample Collection

All samples were selected from drill-core stored at the Kamoa camp, DRC (Fig. 3; Table 3). Samples of the Roan Group underlie the 'grand conglomérat' and should reflect the depositional regime of the basin before the onset of the rifting event associated with the grand conglomérat and the mid-Neoproterozoic glacial event. Several samples of the Dipeta and Mwashya subgroups were collected in order to avoid possible biasing from intraformational variations in detrital zircon age distributions (Zimmermann et al., 2015). Samples of the diamictite and laminated siltstone present in the 'grand conglomérat' were taken to test whether different depositional processes (debrite-dominated vs. suspension-dominated) sampled different sources or biased the results towards particular zircon populations. Samples of diamictite were chosen to avoid large clasts (pebble-sized and larger) as much as possible, to avoid biasing to the dominant large clast type in a given sample. Samples were also chosen to avoid veins and alteration. Samples were examined to evaluate sedimentary texture (angularity and shape of detrital grains) and the dominant rock-forming minerals present in order to classify the rocks (Figs. 10-16). The holes and depths sampled are provided in Figure 3 and Table 3. [e1]

3.2 Zircon extraction, separation, and picking

Samples were comminuted using electronic pulse disaggregation (EPD) at Overburden Drilling Management (ODM), Nepean, Canada following procedures outlined by Cabri et al., (2008). The remaining five samples were comminuted using SelFrag (Edwin et al., 2006) at Queen's University, Kingston, Canada. Heavy mineral separation via Wilfley table and heavy liquids (methylene iodide, 3.32 g/cm^3) was done at Laurentian University (Table 1). No magnetic

separation was done to avoid biasing of zircon populations from removal of the least paramagnetic fraction (Sircombe and Stern, 2002).

In samples containing abundant pyrite a further step ("pyrite float") was undertaken to remove some of the pyrite. The heavy mineral concentrate was submerged in a 1% solution of K-amyl xanthate in 50 ml of distilled water with ~1-3 ml of KOH and then put into an ultrasonic bath for 5 minutes to remove silt/clay sized material from pyrite grains. The solution was decanted and water was introduced into the sample to remove and 'float' the pyrite from the remainder of the heavy minerals. The K-amyl xanthate solution changes the wettability of the pyrite grains so that they become hydrophobic, which is why they 'float' when subjected to water.

All zircon in a sample were picked regardless of colour, size, clarity, and presence of inclusions, to minimise sampling biases (Fig. 17). The rigorous picking of all zircon grains in a sample regardless of their quality causes the data to have a higher proportion of discordant analyses compared to concordant analyses. Most samples in this study have ~60% of the total population of grains lost to discordance, which is primarily due to the inclusion of metamict grains (i.e., dark pink grains) that would normally be discarded before U-Pb analysis in a typical igneous or metamorphic geochronological study. Including the metamict grains is beneficial because it ensures that no detrital zircon population is excluded from the dataset. Having access to discordant analyses offers the possibility to examine the discordant data in order to see if any other conclusions can be drawn from the data (e.g., Sircombe et al., 2002). Zircon grains were embedded in epoxy pucks and polished down to 1 μm paste to expose their interiors.

3.3 Cathodoluminescence and secondary electron imaging

Scanning electron micrographs of the zircon were taken using a JEOL 6400 SEM at Laurentian University, Sudbury, Canada, under secondary electron mode to identify and avoid the location of flaws (e.g., inclusions, fractures) that would affect analyses. Cathodoluminescence (CL) micrographs were taken to locate youngest growth increments of the zircon based on chemical zonation from their CL response (Fig. 18).

3.4 U-Pb Geochronology

Analytical work was conducted at the chemical fingerprinting laboratories at Laurentian University, Sudbury, Canada, using laser ablation-inductively coupled plasma-mass spectrometry (LA-ICP-MS). Samples were ablated using a Coherent CompexPro excimer ArF laser operating at a 193 nm wavelength and transported via N doped He carrier gas into the Ar plasma source of a Thermo X-series II quadrupole mass spectrometer. Each analysis consisted of a 30-second integration time with the laser firing at 6 Hz with a 20-nanosecond pulse duration using a spot size of 22 μm. Before and after each analysis, data were collected for background measurements and to purge the ablated material before the next analysis. Data reduction was conducted using VizualAge (Petrus and Kamber, 2012), which is an add-on for Iolite (Paton et al., 2011), which is a set of procedures for IgorPro (www.wavemetrics.com). Three reference materials [Plesovice (Sláma et al., 2008); 91500 (Wiedenbeck et al., 1995); and AusZ3] were used as external standards at the beginning and end of a sample and generally between every 10-15 unknown grains. The internal errors are calculated at the 2σ level (i.e., 68% confidence interval of a normal distribution). Interpretation and plotting of the results used the AgeDisplay excel macro of Sircombe, (2004). A 5% discordance filter was employed so that any analysis that is ≥ 5% discordant or ≤ 5% reverse discordant was not used when plotting data. Ages that

are >1000 Ma are reported using the Pb^{207}/Pb^{206} age, and ages <1000 Ma are reported using the U^{238}/Pb^{206} age.

The interpretations of the provenance are not significantly affected by the use of the Pb^{207}/Pb^{206} age vs. the U^{238}/Pb^{206} age because the dominant populations are all >1000 Ma. However, the following are two examples that demonstrate why the different isotopic systems are used at the cutoff for 1000 Ma. The two grains of this example demonstrate the differences in the ages and of the uncertainties from younger grains present in the lower KPS (as a disclaimer the ages aren't present in the appendices because they are discordant).

Grain 68: U^{238}/Pb^{206} : 759±25 Ma; Pb^{207}/Pb^{206} : 760±160 Ma. Similar age but huge uncertainties in the latter age.

Grain 96: U^{238}/Pb^{206} : 984±23 Ma; Pb^{207}/Pb^{206} : 1065±98 Ma. This age straddles the boundary of ~1000 Ma and thus the U^{238}/Pb^{206} age was used because of the significantly smaller error associated with that age.

These examples demonstrate that there are significant differences in the age results of the two isotopic ratios, but because the methodology was applied consistently provenance interpretation is not affected.

A comparison of the data when applying a 5% discordance filter compared to a 10% discordance filter demonstrates that there is not a significant difference in the proportions of major detrital zircon age populations, which affect the interpretation of the provenance. Minor zircon populations have increased abundance using a 10% discordance filter (e.g., mid-Neoproterozoic population of the lower KPS), but there is no difference that significantly affects the outcome. A

5% discordance filter was used to ensure that the data used for the interpretations consists of the most robust ages that are unequivocal based on their discordance.

Prior to the advent of rigorous U-Pb geochronology, researchers attempted to interpret zircon provenance based on colour and morphology (i.e., zircon typology; Pupin 1980).In this study, detrital zircon provenance was not interpreted based on morphology or colour. A qualitative examination showed that the most rounded, darkest pink grains are generally older than subrounded, paler grains with remnant crystal shape. Applying zircon typology to interpret the provenance of zircon would be of limited use because of similarities in source area ages among units (i.e., overlapping age ranges) and due to evidence of sedimentary recycling that affects correlations of zircon to primary source areas. The total number of grains needed to characterise adequately the detrital zircon age populations in a sample is still a subject of debate in the detrital zircon community. Dodson et al. (1988) stated that 59 randomly chosen grains (assuming all 59 grains are within the discordance filter) are needed in order to have a 95% probability that a detrital zircon age population representing 5% of the total population is identified. Vermeesch (2004) stated that 117 randomly chosen grains (assuming all 117 are within the concordance filter) are needed to have a 95% chance of identifying every detrital zircon age population that represents 5% of the total population in a given sample. Gehrels (2012) suggested that a reasonable number of grains to capture the total population of detrital zircon for a sample should be around 100 analyses that are within the concordance filter. In the case of this study the number of analyses that fall within the 5% discordance filter used ranges from 39 analyses to 171, but the majority of samples have ~90 concordant analyses. Therefore, based on previous literature and research that has been done to address the statistical validity of the number of grains needed for a detrital zircon study, the samples in this study have an adequate number of

concordant analyses, although some samples are short of the 117 grains needed to ensure every 5% detrital zircon age population is represented.

4.0 Results

4.1 Detrital zircon U-Pb geochronology

4.1.1 Lower Dipeta Subgroup (Roan Group)

A total of 258 zircon was analysed, of which 91 were acceptable using the ±5% discordance filter (Fig. 19). There is a bimodal detrital zircon age distribution with a dominant age population of Mesoproterozoic grains (39%) with a peak at ~1380 Ma and a dominant age population of mid-Paleoproterozoic grains (60%) with a peak at ~1920 Ma. A single early Paleoproterozoic grain ~2400 Ma is present.

4.1.2 Upper Dipeta Subgroup (Roan Group)

A total of 300 zircon was analysed, of which 39 were acceptable using the ±5% discordance filter (Fig. 19). There is a bimodal detrital zircon age distribution with a dominant age population of Mesoproterozoic grains (46%) with a peak at ~1360 Ma and a dominant age population of mid-Paleoproterozoic grains (26%) with a peak at ~1930 Ma. A subordinate population of late Paleoproterozoic grains (20%) with a peak at ~1735 Ma and minor early Paleoproterozoic grains (8%) are also present.

4.1.3 Lower Mwashya Subgroup (Roan Group)

A total of 228 zircon was analysed, of which 101 were acceptable using the ±5% discordance filter (Fig. 20). There is a bimodal detrital zircon age distribution with a dominant age population

of Mesoproterozoic grains (37%) with a peak at ~1360 Ma and a dominant age population of mid-Paleoproterozoic grains (60%) with a peak at ~1910 Ma. Minor Archean grains (3%) that are ~2700-2500 Ma are also present.

4.1.4 Upper Mwashya Subgroup (Roan Group)

A total of 219 zircon was analysed, of which 97 were acceptable using the ±5% discordance filter (Fig. 20). There is a bimodal detrital zircon age distribution with a dominant age population of mid-Paleoproterozoic grains (75%) with a peak at ~1950 Ma and a subordinate age population of Mesoproterozoic grains (22%) with a peak at ~1370 Ma. Minor amounts of Archean and early-Paleoproterozoic grains (3%) that are ~2600-2370 Ma are also present.

4.1.5 Basal diamictite lower package (Nguba Group)

A total of 196 zircon was analysed, of which 93 were acceptable using the ±5% discordance filter (Fig. 21). There is a dominant detrital zircon age distribution of mid-Paleoproterozoic grains (50%) with a peak at ~1960 Ma. There are subordinate populations of Mesoproterozoic grains (11%) with a peak at ~1500 Ma, late-Paleoproterozoic grains (19%) with a peak at ~1770 Ma, and Archean grains (12%) with peaks at ~3260, 2700, 2620, and 2510 Ma.

4.1.6 Basal diamictite upper package (Nguba Group)

A total of 265 zircon was analysed, of which 90 were acceptable using the ±5% discordance filter (Fig. 21). There is a dominant detrital zircon age distribution of mid-Paleoproterozoic

grains (46%) with peaks at ~2050 and 1870 Ma. There are subordinate populations of late Paleoproterozoic grains (21%) with a peak at ~1760 Ma and Archean grains with a peak at ~2500 Ma. Minor Mesoarchean grains (25%) with a peak at ~2980 Ma and one Neoproterozoic grain at ~920 Ma are also present.

4.1.7 Lower Kamoa pyritic siltstone (KPS; Nguba Group)

A total of 304 zircon was analysed, of which 93 were acceptable using the ±5% discordance filter (Fig. 22). There is a dominant detrital zircon age distribution of mid-Paleoproterozoic grains (52%) with a peak at ~1890 Ma and a subordinate age population of Mesoproterozoic grains (15%) with a peak at ~1380 Ma. Minor amounts of Archean grains (5%), early-Paleoproterozoic grains (3%), late-Paleoproterozoic grains (10%), late-Mesoproterozoic grains (11%), and Neoproterozoic grains (4%) are also present. Specifically, there are three mid-Neoproterozoic grains (741±21 Ma, 759±25 Ma, 686±25 Ma).

4.1.8 Middle diamictite (Nguba Group)

A total of 290 zircon was analysed, of which 171 were acceptable using the ±5% discordance filter (Fig. 22). There is a dominant detrital zircon age population of mid-Paleoproterozoic grains (62%) with a peak at ~2000 Ma and a subordinate age population of Archean grains (19%) with a peak at ~2510 Ma. Minor amounts of early-Paleoproterozoic grains (8%), late-Paleoproterozoic grains (4%), Mesoproterozoic grains (6%), and one Neoproterozoic grain ~660 Ma.

4.1.9 Upper diamictite (Nguba Group)

A total of 176 zircon was analysed, of which 97 were acceptable using the ±5% discordance filter (Fig. 23). There is a dominant detrital zircon age distribution of Mesoproterozoic grains

(51%) with a peak at ~1350 Ma and a subordinate population of mid-Paleoproterozoic (1750-2010 Ma) grains. Minor amounts of early Paleoproterozoic and Archean grains are also present.

5.0 Interpretation

5.1 Roan Group

Detrital zircon generally represent either: 1) direct provenance from metamorphic and igneous source areas (primary sources) or 2) recycling from sedimentary rocks (secondary sources). Detrital zircon studies of the upper and lower Roan Group from across the Katangan basin (Fig. 9) provides some insight into the sedimentary dynamics during deposition of the units. The detrital zircon age distributions of samples from across the Katangan basin demonstrate that they all share a similar provenance, with a dominant mid-Paleoproterozoic population and minor amounts of Archean, Mesoproterozoic, and Neoproterozoic grains (Fig. 9; Armstrong et al., 2005; Master et al., 2005; Halpin and Selley, 2010; Liu et al., 2019). The mid-Paleoproterozoic population is ubiquitous in samples, with the exception of the upper diamictite (this study) and the ‘poudingue conglomerate’ (Halpin and Selley, 2010). The mid-Paleoproterozoic population is the dominant population because the basement underlying the Katangan basin consists of the mid-Paleoproterozoic LMC and the related Bangweulu block and Paleoproterozoic basement is exposed in the Irumide belt and in the ‘domes’ inliers. Thus, the dominant source area for strata in the Katangan Supergroup is locally derived, overlying mid-Paleoproterozoic basement. Minor amounts of Archean grains were probably derived through inheritance of recycled Archean grains present in Mesoproterozoic and Paleoproterozoic metasedimentary units (e.g., Muva Supergroup, Kibaran Supergroup) or directly from primary sources such as the Kasai block or the Tanzania craton. Minor Mesoproterozoic grains in the northern margins of the basin were

probably derived from the Mesoproterozoic Kibaran igneous rocks present in the Kibaran belt, whereas in the southern part of the basin they were probably derived from igneous rocks present in the Irumide belt. Minor early-Neoproterozoic (1000-800 Ma) grains were probably derived from local S-type granitoid intrusions present in both the Kibaran and Irumide belts.

Overall, when comparing strata of the lower and upper Roan Group across the basin there are no significant variations in their detrital zircon age distributions, which suggests that strata of the Roan Group were derived primarily from underlying and nearby basement rocks, with only minor contributions from other source areas. The similarity in their detrital zircon age distributions indicates that, despite having different source areas in the northern margin (i.e., Kasai block, Kibaran belt) vs. the southern margin (i.e., Bangweulu block, Irumide belt) of the basin, the basement rocks are similar in age, yielding similar provenance signatures for detrital units from geographically separate areas in the Katangan basin. Comparing different stratigraphic intervals in each part of the basin, there are no differences in their detrital zircon age distributions through time that are evident going up-section.

The only significant difference in the provenance signatures of the upper and lower Roan Group geographically and stratigraphically are that strata from the northwestern part of the basin [i.e., ‘poudingue conglomerate’, RAT, and RGS (Halpin and Selley, 2010), and the Mwashya and Dipeta subgroups (this study)] have a subordinate to dominant population of Mesoproterozoic grains ~1380 Ma. The Mesoproterozoic population has an increased abundance in samples in the NW part of the basin probably because of the proximity of Kibaran-aged igneous intrusions located west of Kolwezi in the Kibaran belt.

The only other Roan Group samples that have significantly different detrital zircon age distributions from the rest of the strata are the ‘poudingue conglomerate’ sample from Kolwezi (Halpin and Selley, 2010), the RGS sample from Lupoto (Halpin and Selley, 2010), and the RAT sample from Ruashi (Halpin and Selley, 2010). The lack of a dominant mid-Paleoproterozoic population in the ‘poudingue conglomerate’ is probably due to a greater proportion of Kibaran-aged detritus, which proportionately decreases the abundance of the mid-Paleoproterozoic population. The wide range of minor grains in the RGS sample around Lupoto is difficult to reconcile, because it is near other RGS samples that do not have the same spectrum (i.e., RGS from Kipushi and Ruashi). Perhaps there are local Mesoproterozoic and Neoproterozoic intrusions that correspond to the peaks in the spectra for Lupoto RGS underlying the Katangan basin in the Lupoto area that are not present at Kipushi or Ruashi. The RAT sample from Ruashi appears to have a significant Mesoproterozoic population ~1100-1000 Ma, but only nine grains were analysed from this sample and therefore the seemingly dominant population is only an artefact of having a statistically insufficient number of concordant analysed zircon.

The samples of the Dipeta and Mwashya subgroups from the present study have similar detrital zircon age distributions as the samples from Halpin and Selley (2010) in the Kolwezi area. The exception is the Mines Subgroup from Kolwezi, which lacks a significant Mesoproterozoic population, probably because during its deposition Kibaran-aged intrusives were not exposed and were covered by Katangan strata. The detrital zircon age distributions of the Dipeta and Mwashya subgroups compared to the Roan Group strata from other parts of the basin share the ubiquitous mid-Paleoproterozoic population but lack the Mesoproterozoic population. The absence of the Mesoproterozoic population in the other Roan Group strata is probably because

they are not near any Kibaran-aged intrusives, whereas samples from the NW part of the basin are relatively close to Kibaran igneous rocks.

The samples of the ‘grand conglomérat’ in the present study share the ubiquitous mid-Paleoproterozoic population with the Roan Group strata. The basal diamictite contains an older Mesoproterozoic population with a peak ~1490 Ma. Rocks of this age are unknown and so the presence of such grains is probably explained by the presence of underlying intrusions of that age that are presently unexposed but that were exposed during deposition of the basal diamictite. The basal and middle diamictite have a subordinate Neoarchean to early Paleoproterozoic population, which is not present in any other strata, and is probably the result of distal glacial transport from the Kasai block ~200 km from Kamoa. The upper diamictite has a detrital zircon age distribution similar to the ‘poudingue conglomerate’ and probably represents local provenance from locally exposed Kibaran intrusions that were not exposed during deposition of the other units of the ‘grand conglomérat’ at Kamoa.

The only detrital zircon data for the ‘grand conglomérat’ apart from this study are those of Master et al. (2005), which consists of six mid-Paleoproterozoic grains (Fig. 8). The number of grains analysed in that study is not statistically robust and precludes any meaningful comparison, especially considering that mid-Paleoproterozoic grains are present in every detrital zircon sample in the Katangan basin. The results of the present study are therefore the first robust detrital zircon dataset for the ‘grand conglomérat’, and no meaningful comparison with this stratigraphic unit as expressed elsewhere in the basin are yet possible.

5.2 Issues with validity of previous detrital zircon studies

The number of grains analysed in detrital zircon studies, especially for a provenance study, is a crucial aspect of fully and accurately representing the source materials that make up the detrital unit (Vermeesch, 2004; Gehrels, 2012). One must analyse a suitable number of representative grains in order to capture all of the major and minor populations present in a sample (n=117; Vermeesch, 2004). An appropriate number of detrital zircon for a given sample should analyse a minimum of ~100 concordant grains.

Many of the detrital zircon samples from previous studies (Master et al., 2005; Armstrong et al., 2005; Halpin and Selley, 2010) have analysed considerably fewer than 100 grains, even when combining the detrital zircon results of several samples from a given stratigraphic unit. The disparity in the number of concordant data-points for samples of a given stratigraphic unit affects the validity of comparisons between samples (e.g., RAT from Ruashi n=9 vs. RAT from Kolwezi n=121; Halpin and Selley, 2010).

Another issue that affects comparisons between different detrital zircon datasets are the analytical techniques used to analyse grains, in this case the differences in precision between sensitive high resolution ion microprobe (SHRIMP) and LA-ICP-MS analyses. SHRIMP analyses have higher analytical precision and accuracy and therefore researchers can present their data using 1σ levels of uncertainty, which results in a greater number of distinct populations. LA-ICP-MS analyses have a lower analytical precision and therefore results are reported using 2σ levels of uncertainty, which results fewer minor distinct populations and the presence of larger overlapping peaks in the detrital zircon age spectra.

Another intrinsic bias in the detrital zircon sampling in the Katangan basin (this study included) is that most samples are from drill-cores near exposed basement inliers. This sampling bias is

difficult to avoid because in the CACB there is a lack of suitable stratigraphically constrained outcrop from which to sample, and exploration efforts are preferentially focused around mineralisation on the peripheries of basement inliers (e.g., Kafue anticline, Nzilo promontory). Samples collected in locations distant from any exposed basement inliers should properly represent a detrital zircon age distribution that is not biased by the predominant exposed basement rock in the area.

Another issue is that significant variations in the detrital zircon age distribution of a given stratigraphic unit can be present depending on the lithology that has been sampled - different sedimentary processes are responsible for different lithologies and can cause sedimentological biasing in zircon populations (Zimmermann et al., 2015). In order to represent the detrital zircon age distribution of a given stratigraphic unit accurately, several samples of different lithofacies should be analysed to ensure that there are no intraformational variations in provenance that arose from the sampling of different lithofacies.

Lastly, for the detrital zircon samples of Halpin and Selley (2010) their data are presented using a 10% discordance filter, whereas the other detrital zircon datasets are presented using a 5% discordance filter; this could possibly influence detrital zircon age distributions.

6.3 Provenance of the Dipeta and Mwashya subgroups

The provenance of the Dipeta and Mwashya subgroups is discussed together because of the similarities in their detrital zircon age distributions (Fig. 24). The Dipeta and Mwashya subgroups have a bimodally distributed population of Mesoproterozoic (~1400-1350 Ma) and mid-Paleoproterozoic (~1900 Ma) grains, with minor Archean (~2700-2500 Ma) and early Paleoproterozoic grains (~2400-2200 Ma).

The Mesoproterozoic population was probably derived from quartzite and conglomerate of the locally exposed Nzilo promontory of the Kibaran Supergroup, with the primary source of the population ~1380-1370 Ma being intrusive rocks of the Kibaran magmatic event (Tack et al., 2010). The mid-Paleoproterozoic population is also probably derived from recycling of Kibaran quartzite, because the Nzilo Group also has a dominant mid-Paleoproterozoic population (Kokonyangi et al., 2007). The primary source of the mid-Paleoproterozoic population is probably gneiss and schist of the Lufubu metamorphic complex (2050-1850 Ma), which underlies the CACB and is exposed as basement inliers in the 'domes' region of Zambia and in the Kafue anticline (Rainaud et al., 2005b). The early-Paleoproterozoic and Neoarchean grains are probably derived from recycling of the Kibaran Supergroup from locally exposed basement in the Kamoa area.

The samples of Dipeta and Mwashya in this study have roughly equal proportions of both Mesoproterozoic and mid-Paleoproterozoic grains based on their detrital zircon age distributions. The Nzilo Group from the Mitwaba area has a dominant mid-Paleoproterozoic population, much like the detrital zircon age distributions of other strata from the Katanga Supergroup, but does not share such a prominent Mesoproterozoic population (Kokonyangi et al., 2007; Halpin and Selley, 2010; Liu et al., 2019).The ubiquitous nature of the mid-Paleoproterozoic population makes it difficult to determine exactly where the population was derived from, because that population is widespread in Katangan strata and in pre-Katangan supracrustal rocks (e.g., Kibaran Supergroup, Muva Supergroup) and pre-Katangan crystalline basement (e.g., Bangweulu block, LMC). The mid-Paleoproterozoic population could have been derived from recycling of Kibaran Supergroup or directly sourced from the LMC, however the LMC would have been covered by older strata of the Katanga Supergroup. The prominent Mesoproterozoic

population in the Dipeta and Mwashya subgroups was probably derived directly from intrusions ~1380-1370 Ma in the Kibaran belt to the west and north of Kamoa in order to account for the increase in Mesoproterozoic grains. The lack of a distally derived detrital zircon population, and the similarities between the detrital zircon age distributions of the four samples of Dipeta and Mwashya subgroups, suggests that they were locally sourced through sedimentary recycling of Kibaran Supergroup strata exposed on the Nzilo promontory, and that during deposition of these strata in the first rifting stage of the Katangan basin there were no major changes in sediment transport.

6.4 Provenance of the basal diamictite

The lower and upper packages of the basal diamictite (Fig. 25) have a unimodal distribution of mid-Paleoproterozoic grains (~2000-1900 Ma), with subordinate populations of Neoarchean to early Paleoproterozoic grains (~2600-2400 Ma) and Mesoproterozoic grains (~1500-1400 Ma). Minor amounts of Mesoarchean grains (~3200-3000 Ma) are also present in both units. A single early Neoproterozoic grain is present (~990 Ma) in the upper package of the basal diamictite.

The mid-Paleoproterozoic population dominates both samples. The basal diamictite upper package has two distinct peaks in the mid-Paleoproterozoic population with an older peak ~2050 Ma and a younger peak ~1870 Ma. The separation of the two peaks is also evident in other Katangan detrital zircon samples (e.g., lower Roan Group; Liu et al., 2019) and probably derives from two distinct ages in the LMC, as, for example, in the Kafue anticline (Rainaud et al., 2005b).The mid-Paleoproterozoic population is probably originally derived from recycling of Dipeta and Mwashya subgroups and from Kibaran metasedimentary rocks.

Apart from the ubiquitous mid-Paleoproterozoic population, the basal diamictite has a distinctly different detrital zircon age distribution from that of the underlying Dipeta and Mwashya subgroups. The Mesoproterozoic population is significantly smaller and has shifted from a population peak ~1380 Ma in the upper Roan Group to a peak ~1500 Ma in the basal diamictite. The 1500 Ma material is too old (>100 m.y.) to be derived from Kibaran intrusive rocks, and the only known rocks of that age range in central Africa are granitoids in the Irumide belt (De Waele et al., 2006). The Irumide belt is an unlikely source for detritus delivered to the Kamoa sub-basin because it is on the opposite flank of the Katangan rift (Fig. 5); the dominant source area for detritus in the Kamoa sub-basin would be from source areas near the northern and western margin based on the general orientation of the Katangan rift axis (Selley et al., 2018). There could be hitherto unknown rocks ~1500 Ma in the Kibaran belt or hidden beneath Phanerozoic cover rocks to the NW of Kamoa (Linol et al., 2016).

A second major difference between the detrital zircon age distributions of the basal diamictite and the underlying Dipeta and Mwashya subgroups is the significant Neoarchean to early Paleoproterozoic population (~2500-2300 Ma) present in the basal diamictite. Neoarchean to early Paleoproterozoic grains are common in the Katanga Supergroup, but never as substantial populations. The absence of the Neoarchean to early Paleoproterozoic population from the Dipeta and Mwashya subgroups, together with the decrease in the Mesoproterozoic population that was prominent in the underlying Dipeta and Mwashya subgroups, suggests that the sediment supply may not have been only locally sourced during deposition of the basal diamictite, and that other primary source areas contributed to the sediment supply at Kamoa, such as the Kasai block.

A Mesoarchean population is absent from the Dipeta and Mwashya subgroups but is present in the Nzilo Group from the Mitwaba area (~200 km northeast of Kamoa; Kokonyangi et al., 2007)

and in other Katangan strata (Fig. 9). The Mesoarchean population was probably sourced from the Likasi terrane through recycling of Kibaran Supergroup rocks (Rainaud et al., 2003). The small population of early Neoproterozoic grains present in the basal diamictite is probably derived from post-Kibaran granitoids dated ~977 Ma that may be present in the Nzilo promontory near Kolwezi (Kokonyangi et al., 2004). The presence of the early Neoproterozoic grains and Mesoarchean grains does not affect the interpretation of the basal diamictite's provenance

The basal diamictite was probably mostly derived by recycling of Kibaran metasedimentary rocks, which are locally exposed in the Nzilo promontory north of Kamoa and a larger area of Kibaran bedrock west of Kamoa, and was not produced simply by recycling sediment from the underlying Dipeta and Mwashya subgroups; this is clearly indicated by the absence of the dominant Mesoproterozoic ~1380 Ma population that is present in the Dipeta and Mwashya subgroups. The basal diamictite detrital zircon age spectrum is more similar to the Nzilo Group spectrum of Kokonyangi et al. (2007) than it is to the upper Roan Group spectra from the present study. There is evidence that the basal diamictite may have received a small amount of material from distal primary source areas (e.g., Kasai block) that were responsible for the Neoarchean to early Paleoproterozoic population, which is absent in the Dipeta and Mwashya subgroups.

6.5 Provenance of the lower KPS

The lower KPS has a unimodal detrital zircon age distribution with a dominant mid-Paleoproterozoic population (~1900 Ma) and a subordinate Mesoproterozoic population (~1400 Ma and 1100 Ma; Fig. 26). Minor amounts of Archean, early Paleoproterozoic and mid-Neoproterozoic grains are also present.

The detrital zircon age distribution of the lower KPS differs from that of the Dipeta and Mwashya subgroups, the basal diamictite below it, and the middle diamictite above it. The mid-Paleoproterozoic population is ubiquitous and has limited use for differentiating provenance, and thus subordinate populations prove more useful for diagnosing provenance of the lower KPS. The most significant differences in the detrital zircon age distribution of the lower KPS, as compared to the underlying basal diamictite, are a decrease in the Neoarchean to early Paleoproterozoic population and the presence of a Mesoproterozoic population ~1100 Ma. The near-absence of the Neoarchean to early Paleoproterozoic population suggests that sediment delivery from the Kasai block no longer took place during deposition of the lower KPS. The lower KPS has a Mesoproterozoic population ~1380 Ma, which suggests that metasedimentary rocks of the Kibaran Supergroup were being sourced together with input from primary Kibaran intrusives ~1380-1370 Ma that belong to the Kibaran magmatic event of Tack et al. (2010) , which resulted in an increase in the mid-Mesoproterozoic population, as compared to the spectrum for the basal diamictite. The difference in the size of the mid-Mesoproterozoic population of the lower KPS compared to the Dipeta and Mwashya subgroups is probably because the Kibaran intrusives were not the dominant source of Mesoproterozoic grains during that time and that the Mesoproterozoic population of the lower KPS was mainly derived from recycling of Kibaran metasedimentary rocks.

The presence of the Mesoproterozoic population ~1100 Ma, which was absent in underlying units, indicates that during deposition of the lower KPS a new source area contributed sediment to the Kamoa sub-basin. Granitoid intrusions of this age are located in both the Irumide and Kibaran belts (Kokonyangi et al., 2004, 2006; De Waele et al., 2006b). The probable source of grains ~1100 Ma is post-Kibaran S-type “tin” granitoids in the Kibaran belt, the closest of which

are ~60 km away; unfortunately, there is no geochronology for intrusives in the nearby Kibaran basement to show whether the intrusions belong to the Kibaran intrusive suite ~1380 Ma or the post-Kibaran, ~1000 Ma “tin” granitoids. The most significant difference in the detrital zircon age distribution of the lower KPS is the presence of mid-Neoproterozoic grains (~700 Ma; n=3). The mid-Neoproterozoic population is probably derived either from the mafic volcanic unit intercalated between the lower KPS and middle diamictite at Kamoa or from related mafic volcanic units that outcrop to the south in Zambia (Selley et al., 2005). The presence of rift-related tholeiitic basalts that are ~700 Ma is well documented throughout the CACB (e.g., Kampunzu et al., 2000; Key et al., 2001; Barron, 2003). The provenance of the lower KPS contrasts with the provenance of the underlying basal diamictite and may represent a period of glacial waning in which the sediment was more locally derived.

The provenance of the lower KPS could be an effect of sedimentary biasing due to the difference in grain size of the lower KPS compared to the diamictite of the ‘grand conglomérat’ (i.e., siltstone vs. poorly sorted conglomerate). An analysis of the cathodoluminescence images of zircon from samples analysed for this study was done to determine if there are any differences in the zircon (e.g., size, shape, internal textures), which would indicate that zircon from different age populations have identifying characteristics. Differences in zircon grain size specifically would apply to sedimentary biasing of the lower KPS, because it would be expected that larger zircon would not be a significant component of the lower KPS and would result in sedimentary biasing based on preferential grain sorting for certain age populations. However, the variability in zircon characteristics for different age populations (e.g., Mesoproterozoic vs. mid-Paleoproterozoic) indicates that there are no major differences between zircon populations and that sedimentary biasing did not affect the provenance of the lower KPS.

6.6 Provenance of the middle diamictite

The middle diamictite has a unimodal detrital zircon age distribution with a dominant mid-Paleoproterozoic population (~1900 Ma) and a subordinate population of Neoarchean to early Paleoproterozoic grains (~2500-2400 Ma). Minor amounts of Mesoarchean grains (~3200-2900 Ma) and Mesoproterozoic grains (~1400-1300 Ma) are also present. The middle diamictite spectrum resembles that of the underlying basal diamictite but is significantly different from the underlying lower KPS and the overlying upper diamictite (Fig. 26, 27).

An important difference between the middle diamictite and the other units in this study is that the minor Mesoproterozoic population has a peak ~1290 Ma rather than the peak ~1500 Ma present in the basal diamictite and the peak ~1380 Ma that is present in the Dipeta and Mwashya subgroups, the lower KPS, and the upper diamictite. There are no known source rocks of that age in the area surrounding the CACB, and thus it is probable that this population was derived from rare intrusions ~1290 Ma hidden beneath Phanerozoic cover to the north or currently unexposed in the Kibaran belt. Sedimentary recycling of underlying Katangan strata may have contributed less to the sediment budget of the Kamoa sub-basin during deposition of the basal and middle diamictite (indicated from the distally sourced Neoarchean to early Paleoproterozoic population), resulting in a decrease of Mesoproterozoic grains compared to the Dipeta and Mwashya subgroups. The decrease in the Mesoproterozoic zircon population and the reappearance of the Neoarchean to early Paleoproterozoic population suggests that recycling of underlying strata of the Dipeta and Mwashya subgroups and of the Kibaran Supergroup was not the only source of sediment during deposition of the middle diamictite, and suggests that distal primary source areas, such as the Kasai block, also contributed to the sediment budget, similar to the provenance of the basal diamictite.

6.7 Provenance of the upper diamictite

The upper diamictite has a unimodal detrital zircon age distribution with a dominant Mesoproterozoic population (~1350 Ma) and a subordinate mid-Paleoproterozoic population (~2100-1700 Ma). Minor amounts of Archean and early Paleoproterozoic grains are also present, but young Mesoproterozoic and Neoproterozoic grains are absent. This detrital zircon age distribution is significantly different from that all underlying components of the grand conglomérat (Fig. 27).

The change in the proportions of the Mesoproterozoic and mid-Paleoproterozoic populations suggests sediment sourcing from the underlying Dipeta and Mwashya subgroups and from the metasedimentary rocks of the locally exposed Kibaran basement. However, the proportion of mid-Paleoproterozoic grains in the upper diamictite is significantly lower than that in the Dipeta and Mwashya subgroups, which suggests that primary Mesoproterozoic rocks (orthogneisses and granitoid intrusions of the Kibaran magmatic event ~1380-1370 Ma) contributed abundant detritus to the Kamoa sub-basin during deposition of the upper diamictite. Mesoproterozoic intrusions are present in the vicinity of the Kamoa sub-basin, which suggests that, along with the absence of the Neoarchean to early Paleoproterozoic population, the upper diamictite records a more locally derived provenance as compared to the other diamictite units in the ‘grand conglomérat’. The minor amounts of Archean grains were probably derived from recycled detritus of underlying units.

The provenance changes throughout the ‘grand conglomérat’ have significant implications for the current understanding of sediment dynamics at Kamoa. Recent sedimentological research suggested that the diamictite of the ‘grand conglomérat’ at Kamoa was almost exclusively

locally sourced from underlying units, and especially by resedimentation of rift-margin conglomerates (Kennedy et al., 2018).

The data produced by the present detrital zircon study contradicts that interpretation, because of the significant differences in the detrital zircon age populations among the different clastic units of the ‘grand conglomérat’, as compared to those of the underlying Dipeta and Mwashya subgroups. The ‘grand conglomérat’ exhibits variations in provenance throughout its stratigraphy and contains elements that show clearly that it was not derived solely from underlying units (Mwashya subgroup; ‘poudingue’) during rift-margin faulting, as suggested by Kennedy et al. (2018). Other factors had to have contributed to the provenance of the ‘grand conglomérat’ in the Kamoa sub-basin, and based on the evidence from this study, it is logical to suggest that variations in glacial dynamics during deposition of the ‘grand conglomérat’ resulted in significantly different detrital zircon age distributions documented in this study. Tectonic controls were clearly dominant, but were not the only factor contributing to sediment supply at Kamoa during deposition of the ‘grand conglomérat’.

In summary, sediment delivery to the ‘grand conglomérat’ started as comparatively broad in the basal diamictite (i.e., included a modest component from the ~100 km distant Kasai block), but became more local in the KPS, during which time subaqueous volcanics were extruded both at and (more thickly) west of Kamoa, and then cannibalised into the ‘grand conglomérat’ sediment, and presumably local, young Mesoproterozoic sources (~1.0 Ga) contributed substantially for the only time in the succession. A third regime, involving reworked mid-Paleoproterozoic material but only a sparse Mesoproterozoic intrusive component (~1370 Ma), together with a renewed Neoarchean to early Paleoproterozoic component from the Kasai craton, reflects dominance of a broader provenance during deposition of the middle diamictite. Lastly, a local provenance is

indicated for the upper diamictite, which has little Archean to early Paleoproterozoic material and is dominated by a Kibaran Mesoproterozoic intrusive source, together with the ubiquitous mid-Paleoproterozoic material reworked from the Kibaran Supergroup. This history demonstrates that the detrital zircon spectra from Kamoa's 'grand conglomérat' were affected by local, dramatic rift processes, glacial dynamics, and variable unroofing of sources in the Kibaran basement, mid-Paleoproterozoic, previously reworked material and several ages of Mesoproterozoic intrusives (~1370 Ma and 1100 Ma). This history is also compatible with Kennedy's (2018) three-stage evolution of the Kamoa sub-basin, after a modest contribution from changing glacial dynamics has been added to the interpretation: glaciation started locally and at the same time as thermal doming and rifting, became more regional (provenance still limited to within ~100 km of the rift) during maximum subsidence in the rift, and then contracted during late-stage glaciation and waning of rift tectonism.

7.0 DISCUSSION

7.1 Zircon provenance, basin evolution, and sedimentary dynamics

The provenance of the pre- and syn-glacial strata at Kamoa yields important information regarding the sedimentary dynamics of the Kamoa sub-basin, which may have wider implications for the Katangan basin and possibly to mid-Neoproterozoic ('Sturtian') successions elsewhere in the world.

Results of this study identify at least seven distinct sources that variably supplied zircon to the Kamoa sub-basin during deposition of the upper Roan Group and 'grand conglomérat' (Table 4).

(1) Kibaran metasedimentary rocks containing reworked zircon having a major peak ca. 1.86 Ga, a minor peak ca. 1.4-1.37 Ga, and small amounts of Neoarchean and Mesoarchean grains.
(2) Mesoproterozoic ca. 1.38-1.37 Ga intrusives that cross-cut metasedimentary rocks of the Kibaran Supergroup.
(3) Reworked Roan Group sediment [derived from (1) and (2)].
(4) Intrusive post-tectonic granitoids located in the Kibaran belt ca. 1.1-1.0 Ga of unknown nature and location.
(5) The Neoarchean to early Paleoproterozoic Kasai block that is responsible for grains ca. 2.4-2.6 Ga.
(6) Neoproterozoic granite ca.0.9 Ga [minimal; one unit only (Dipeta)].
(7) Neoproterozoic mafic extrusive rocks 0.7 Ga (well known in Kamoa area).

It is interesting that although the details of sediment supply fluctuated throughout upper Roan Group and ‘grand conglomérat’ deposition, the Kasai block only contributed significantly to the zircon profile of any of the basal and middle diamictite, suggesting that all sediment delivered during this time was quite locally derived, and therefore that the Mesoproterozoic (1.1 Ga) sources are probably local components of the Kibaran block that have not yet been recognised. An exclusively local source with only minimal extrabasinal input from Kasai for the entire ‘grand conglomérat’ suggests that glacial influence was similarly localised, either because uplifted rift margins caused sediment transport to be predominantly away from the rift, except in its immediate vicinity, or because glaciation was of geographically limited extent.

The pre-glacial Dipeta and Mwashya subgroups have detrital zircon age distributions that indicate that they were locally sourced. Kibaran basement was exposed during rifting of the

Kamoa sub-basin along scarps of syndepositional normal faults (Kennedy et al., 2018; Twite et al., 2019) and provided the bulk of the sediment during deposition of the Dipeta and Mwashya subgroups as indicated from their detrital zircon age distributions.

The significant ~1.38-1.37 Ga Mesoproterozoic population and the similarity of the detrital zircon age spectra of the Dipeta and Mwashya subgroups to the detrital zircon age spectra of the Nzilo Group supports this interpretation. The predominant clast population in the conglomerate-dominated facies of the Mwashya Subgroup is quartzite of the Kibaran Supergroup exposed in the Nzilo block, which further supports the local provenance of the Dipeta and Mwashya subgroups (Kennedy et al., 2018).

The syn-rift, syn-glacial ‘grand conglomérat’ has detrital zircon age distributions that suggest both local and regional provenance. The basal and middle diamictite share the ubiquitous mid-Paleoproterozoic population that is present in the pre-glacial units, but lacks the significant Mesoproterozoic population that is present in the Dipeta and Mwashya subgroups and the upper diamictite. The appearance of the Neoarchean to early Paleoproterozoic population in the basal and middle diamictite, which was not present in the Nzilo Group or in the underlying Dipeta and Mwashya subgroups, indicates that the basal and middle diamictite do not share the same provenance as the other Dipeta and Mwashya subgroups or the upper diamictite. The Dipeta and Mwashya subgroups are interpreted to have been locally derived, and therefore the differences in their detrital zircon age distributions as compared to those of the basal and middle diamictite suggests that the latter units had a broader provenance and source areas that did not supply sediment during deposition of the underlying units.

The lower KPS has the ubiquitous mid-Paleoproterozoic populations, lacks the Neoarchean to early Paleoproterozoic population; it contains the typical Kibaran Mesoproterozoic population ~1380 Ma but also has a Mesoproterozoic population ~1100 Ma that is not present in other strata of the 'grand conglomérat' or in the underlying units. Although there is no obvious source for this ~1000 Ma population from known geochronology of Kibaran igneous rocks, it is probable that Mesoproterozoic intrusions in the Kamoa area that have not yet been dated could be the ~1100-1000 Ma source of this population. The presence of the Mesoproterozoic population ~1100 Ma indicates that the provenance consists of a slightly different combination of sources compared to that of the Dipeta and Mwashya subgroups and that of the diamictite of the 'grand conglomérat', and thus that it too may have had a broader provenance.

The upper diamictite records the most significant change in the detrital zircon age distributions of the 'grand conglomérat' at Kamoa, because it has a dominant Mesoproterozoic population and only a subordinate mid-Paleoproterozoic population. The latter detrital zircon population dominates all other units in this study and is dominant in almost all other strata of the Katanga Supergroup. The significant increase in the Mesoproterozoic population, compared to the other units of the 'grand conglomérat' and compared to the Nzilo Group from Kokonyangi et al. (2007), along with the decrease in the mid-Paleoproterozoic population compared to all other units in this study, indicates that primary sources of Mesoproterozoic grains ~1370 Ma, such as the Mesoproterozoic intrusive rocks of unknown age ~60 km west of Kamoa and ~100 km north that were probably associated with the Kibaran magmatic event became a more important source of detritus contributing to the sediment supply at Kamoa during deposition of the upper diamictite. The increase in the Mesoproterozoic population and the lack of the Neoarchean to early Paleoproterozoic population suggests that the upper diamictite had a local provenance

compared to the other units of the ‘grand conglomérat’, and that most of the sediment supply at Kamoa during deposition of the upper diamictite was derived from local Mesoproterozoic intrusives located within ~100 km of Kamoa. The decrease in the mid-Paleoproterozoic population is probably because the dominant source areas of mid-Paleoproterozoic grains (i.e., LMC) were not exposed in the later stages of the rifting in the Katangan basin due to sedimentary cover by older Katangan strata. Another possible explanation is that the proportion of Mesoproterozoic intrusive detritus compared to recycled detritus from Kibaran metasedimentary rocks and sedimentary rocks of the Roan Group was significantly increased, producing the dominant Mesoproterozoic population and the subordinate mid-Paleoproterozoic population. In any case, the detrital zircon age distributions of the diamictite at Kamoa indicate that they were not simply derived from underlying stratigraphic units, because of the differences in provenance between the basal and middle diamictite, and between the upper diamictite and the lower KPS (Fig. 28).

Another possible explanation for temporal fluctuations in the provenance of the ‘grand conglomérat’ would be the progressive unroofing of previously unexposed source areas that then contributed to the sediment supply at Kamoa. This could be a possible explanation for the increase in the Mesoproterozoic population of the upper diamictite: Kibaran intrusive rocks could have been exposed comparatively late, along fault scarps through progressive rifting, and then eroded to provide sediment to the Kamoa sub-basin late in the accumulation of the diamictite succession, with an increased proportion of the material coming from the newly exposed Kibaran intrusive rocks. Glaciation would then not necessarily be required to explain provenance variation in the ‘grand conglomérat’. This alternative interpretation, however, cannot explain the presence of the Neoarchean to early Paleoproterozoic population derived from the

distal Kasai block. Fluvial or glaciofluvial processes might possibly explain the presence of the distally derived population and the temporal fluctuations, but because the margins of the Katangan basin were topographically uplifted during rifting, because of thermal doming, physically there would be no way for a fluvial system to deliver sediment to the Kamoa sub-basin across the uplifted rift margin.

7.2 Detrital zircon geochronology of comparable Cryogenian units

In rift basins from other 'Sturtian' sedimentary successions it is known that the provenance of sedimentary units reflects locally exposed basement rocks in the basin that were exposed due to extensional normal faults (Figueiredo et al., 2016). The sediment supply of mid-Neoproterozoic rift basins that have 'Sturtian' diamictite was also shown to be controlled by what was locally exposed, not due to faulting but from selective erosion of glaciers or glacio-fluvial streams (Figueiredo et al., 2009). Previous studies of mid-Neoproterozoic diamictite in Brazil concluded that the majority of the sediment in their respective basins was derived from local sources; however, there are detrital zircon populations that are enigmatic and probably sourced from distal source area(s), possibly as far away as ~1500 km or from unknown sources not on the São Francisco craton (Babinski et al., 2012; Babinski et al., 2013; Kuchenbecker et al., 2015).

Similar studies done in Namibia have come to similar conclusions. A study of four different diamictite units from Namibia found that, although the provenance of the glacially influenced strata was predominantly local, it was not exclusively local because of the lack of a distinctive population whose source area was close to the depositional area (Hofmann et al., 2015).

A detrital zircon study of glacially influenced diamictite from five different stratigraphic sections of the Cryogenian Perry Canyon Formation (Utah, USA) identified vertical and lateral changes

in their detrital zircon age distributions. During initial rifting, local sources provided the bulk of detritus to pre-glacial sandstone units, but during subsidence and deposition of pre-glacial mudstone units a change to distal source areas appeared. This was followed by volcanism and deposition of syn-glacial diamictite that identified that local sources once again became the dominant sediment supply. Detrital zircon of the lower diamictite unit yielded some young ages of 703±6 Ma and 667±5 Ma (U-Pb SHRIMP; Balgord et al., 2013)

A study of ‘Sturtian’ diamictite from Ethiopia identified detrital zircon populations that were derived from underlying volcanic and metasedimentary rocks. The detrital zircon data combined with analysis of clast populations in the diamictite may indicate proximal provenance from basement source areas underlying the diamictite (Avigad et al., 2007).

A study of ‘Sturtian’ diamictite from the Bolla Bollana Formation (South Australia) showed that detrital zircon age distributions from diamictite identified local provenance from nearby basement source areas and from recycling of paragneisses (Cox et al., 2018). The authors identified zircon from a tuff bed in the upper Wilyerpa Formation, another glacial diamictite unit associated with the ‘Sturtian’, placing the termination of the ‘Sturtian’ glaciation ~663±0.76 Ma (CA-ID-TIMS; Cox et al., 2018).

Previous studies of the provenance of ‘Sturtian’ diamictite from basins in various continents have confirmed that, due to rift dynamics, sediment provenance is overwhelmingly local, but that intraformational variability resulted from differential glacial erosion and also possibly from unknown distal extrabasinal source areas. Changes in provenance of the ‘grand conglomérat’ could be explained by similar conditions, in which syndepositional extensional normal faults exposed and exhumed basement rocks that had been previously under sedimentary cover.

In the case of the Kamoa sub-basin, there is no known basement of Neoarchean to early Paleoproterozoic age (~2700-2400 Ma) in the area. Processes other than rift development contributed to a changing sediment supply in the Kamoa sub-basin. Glacial or related glaciogenic processes may be the cause of variations in provenance at Kamoa, providing detritus not only from nearby source areas but also probably at least slightly more distal source areas.

The current understanding of sediment dynamics at Kamoa is that the ‘grand conglomérat’ was locally derived from recycling and mixing of sediment from underlying units, which is based primarily on sedimentology and the predominant clast-type of the diamictite (Kennedy et al., 2018); this interpretation is challenged by the detrital zircon data produced in the present study. Changes in the proportions of detrital zircon age populations (e.g., Mesoproterozoic vs. mid-Paleoproterozoic) indicate that individual diamictite units at Kamoa had variable provenance, and that their provenance differed from that of the underlying Dipeta and Mwashya subgroups. The detrital zircon age populations of the pre-glacial and syn-glacial strata would be identical if the latter had been derived solely through local recycling, but this is not the case. Therefore, the sediment supply of the ‘grand conglomérat’ was not simply a matter of local provenance from recycling of underlying units; various source areas contributed detritus variably during deposition of the ‘grand conglomérat’. The main depositional influence in the Kamoa sub-basin was tectonically driven syndepositional faulting, but sediment supply was also influenced by glacial activity or other processes in order to account for variable proportions of locally and distally sourced material. Not all of the units in the ‘grand conglomérat’ have detrital zircon age distributions suggesting a broader, more distal provenance (i.e., upper diamictite), but the temporal variability in its general provenance suggests that during the evolution of the Kamoa

sub-basin, processes other than resedimentation from rift shoulders, possibly including glaciation, influenced the sediment supply of the basin.

7.3 Mid-Neoproterozoic detrital zircon geochronology on the timing and dynamics of 'Sturtian' glaciation

The mid-Neoproterozoic 'Sturtian' glaciation is the oldest of the postulated Neoproterozoic 'snowball Earth' glaciations. The 'snowball Earth' hypothesis postulates that the 'Sturtian' glaciation was a globally synchronous event in which the entire surface of Earth was covered in ice sheets (Kirschvink, 1992; Hoffman et al., 1998; Schrag et al., 2002). Alternative theories, such as the 'zipper-rift' theory, postulate that 'Sturtian' glaciations were instead a series of regional glaciations that developed diachronously along the uplifted rift-shoulders of Rodinia during its protracted break-up (Eyles and Januszczak, 2004; Allen and Etienne, 2008). An important test for the 'snowball Earth' theory is the timing of 'Sturtian' glacial deposits from basins throughout the world.

In the CACB, the previous age constraints on deposition of the 'grand conglomérat' were between 765±5 and 735±5 Ma (Key et al., 2001). The ages that Key et al. (2001) produced from volcanic rocks in the underlying Mwashya Subgroup and overlying Kakontwe Formation may not be reliable, because (a) the stratigraphic position of the volcanic rocks intercalated in the Mwashya Subgroup is poorly constrained, and (b) the "volcanic centres" dated in the Kakontwe Formation are poorly geologically constrained, with no stratigraphic position and inadequate defence of their volcanic origin (could be intrusive).

In the present study, the ages of two mid-Neoproterozoic grains from the lower KPS (715±16 and 686±25 Ma) conflict with previous age constraints for the 'grand conglomérat' suggesting

that its maximum possible depositional age may be millions of years younger than previously assumed. Geochronological data from other ‘Sturtian’ correlatives in Africa that conflict with the previous age constraints include 694±4 Ma from the lower diamictite formation, West Congo belt (Straathof, 2011), and 727.3±4.9 for the Mwashya Subgroup (Rooney et al., 2015). The <765±5 Ma age (Key et al., 2001) from felsic volcanic rocks intercalated in the Mwashya Subgroup and the 727.3±4.9 Ma age of black shale in the Mwashya Subgroup (Rooney et al., 2015) highlight an age discrepancy of at least 36 m.y. The detrital zircon with a maximum depositional age of 686±25 Ma from the lower KPS in the ‘grand conglomérat’ compared to the maximum depositional age of 765±5 Ma is a discrepancy up to 49 m.y. (factoring in the large error bars of the former age). These examples of the discrepancy in the maximum depositional ages of the ‘grand conglomérat’ from geographically close areas in Africa (within a few 100 kms) suggest that the onset of the mid-Neoproterozoic glaciation may have been diachronous (Fig. 29).

The depositional age of mid-Neoproterozoic (‘Sturtian’) diamictite around the world suggests that glaciations may have been diachronous. The following geochronological data are from glacial deposits associated with the ‘Sturtian’ diamictite from around the globe (Fig. 30). The minimum depositional age of ‘Sturtian’ diamictite in central Australia is constrained to 657±5 Ma (Re-Os black shale; (Kendall et al., 2006) from the basal Aralka Formation directly overlying diamictite of the Areyonga Formation. In southern Australia, the minimum depositional age is 643±2.4 Ma (Re-Os black shale; Kendall et al., 2006) from the basal Tapley Hill Formation, overlying the Sturtian Formation (type locality of ‘Sturtian’ diamictite). The discrepancy between the minimum depositional ages of the ‘Sturtian’ glacial diamictite from central and southern Australia could be up to 20 m.y.

Geochronological data from ‘Sturtian’ diamictite in northwestern Canada also suggest diachroneity of the ‘Sturtian’ glaciation. A 711±0.24 Ma maximum depositional age from a detrital zircon in the Rapitan Formation, Northwest Territories, Canada (U-Pb zircon ID-TIMS; Baldwin et al., 2016) and a 717±0.14 Ma age from a tuff in the Mount Harper Group, Yukon, (U-Pb zircon ID-TIMS; Macdonald et al., 2010), suggests that there could be up to 6 m.y. discrepancy in the onset of the ‘Sturtian’ glaciation in northwestern Canada.

Geochronological data from ‘Sturtian’ glacial deposits in southern Idaho, U.S.A., include a detrital zircon from the South Mountain Member of the Pocatello Formation of 709±5 Ma (U-Pb zircon SHRIMP; Fanning and Link, 2004) and a maximum depositional age of a cap-carbonate directly above the South Mountain Member from a reworked tuff has an age of 667±5 Ma (U-Pb zircon SHRIMP; Fanning and Link, 2004). The correlative Edwardsburg Formation in central Idaho, USA. from rhyolite flows intercalated near the top and bottom of the diamictite provides ages of 685±7 Ma and 684±4 Ma, respectively (U-Pb zircon SHRIMP; Lund et al., 2003). The discrepancy between the maximum depositional ages of the Pocatello Formation and the Edwardsburg Formation is at least 24 m.y. and the discrepancy in the minimum depositional ages is at least 17 m.y.

There are several different geochronological constraints on ‘Sturtian’ diamictite in China, which includes a minimum depositional age of 663±4 Ma (U-Pb TIMS of grain fractions; Zhou et al., 2004) from the lower Datangpo Formation, which overlies ‘Sturtian’ diamictite of the Gucheng Formation and a maximum depositional age of 715.9±2.8 Ma age from a tuffaceous siltstone bed in the Jiangkou Formation (U-Pb zircon SIMS; Lan et al., 2014).

Geochronological data from ‘Sturtian’ glacial deposits in Oman provide an age of 711±8 Ma for the Ghubrah diamictite of the Huqf Supergroup from a tuffaceous bed intercalated in the diamictite (Leather et al., 2002). Another age for the Ghubrah diamictite in Oman from the base of the diamictite is 713.7±0.5 Ma (detrital ID-TIMS zircon; Bowring et al., 2007). A dacite sill intercalated at the base of the ‘Sturtian’ Chuos Formation, Namibia, provides an age of 757±5 Ma (U-Pb zircon SHRIMP; Nascimento et al., 2016). Detrital zircon from the ‘Sturtian’ Puga Formation, Brazil, provides an age of 706±9 Ma (U-Pb zircon SHRIMP; Babinski et al., 2013).

The geochronology from ‘Sturtian’ deposits from across the globe highlights various different maximum and minimum depositional ages for ‘Sturtian’ diamictite and demonstrates variable timing for the ‘Sturtian’ glaciation. An unavoidable caveat of the argument for or against a synchronous ‘snowball Earth’ glaciation is that depending on which ages one decides to present there can be very different outcomes in regard to the timing of the ‘Sturtian’ glaciation, with geochronology from different sources being used to argue for and against the diachroneity of the ‘Sturtian’ glaciation. Excellent resources with summaries of the various ages of ‘Sturtian’ and ‘Marinoan’ diamictite include Allen and Etienne (2008) and Rooney et al. (2015). Further geochronology and detailed stratigraphy must be done on ‘Sturtian’ glacial deposits from other basins in order to determine the extent and timing of the ‘Sturtian’ glaciation, and one must be prudent when presenting and interpreting geochronological data and the stratigraphic context of the material dated [e2]

7.4 Exploration Implications

The Katanga region of southern DRC, where Kamoa is located, has very little exposure and thus exploration drilling is done with little knowledge of which stratigraphic unit of the ‘grand

conglomérat' is being intersected. The ore-bearing basal diamictite of the 'grand conglomérat' is of great economic interest because it hosts the mineralisation at the Kamoa deposit. Now that baseline detrital zircon spectra for the 'grand conglomérat' have been established, it may be possible to correlate the stratigraphy of the 'grand conglomérat' elsewhere in the Kamoa area and possibly elsewhere in the Katangan basin. More work is required to test the lateral variations (if any) in the detrital zircon spectra threough the diamictite in the Kamoa sub-basin. Given that the 'grand conglomérat' has no simple way of diagnosing its stratigraphic subdivisions, the ability to correlate based on detrital zircon spectra could assist exploration targetting of the ore-bearing diamictite in new areas where the geology is poorly known.

7.5 Further Work

A summary of future work that should be done:

-Increase the number of concordant analyses of samples that were studied for this project in order to be statistically adequate (i.e., minimum 117 concordant analyses in each sample).

-Collect units of the stratigraphy at Kamoa that were not initially sampled (e.g., uppermost diamictite Ng 1.1.6, upper KPS).

-Collect diamictite samples from the same stratigraphic units but from different drill-holes geographically distant from drill-holes sampled in this study to test lateral variations in the detrital zircon spectra. This will also test whether the stratigraphic units in the western foreland, and particularly in the 'grand conglomérat', can be correlated using detrital zircon geochronology.

-Duplicate samples of previously sampled units from the same drill-holes and close to the same sampled interval in order to test the reproducibility of the results and to see if there are significant differences from sample to sample within the same stratigraphic unit.

-Sampling from several stratigraphic intervals of the same diamictite unit especially if it is particularly thick and if intervals of the diamictite are separated by siltstone interbeds. Sampling of the siltstone units.

-Sampling of basement units locally exposed in the Nzilo promontory, including Kibaran metasedimentary rocks and Kibaran intrusive rocks, to represent the basement geochronology of the area better and thereby improve interpretation of provenance.

-Increase the number of mid-Neoproterozoic grains analysed from the lower KPS in order to have a statistically valid number of grains for a maximum depositional age. Also, analysing the mid-Neoproterozoic grains using a more accurate analytical instrument that yields smaller uncertainties (e.g., using SHRIMP or TIMS instead of LA-ICP-MS).

-Using U/Th ratios in order to classify grains into distinct groups to see if that could assist in provenance interpretation. Also, using other geochemical indicators from the zircon for better provenance interpretation (e.g., REE, Lu-Hf).

-Using different methods of displaying data and for ensuring statistical validity of the data (e.g., using a kernel density estimation instead of the probability density distribution; using a K-S test to check for reasonable data).

8.0 Conclusions

Detrital zircon geochronology (U-Pb LA-ICP-MS) of the pre-glacial Dipeta and Mwashya subgroups at Kamoa, DRC, indicates that the main source of sediment during their deposition was recycling from locally exposed basement of the Mesoproterozoic Kibaran Supergroup, which is dominated by mid-Paleoproterozoic zircon with minor Mesoproterozoic zircon, together with Mesoproterozoic zircon directly sourced from intrusive bodies that cross-cut the Kibaran Supergroup in the Kamoa area. The provenance of the syn-glacial, up to 1800-m-thick 'grand conglomérat' indicates that there were variations in sediment supply at Kamoa during its deposition. At least seven source types are identified: (1) Kibaran metasedimentary rocks containing reworked zircon having a major peak ca. 1.86 Ga, a minor peak ca. 1.4-1.38 Ga, and small amounts of Neoarchean and Mesoarchean grains; (2) Mesoproterozoic ca. 1.38-1.37 Ga intrusives that cross-cut metasedimentary rocks of the Kibaran Supergroup; (3) Reworked Roan Group sediment [derived from (1) and (2)]; (4) Intrusive post-tectonic granitoids in the Kibaran belt ca. 1.1-1.0 Ga of unknown nature and location; (5) the Neoarchean to early Paleoproterozoic Kasai block, which is responsible for grains ca. 2.4-2.6 Ga; (6) Neoproterozoic granite ca.0.9 Ga [negligible; one unit only (Dipeta)]; (7) Neoproterozoic mafic extrusive rocks (well known in Kamoa area).

The nearby Archean Kasai block is represented by a subordinate peak in the basal and middle diamictite in the detrital zircon spectrum of the 'grand conglomérat'; together with the identities of the seven source types, this points to uniquely local but temporally fluctuating source areas and minor distal input. These provenance data suggest that during the 'Sturtian' glaciation, even though the predominant control on the deposition of the clastic units at Kamoa was rift-related syndepositional faulting, sediment supply at Kamoa was also influenced to at least some extent by glacial activity.

The maximum possible depositional age of 686±25 Ma of the ‘grand conglomérat’ at Kamoa indicates that it is probably younger than was previously thought, conflicting with previous age constraints (765±5-735±5 Ma; Key et al., 2001). The new maximum depositional age also clarifies the timing of the second episode of rifting in the Katangan basin. The depositional age of the ‘grand conglomérat’ also questions the timing of the ‘Sturtian’ glaciation. Discrepancies of the maximum depositional age of the ‘grand conglomérat’ and to its putative ‘Sturtian’ equivalents in Namibia (i.e., Chuos Fm.) and in the West Congo (i.e., lower Diamictite fm.) and compared to elsewhere in the world suggest that the ‘Sturtian’ glaciation may have developed diachronously, as discrete events along rift-margins of Rodinia. Further work on the provenance of the ‘grand conglomérat’ in the Katangan basin, as well as ‘Sturtian’ glacial deposits from other basins elsewhere in the world, needs to be done to test if other examples of ‘Sturtian’ diamictite have local or regional provenance. More detailed geochronology and stratigraphic studies of ‘Sturtian’ diamictites should be done as well, to constrain more precisely the timing of the ‘Sturtian’ glaciation.

References Cited

Allen, P.A., Etienne, J.L., 2008. Sedimentary challenge to Snowball Earth. Nat. Geosci. 1, 817–825. https://doi.org/10.1038/ngeo355

Armstrong, R.A., Master, S., Robb, L.J., 2005. Geochronology of the Nchanga Granite, and constraints on the maximum age of the Katanga Supergroup, Zambian Copperbelt. J. African Earth Sci. 42, 32–40. https://doi.org/10.1016/j.jafrearsci.2005.08.012

Avigad, D., Stern, R.J., Beyth, M., Miller, N., McWilliams, M., 2007. Detrital zircon U-Pb geochronology of Cryogenian diamictites and Lower Paleozoic sandstone in Ethiopia (Tigrai): age constraints on Neoproterozoic glaciation and crustal evolution of the southern Arabian-Nubian Shield. Precambiran Res. 154, 88–106. https://doi.org/10.1016/j.precamres.2006.12.004

Babinski, M., Boggiani, P.C., Trindade, R.I.F., Fanning, C.M., 2013. Detrital zircon ages and geochronological constraints on the Neoproterozoic Puga diamictites and associated BIFs in

the southern Paraguay Belt , Brazil. Gondwana Res. 23, 988–997. https://doi.org/10.1016/j.gr.2012.06.011

Babinski, M., Pedrosa-soares, A.C., Trindade, R.I.F., Martins, M., Noce, C.M., Liu, D., 2012. Neoproterozoic glacial deposits from the Araçuaí orogen, Brazil: Age, provenance and correlations with the São Francisco craton and West Congo belt. Gondwana Res. 21, 451–465. https://doi.org/10.1016/j.gr.2011.04.008

Baldwin, G.J., Turner, E.C., Kamber, B.S., 2016. Tectonic controls on distribution and stratigraphy of the Cryogenian Rapitan iron formation, northwestern Canada. Precambrian Res. 278, 303–322. https://doi.org/10.1016/j.precamres.2016.03.014

Balgord, E.A., Yonkee, W.A., Link, P.K., Fanning, C.M., 2013. Stratigraphic, geochronologic, and geochemical record of the Cryogenian Perry Canyon Formation, northern Utah: Implications for Rodinia rifting and snowball Earth glaciation. GSA Bull. 125, 1442–1467. https://doi.org/10.1130/B30860.1

Barron, J., Broughton, D., Armstrong, R.A., Hitzman, M., 2003. Petrology, geochemistry and age of gabbroic bodies in the Solwezi area, northwestern Zambia, in: Proterozoic Sediment-Hosted Base Metal Deposits of Western Godwana, Contributions Presented at the 3rd IGCP-450 Conference and Guide Book of the Field Workshop, Lubumbashi. pp. 75–77.

Batumike, J.M., Griffin, W.L., O'Reilly, S.Y., Belousova, E.A., Pawlitschek, M., 2009. Crustal evolution in the central Congo-Kasai Craton, Luebo, D.R. Congo: Insights from zircon U-Pb ages, Hf-isotope and trace-element data. Precambrian Res. 170, 107–115. https://doi.org/10.1016/j.precamres.2008.12.001

Batumike, M.J., Cailteux, J.L.H., Kampunzu, A.B., 2007. Lithostratigraphy, basin development, base metal deposits, and regional correlations of the Neoproterozoic Nguba and Kundelungu rock successions, central African Copperbelt. Gondwana Res. 11, 432–447. https://doi.org/10.1016/j.gr.2006.04.012

Batumike, M.J., Kampunzu, A.B., Cailteux, J.H., 2006. Petrology and geochemistry of the Neoproterozoic Nguba and Kundelungu Groups, Katangan Supergroup, southeast Congo: Implications for provenance, paleoweathering and geotectonic setting. J. African Earth Sci. 44, 97–115. https://doi.org/10.1016/j.jafrearsci.2005.11.007

Boniface, N., Appel, P., 2018. Neoproterozoic reworking of the Ubendian Belt crust: Implication for an orogenic cycle between the Tanzania Craton and Bangweulu Block during the assembly of Gondwana. Precambrian Res. 305, 358–385. https://doi.org/10.1016/j.precamres.2017.12.011

Boniface, N., Schenk, V., Appel, P., 2014. Mesoproterozoic high-grade metamorphism in pelitic rocks of the northwestern Ubendian Belt: Implication for the extension of the Kibaran intra-continental basins to Tanzania. Precambrian Res. 249, 215–228. https://doi.org/10.1016/j.precamres.2014.05.010

Boniface, N., Schenk, V., Appel, P., 2012. Paleoproterozoic eclogites of MORB-type chemistry

and three Proterozoic orogenic cycles in the Ubendian Belt (Tanzania): Evidence from monazite and zircon geochronology, and geochemistry. Precambrian Res. 192–195, 16–33. https://doi.org/10.1016/j.precamres.2011.10.007

Bowring, S.A., Grotzinger, J.P., Condon, D.J., Ramezani, J., Newall, M.J., Allen, P.A., 2007. Geochronologic constraints on the chronostratigraphic framework of the neoproterozoic Huqf Supergroup, Sultanate of Oman. Am. J. Sci. 307, 1097–1145. https://doi.org/10.2475/10.2007.01

Broughton, D., Rogers, T., 2010. Discovery of the Kamoa Copper Deposit, Central African Copperbelt, D.R.C. Soc. Econ. Geol. Spec. Publ. 15 1, 287–297.

Budyko, M., 1940. The effect of solar radiation variations on the climate of the Earth. Ecology 21, 438–450. https://doi.org/10.3402/tellusa.v21i5.10109

Bull, S., Selley, D., Broughton, D., Hitzman, M., Cailteux, J., Large, R., McGoldrick, P., 2011. Sequence and carbon isotopic stratigraphy of the Neoproterozoic Roan Group strata of the Zambian copperbelt. Precambrian Res. 190, 70–89. https://doi.org/10.1016/j.precamres.2011.07.021

Cabri, L.J., Rudashevsky, N.S., Rudashevsky, V.N., Oberthür, T., 2008. Electric-Pulse Disaggregation (Epd), Hydroseparation (Hs) and Their Use in Combination for Mineral Processing and Advance Characterization of Ores, in: 40th Annual Meeting of the Canadian Mineral Processors. pp. 211–235.

Cailteux, J.L.H., 1994. Lithostratigraphy of the Neoproterozoic Shaba-type (Zaire) Roan Supergroup and metallogenesis of associated stratiform mineralization. J. African Earth Sci. 19, 279–301.

Cailteux, J.L.H., De Putter, T., 2018. The Neoproterozoic Katanga Supergroup (D. R. Congo): State-of-the-art and revisions of the lithostratigraphy, sedimentary basin and geodynamic evolution. J. African Earth Sci. 0–1. https://doi.org/10.1016/j.jafrearsci.2018.07.020

Cailteux, J.L.H., Kampunzu, A.B., Lerouge, C., 2007. The Neoproterozoic Mwashya-Kansuki sedimentary rock succession in the central African Copperbelt, its Cu-Co mineralisation, and regional correlations. Gondwana Res. 11, 414–431. https://doi.org/10.1016/j.gr.2006.04.016

Collins, A.S., Reddy, S.M., Buchan, C., Mruma, A., 2004. Temporal constraints on Palaeoproterozoic eclogite formation and exhumation (Usagaran Orogen, Tanzania). Earth Planet. Sci. Lett. 224, 175–192. https://doi.org/10.1016/j.epsl.2004.04.027

Cox, G.M., Isakson, V., Ho, P.F., Gernon, T.M., Schmitz, M.D., Shahin, S., Collins, A.S., Preiss, W., Blades, M.L., Mitchell, R.N., Nordsvan, A., 2018. South Australian U-Pb zircon (CA-ID-TIMS) age supports globally synchronous Sturtian deglaciation. Precambrian Res. 315, 257–263. https://doi.org/10.1016/j.precamres.2018.07.007

De Waele, B., 2005. The Proterozoic geological history of the Irumide belt, Zambia. PhD Thesis.

Curtin University of Technology, Perth, 468 pp.

De Waele, B., Fitzsimons, I.C.W., 2007. The nature and timing of Palaeoproterozoic sedimentation at the southeastern margin of the Congo Craton; zircon U-Pb geochronology of plutonic, volcanic and clastic units in northern Zambia. Precambrian Res. 159, 95–116. https://doi.org/10.1016/j.precamres.2007.06.004

De Waele, B., Fitzsimons, I.C.W., Wingate, M.T.D., Mapani, B.S.E., 2003. Untying the Kibaran knot: A reassessment of Mesoproterozoic correlations in southern Africa based on SHRIMP U-Pb data from the Irumide belt. Geol. Soc. Am. 31, 509–512. https://doi.org/10.1016/j.precamres.2008.12.001

De Waele, B, Kampunzu, A.B., Mapani, B.S.E., Tembo, F., 2006a. The Mesoproterozoic Irumide belt of Zambia. J. African Earth Sci. 46, 36–70. https://doi.org/10.1016/j.jafrearsci.2006.01.018

De Waele, Bert, Liégeois, J., Nemchin, A.A., Tembo, F., 2006b. Isotopic and geochemical evidence of proterozoic episodic crustal reworking within the irumide belt of south-central Africa , the southern metacratonic boundary of an Archaean Bangweulu Craton. Precambrian Res. 148, 225–256. https://doi.org/10.1016/j.precamres.2006.05.006

De Waele, B., Johnson, S.P., Pisarevsky, S.A., 2008. Palaeoproterozoic to Neoproterozoic growth and evolution of the eastern Congo Craton: Its role in the Rodinia puzzle. Precambrian Res. 160, 127–141. https://doi.org/10.1016/j.precamres.2007.04.020

De Waele, B., Fitzsimons, I.C.W., Wingate, M.T.D., Tembo, F., Mapani, B., Belousova, E.A., 2009. The geochronological framework of the irumide belt: A prolonged crustal history along the margin of the Bangweulu Craton. Am. J. Sci. 309, 132–187. https://doi.org/10.2475/02.2009.03

Debruyne, D., Wilderode, J. Van, Balcaen, L., Vanhaecke, F., Muchez, P., 2014. Geochemistry and isotopic evolution of the central African Domes, Bangweulu and Irumide regions: Evidence for cryptic Archean sources and a Paleoproterozoic continental arc. J. African Earth Sci. 100, 145–163. https://doi.org/10.1016/j.jafrearsci.2014.06.013

Dodson, M.H., Compston W., Williams, I.S., Wilson, J.F., (1988) A search for ancient detrital zircons in Zimbabwean sediments. J Geol Soc London 145, 977-983.

Edwin, G., Daniel, K., Urs, E., 2006. Electrodynamic disaggregation of geologic material, in: 4th Swiss Geoscience Meeting. pp. 3–5.

Eyles, N., Januszczak, N., 2004. “Zipper-rift”: A tectonic model for Neoproterozoic glaciations during the breakup of Rodinia after 750 Ma. Earth-Science Rev. 65, 1–73. https://doi.org/10.1016/S0012-8252(03)00080-1

Fairchild, I.J., Kennedy, M.J., 2007. Neoproterozoic glaciation in the Earth System. J. Geol. Soc. London. 164, 895–921. https://doi.org/10.1144/0016-76492006-191

Fanning, C.M., Link, P.K., 2004. U-Pb SHRIMP ages of Neoproterozoic (Sturtian) glaciogenic Pocatello Formation, southeastern Idaho. Geology 32, 881–884. https://doi.org/10.1130/G20609.1

Fedo, C.M., Sircombe, K.N., Rainbird, R.H., 2003. Detrital zircon analysis of the sedimentary record. Rev. Mineral.53, 277–303. https://doi.org/10.2113/0530277

Gehrels, G.E., 2012. Detrital zircon U-Pb geochronology: current methods and new opportunities, in: Tectonics of Sedimentary Basins: Recent Advances. pp. 47–62. Edited by Cathy Busby and Antonio Azor. Published by Blackwell Publishing Ltd.

Gilchrist, G., 2019. Ivanhoe Mines Ltd. Press Release.https://ivanhoemines.com/projects/kamoa-kakula-project/

Godderis, Y., Nedelec, A., Meert, J.G., 2004. A " Snowball Earth " climate triggered by continental break-up through changes in runoff by continental break-up through. https://doi.org/10.1038/nature02408

Halpin, J.A., Selley, D., 2010. Insights to geometry and structural evolution of the Central African Copperbelt from zircon provenance analysis Zambia 33–48.

Hanson, R.E., 2003. Proterozoic geochronology and tectonic evolution of southern Africa. Geol. Soc. London, Spec. Publ. 206, 427–463. https://doi.org/10.1144/GSL.SP.2003.206.01.20

Hitzman, M.W., Broughton, D., Selley, D., Woodhead, J., Wood, D., Bull, S., 2012. The Central African Copperbelt: Diverse Stratigraphic, Structural, and Temporal Settings in the World's Largest Sedimentary Copper District. Soc. Econ. Geol. Spec. Publ. 16, 487–514.

Hoffman, P.F., Kaufman, A.J., Halverson, G.P., Schrag, D.P., 1998. A Neoproterozoic Snowball Earth. Science (80). 281, 1342–1346.

Hoffman, P.F., Schrag, D.P., 2002. Review article The snowball Earth hypothesis: testing the limits of global change. Terra 14, 129–155. https://doi.org/10.1080/713604466

Hoffmann, K.H., Condon, D.J., Bowring, S.A., Crowley, J.L., 2004. U-Pb zircon date from the Neoproterozoic Ghaub Formation , Namibia : Constraints on Marinoan glaciation. Geol. Soc. Am. 32, 817–820. https://doi.org/10.1130/G20519.1

Hofmann, M., Linnemann, U., Hoffmann, K., Germs, G., Gerdes, A., Marko, L., Eckelmann, K., Gärtner, A., Krause, R., 2015. The four Neoproterozoic glaciations of southern Namibia and their detrital zircon record: The fingerprints of four crustal growth events during two supercontinent cycles. Precambrian Res. 259, 176–188. https://doi.org/10.1016/j.precamres.2014.07.021

Hyde, W.T., Crowley, T.J., Baum, S.K., Peltier, W.R., 2000. Neoproterozoic "snowball Earth" simulations with a coupled climate/ice-sheet model. Nature 405, 425–429. https://doi.org/10.1038/35013005

Jackson, M.P.A., Warin, O.N., Woad, G.M., Hudec, M.R., 2003. Neoproterozoic allochthonous salt tectonics during the Lufilian orogeny in the Katangan Copperbelt, central Africa. Bull. Geol. Soc. Am. 115, 314–330. https://doi.org/10.1130/0016-7606(2003)115<0314:NASTDT>2.0.CO;2

Kampunzu, A.B., Tembo, F., Matheis, G., Kapenda, D., Huntsman-Mapila, P., 2000. Geochemistry and Tectonic Setting of Mafic Igneous Units in the Neoproterozoic Katangan Basin, Central Africa: Implications for Rodinia Break-up. Gondwana Res. 3, 125–153.

Kazimoto, E.O., Schenk, V., Berndt, J., 2014. Neoarchean and Paleoproterozoic crust formation in the Ubendian Belt of Tanzania: Insights from zircon geochronology and geochemistry. Precambrian Res. 252, 119–144. https://doi.org/10.1016/j.precamres.2014.06.020

Kendall, B., Creaser, R.A., Selby, D., 2006. Re-Os geochronology of postglacial black shales in Australia: Constraints on the timing of “Sturtian” glaciation. Geology 34, 729–732. https://doi.org/10.1130/G22775.1

Kennedy, K., Eyles, N., Broughton, D., 2018. Basinal setting and origin of thick (1.8 km) mass-flow dominated Grand Conglomérat diamictites, Kamoa, Democratic Republic of Congo: Resolving climate and tectonic controls during Neoproterozoic glaciations. Sedimentology. https://doi.org/10.1111/sed.12494

Key, R.M., Liyungu, a. K., Njamu, F.M., Somwe, V., Banda, J., Mosley, P.N., Armstrong, R. A., 2001. The western arm of the Lufilian Arc in NW Zambia and its potential for copper mineralization. J. African Earth Sci. 33, 503–528. https://doi.org/10.1016/S0899-5362(01)00098-7

Kirschvink, J.L., 1992. Late Proterozoic low-latitude global glaciation: the snowball Earth. Proterozoic Biosph. 52, 51–52.

Kokonyangi, J., Armstrong, R., Kampunzu, A.B., Yoshida, M., Okudaira, T., 2004. U-Pb zircon geochronology and petrology of granitoids from Mitwaba (Katanga, Congo): Implications for the evolution of the Mesoproterozoic Kibaran belt. Precambrian Res. 132, 79–106. https://doi.org/10.1016/j.precamres.2004.02.007

Kokonyangi, J.W., Kampunzu, A.B., Armstrong, R., Yoshida, M., Okudaira, T., Arima, M., Ngulube, D.A., 2006. The Mesoproterozoic Kibaride belt (Katanga, SE D.R. Congo). J. African Earth Sci. 46, 1–35. https://doi.org/10.1016/j.jafrearsci.2006.01.017

Kokonyangi, J.W., Kampunzu, A.B., Armstrong, R., Arima, M., Yoshida, M., Okudaira, T., 2007. U - Pb SHRIMP Dating of Detrital Zircons from the Nzilo Group (Kibaran Belt): Implications for the Source of Sediments and Mesoproterozoic Evolution of Central Africa J. Geol. 115, 99–113.

Kuchenbecker, M., Pedrosa-soares, A.C., Babinski, M., Fanning, M., 2015. Detrital zircon age patterns and provenance assessment for pre-glacial to post-glacial successions of the Neoproterozoic Araçuaí orogen , Brazil. Precambrian Res. 266, 12–26. https://doi.org/10.1016/j.precamres.2015.04.016

Lan, Z., Li, X., Zhu, M., Chen, Z.Q., Zhang, Q., Li, Q., Lu, D., Liu, Y., Tang, G., 2014. A rapid and synchronous initiation of the wide spread Cryogenian glaciations. Precambrian Res. 255, 401–411. https://doi.org/10.1016/j.precamres.2014.10.015

Leather, J., Allen, P.A., Brasier, M.D., Cozzi, A., Ueni, J.L., 2002. Neoproterozoic snowball Earth under scrutiny: Evidence from the Fiq glaciation of Oman. Geol. Soc. Am. 30, 891–894. https://doi.org/10.1130/0091-7613(2002)030<0891

Lenoir, J.L., Liégeois, J.P., Theunissen, K., Klerkx, J., 1994. The Palaeoproterozoic Ubendian shear belt in Tanzania: geochronology and structure. J. African Earth Sci. 19, 169–184. https://doi.org/10.1016/0899-5362(94)90059-0

Link, K., Koehn, D., Barth, M.G., Aanyu, K., Foley, S.F., 2010. Continuous cratonic crust between the Congo and Tanzania blocks in western Uganda. Int. J. Earth Sci. 99, 1559–1573. https://doi.org/10.1007/s00531-010-0548-8

Linol, B., Wit, Maarten De, Barton, E., Wit, Michiel De, Guillocheau, F., 2016. U–Pb detrital zircon dates and source provenance analysis of Phanerozoic sequences of the Congo Basin, central Gondwana. Gondwana Res. 29, 208–219.

Liu, C., Zhang, J., Tang, L., Yang, F., Guo, J., Zhou, C., Cai, Z., Bian, X., Manikyamba, C., 2019. Lower Roan Group, Chambishi Basin, North-eastern Zambia: Implication for Detrital zircon U–Pb geochronology and provenance of the Neoproterozoic Lower Roan Group , Chambishi Basin, North - eastern Zambia: Implication for rift evolution of the Congo Craton. Geol. J. 1–17. https://doi.org/10.1002/gj.3491

Lund, K., Aleinikoff, J.N., Evans, K. V, Survey, U.S.G., Fanning, C.M., 2003. SHRIMP U-Pb geochronology of Neoproterozoic Windermere Supergroup, central Idaho: Implications for rifting of western Laurentia and synchroneity of Sturtian glacial deposits 349–372.

Macdonald, F.A., Schmitz, M.D., Crowley, J.L., Roots, C.F., Jones, D.S., Maloof, A.C., Strauss, J. V, Cohen, P.A., Johnston, D.T., Schrag, D.P., 2010. Calibrating the Cryogenian. Science (80). 327, 1241–1243.

Master, S., Rainaud, C., Armstrong, R.A., Phillips, D., Robb, L.J., 2005. Provenance ages of the Neoproterozoic Katanga Supergroup (Central African Copperbelt), with implications for basin evolution. J. African Earth Sci. 42, 41–60. https://doi.org/10.1016/j.jafrearsci.2005.08.005

Master, S., Wendorff, M., 2011. Neoproterozoic glaciogenic diamictites of the Katanga Supergroup, Central Africa. Geol. Soc. London, Mem. 36, 173–184. https://doi.org/10.1144/M36.12

Mudd, G.M., Weng, Z., Jowitt, S.M., 2013. A detailed assessment of global Cu resource trends and endowments. Econ. Geol. 108, 1163–1183. https://doi.org/10.2113/econgeo.108.5.1163

Nascimento, D.B., Ribeiro, A., Trouw, R.A.J., Schmitt, R.S., Passchier, C.W., 2016. Stratigraphy of the Neoproterozoic Damara Sequence in northwest Namibia: Slope to basin sub-marine

mass-transport deposits and olistolith fields. Precambrian Res. 278, 108–125. https://doi.org/10.1016/j.precamres.2016.03.005

Paton, C., Hellstrom, J., Paul, B., Woodhead, J., Hergt, J., 2011. Iolite: Freeware for the visualisation and processing of mass spectrometric data. J. Anal. At. Spectrom. 26, 2508. https://doi.org/10.1039/c1ja10172b

Petrus, J.A., Kamber, B.S., 2012. VizualAge: A Novel Approach to Laser Ablation ICP-MS U-Pb Geochronology Data Reduction. Geostand. Geoanalytical Res. 36, 247–270. https://doi.org/10.1111/j.1751-908X.2012.00158.x

Prave, A.R., Condon, D.J., Hoffmann, K.H., Tapster, S., Fallick, A.E., 2016. Duration and nature of the end-Cryogenian (Marinoan) glaciation. Geology 44, 631–634. https://doi.org/10.1130/G38089.1

Pupin, J.P., (1980) Zircon and granite petrology. Contrib Mineral Petrol 73, 207-220.

Rainaud, C., Master, S., Armstrong, R.A., Robb, L.J., 2003. A cryptic Mesoarchaean terrane in the basement to the Central African Copperbelt. J. Geol. Soc. London. 160, 11–14. https://doi.org/10.1144/0016-764902-087

Rainaud, C, Master, S., Armstrong, R.A., Phillips, D., Robb, L.J., 2005a. Monazite U–Pb dating and 40 Ar–39 Ar thermochronology of metamorphic events in the Central African Copperbelt during the Pan-African Lufilian Orogeny. J. African Earth Sci. 42, 183–199. https://doi.org/10.1016/j.jafrearsci.2005.08.007

Rainaud, Christine, Master, S., Armstrong, R.A., Robb, L.J., 2005b. Geochronology and nature of the Palaeoproterozoic basement in the Central African Copperbelt (Zambia and the Democratic Republic of Congo), with regional implications. J. African Earth Sci. 42, 1–31. https://doi.org/10.1016/j.jafrearsci.2005.08.006

Reddy, S.M., Collins, A.S., Mruma, A., 2003. Complex high-strain deformation in the Usagaran Orogen, Tanzania: structural setting of Palaeoproterozoic eclogites. Tectonophysics 375, 101–123. https://doi.org/10.1016/S0040-1951(03)00335-4

Rooney, A.D., Strauss, J. V., Brandon, A.D., Macdonald, F.A., 2015. A Cryogenian chronology: Two long-lasting synchronous neoproterozoic glaciations. Geology 43, 459–462. https://doi.org/10.1130/G36511.1

Schmandt, D., Broughton, D., Hitzman, M.W., Plink-Bjorklund, P., Edwards, D., Humphrey, J., 2013. The Kamoa copper deposit, democratic republic of Congo: Stratigraphy, diagenetic and hydrothermal alteration, and mineralization. Econ. Geol. 108, 1301–1324. https://doi.org/10.2113/econgeo.108.6.1301

Schrag, D.P., Berner, R.A., Hoffman, P.F., Halverson, G.P., 2002. On the initiation of a snowball Earth. Geochemistry, Geophys. Geosystems 3, 1–21. https://doi.org/10.1029/2001GC000219

Selley, D, Broughton, D., Scott, R., Hitzman, M., Bull, S., Large, R., McGoldrick, P., Croaker, M., Pollington, N., 2005. A new look at the geology of the Zambian Copperbelt. A new look Geol. Zambia Copperbelt. Econ. Geol. 100th Anniv. Vol. 965–1000.

Selley, David, Broughton, D., Scott, R., Hitzman, M., Bull, S., Large, R., McGoldrick, P., Croaker, M., Pollington, N., 2005. A New Look at the Geology of the Zambian Copperbelt. Soc. Econ. Geol. 15, 965–1000.

Selley, D., Scott, R., Emsbo, P., Koziy, L., Hitzman, M.W., Bull, S.W., Duffett, M., Sebagenzi, S., Halpin, J., Broughton, D.W., 2018. Structural Configuration of the Central African Copperbelt: Roles of Evaporites in Structural Evolution, Basin Hydrology, and Ore Location. SEG Spec. Publ. 115–156. https://doi.org/10.5382/sp.21.07

Sircombe, K.N., 2004. AgeDisplay: An EXCEL workbook to evaluate and display univariate geochronological data using binned frequency histograms and probability density distributions. Comput. Geosci. 30, 21–31. https://doi.org/10.1016/j.cageo.2003.09.006

Sircombe, K.N., Stern, R.A., 2002. An investigation of artificial biasing in detrital zircon U-Pb geochronology due to magnetic separation in sample preparation. Geochim. Cosmochim. Acta 66, 2379–2397. https://doi.org/10.1016/S0016-7037(02)00839-6

Sláma, J., Košler, J., Condon, D.J., Crowley, J.L., Gerdes, A., Hanchar, J.M., Horstwood, M.S.A., Morris, G.A., Nasdala, L., Norberg, N., Schaltegger, U., Schoene, B., Tubrett, M.N., Whitehouse, M.J., 2008. Plešovice zircon—A new natural reference material for U–Pb and Hf isotopic microanalysis. Chem. Geol. 249, 1–35. https://doi.org/10.1016/j.chemgeo.2007.11.005

Sommer, H., Kröner, A., Muhongo, S., Hauzenberger, C., 2005. SHRIMP zircon ages for post-Usagaran granitoid and rhyolitic rocks from the Palaeoproterozoic terrain of southwestern Tanzania. South African J. Geol. 108, 247–256. https://doi.org/10.2113/108.2.247

Spencer, C.J., Kirkland, C.L., Taylor, R.J.M., 2016. Strategies towards statistically robust interpretations of in situ U-Pb zircon geochronology. Geosci. Front. 7, 581–589. https://doi.org/10.1016/j.gsf.2015.11.006

Straathof, G.B., 2011. Neoproterozoic low latitude glaciations: an african perspective. PhD Thesis. University of Edinburgh, Edinburgh, 285 pp.

Tack, L., Wingate, M.T.D., De Waele, B., Meert, J., Belousova, E., Griffin, B., Tahon, A., Fernandez-Alonso, M., 2010. The 1375 Ma “Kibaran event” in Central Africa: Prominent emplacement of bimodal magmatism under extensional regime. Precambrian Res. 180, 63–84. https://doi.org/10.1016/j.precamres.2010.02.022

Thomas, R.J., Jacobs, J., Elburg, M., Mruma, A., Kamihanda, G., Kankila, A., Masanja, A., Saidi, H., 2018. New U-Pb-Hf zircon isotope data forthe Paleoproterozoic Ubendian belt in the Chimala area, SW Tanzania. Geosci. Front. 1–15. https://doi.org/10.1016/j.gsf.2018.05.010

Tulibonywa, T., Manya, S., Maboko, M.A.H., 2015. Palaeoproterozoic volcanism and granitic magmatism in the Ngualla area of the Ubendian Belt , SW Tanzania: Constraints from SHRIMP U–Pb zircon ages , and Sm – Nd isotope systematics. Precambrian Res. 256, 120–130. https://doi.org/10.1016/j.precamres.2014.11.003

Twite, F., Broughton, D., Nex, P., Kinnaird, J., Gilchrist, G., Edwards, D., 2019. Lithostratigraphic and structural controls on sulphide mineralisation at the Kamoa copper deposit, Democratic Republic of Congo. J. African Earth Sci. 151, 212–224. https://doi.org/10.1016/j.jafrearsci.2018.12.016

Vermeesch, P., 2004. How many grains are needed for a provenance study? Earth Planet. Sci. Lett. 224, 441–451. https://doi.org/10.1016/j.epsl.2004.05.037

Wendorff, M., Key, R.M., 2009. The relevance of the sedimentary history of the Grand Conglomerat Formation (Central Africa) to the interpretation of the climate during a major Cryogenian glacial event. Precambrian Res. 172, 127–142. https://doi.org/10.1016/j.precamres.2009.03.013

Wiedenbeck, M., Allé, P., Corfu, F., Griffin, W.L., Meier, M., Oberli, F., Von Quadt, A., Roddick, J.C., Spiegel, W., 1995. Three Natural Zircon Standards For U-Th-Pb, Lu-Hf, Element And REE Analyses. Geostand. Newsl. 19, 1–23.

Zhou, C., Tucker, R., Xiao, S., Peng, Z., Yuan, X., Chen, Z., 2004. New constraints on the ages of Neoproterozoic glaciations in south China. Geology 32, 437–440. https://doi.org/10.1130/G20286.1

Zimmermann, U., Andersen, T., Madland, M.V., Larsen, I.S., 2015. The role of U-Pb ages of detrital zircons in sedimentology-An alarming case study for the impact of sampling for provenance interpretation. Sediment. Geol. 320, 38–50. https://doi.org/10.1016/j.sedgeo.2015.02.006

Tables

References	Location	Strat Unit	Rock Type	ample Nam	Method	# Grains Analysed	Age Range (Ma)		Major Population Peaks			
							Max	Min	Neopro	Mesopro	Paleopro	Archean
Armstrong et al., 2005	Nchanga (Kafue Anticline), Zambia	Lower Roan Group	Sandstone and a	DDH P322	SHRIMP	73	2018	841	880	NA	1900	NA
Master et al., 2005	Likasi	Mwashya Subggroup	Sandstone	S27-32	SHRIMP	3	1870	983	983	1047	1870	NA
Master et al., 2005	Kipushi, DRC	grand conglomérat' (Mw	Diamictite	K30-41	SHRIMP	10	1945	729*only	822	1025	1945-1846	NA
Master et al., 2005	South of Luina Dome, Zambia	Lower Roan Group	Arkosic Sandstor	SPOTMU	SHRIMP	48	2120	1810	NA	NA	1915	NA
Master et al., 2005	South of Luina Dome, Zambia	Lower Roan Group	Arkosic Sandstor	MUS3	SHRIMP	10	2066	1883	NA	NA	2050	NA
Master et al., 2005	Southeast of Luina Dome, Zambia	Lower Roan Group	Arkosic Sandstor	KNS7	SHRIMP	14	1996	1913	NA	NA	1945	NA
Master et al., 2005	Chambishi, Zambia	Lower Roan Group	Arkosic Sandstor	RCB24	SHRIMP	14	2062	908	908	NA	1890, 1960, 2062	NA
De Waele and Fitzsimons, 2007	Bangweulu, Zambia	Muva Supergroup, Mkpo	Quartzite	MA6	SHRIMP	31	2710	1824	NA	NA	1800-1900; 1950-2050	minor ~2500, 2700
De Waele and Fitzsimons, 2007	Bangweulu, Zambia	Muva Supergroup, Kasan	Quartzite	KAS	SHRIMP	33	2593	1434	NA	1 at 1434	1900-2050	one ~2168; one ~259
De Waele and Fitzsimons, 2007	Irumide Belt, Zambia	Muva Supergroup, Mans	Quartzite	IL14	SHRIMP	47	3011	1882		NA	2000-2050	minor ~2100, 2200, 2
De Waele and Fitzsimons, 2007	Irumide Belt, Zambia	Muva Supergroup, Kanor	Conglomerate	MK8	SHRIMP	7	NA	NA	NA	NA	avg @ 2053	NA
Kokonyangi et al., 2007	Kibaran belt, Mitwaba, DRC	Kibaran Supergroup, Nzi	Conglomerate	KB10.7	SHRIMP	33	2434	1329	NA	1380	1850	NA
Kokonyangi et al., 2007	Kibaran belt, Mitwaba, DRC	Kibaran Supergroup, Nzi	Schist	KB8.7	SHRIMP	39	2004	1368	NA	1380; 1 single an	1850	NA
Kokonyangi et al., 2007	Kibaran belt, Mitwaba, DRC	Kibaran Supergroup, Nzi	Quartzite	KB12.7	SHRIMP	39	2718	1399	NA	1410	1850	two ~2600 and 2700
Kokonyangi et al., 2007	Kibaran belt, Mitwaba, DRC	Kibaran Supergroup, Nzi	Quartzite	KB11.7	SHRIMP	40	3214	1333	NA	1380	?	minor ~2400-2800, 3
Halpin and Selley, 2010	Kolwezi Autochton, DRC	Upper Kundelungu Grou	?	NA	LA-ICP-MS	64	2967	736	736	1378, 1192, 1037	1885	minor ~2352-2476, 2
Halpin and Selley, 2010	Kolwezi Autochton, DRC	Poudingue Conglomerat	Conglomerate	NA	LA-ICP-MS	91	2942	1400	NA	1400, 1572	1806, 1967, 2059	minor ~2533-2942
Halpin and Selley, 2010	Kolwezi, DRC	RGS, Upper Roan Group	Siltstone/Sandst	NA	LA-ICP-MS	20	789	2710	789	1385	1868, 2027	2710
Halpin and Selley, 2010	Kolwezi, DRC	Mines, Lower Roan Grou	Siltstone	NA	LA-ICP-MS	125	1386	2309	NA	1386	1897	2309
Halpin and Selley, 2010	Kolwezi, DRC	RAT, Lower Roan Group	Sandstone	NA	LA-ICP-MS	121	1067	2686	NA	1395, 1213-1263,	1892	2686
Halpin and Selley, 2010	Tenke, DRC	RGS, Upper Roan Group	Siltstone/Sandst	NA	LA-ICP-MS	52	1357	1935	NA	1357	1871	NA
Halpin and Selley, 2010	Tenke, DRC	Mines, Lower Roan Grou	Siltstone	NA	LA-ICP-MS	48	1033	2808	NA	1033	1887	2808
Halpin and Selley, 2010	Tenke, DRC	RAT, Lower Roan Group	Sandstone	NA	LA-ICP-MS	58	1168	2649	NA	1399	1885	2549-2649
Halpin and Selley, 2010	Kamoya, DRC	RAT, Lower Roan Group	Sandstone	NA	LA-ICP-MS	69	956	3093	NA	1371	1868	minor 2483, 3093
Halpin and Selley, 2010	Ruashi, DRC	RGS, Upper Roan Group	Siltstone/Sandst	NA	LA-ICP-MS	11	1861	2112	NA	NA	1861-1967	NA
Halpin and Selley, 2010	Ruashi, DRC	RAT, Lower Roan Group	Sandstone	NA	LA-ICP-MS	9	987	1970	987	1591, 1081	1827, 1970	NA
Halpin and Selley, 2010	Lupoto, DRC	RGS, Upper Roan Group	Siltstone/Sandst	NA	LA-ICP-MS	47	808	2131	808	1067-1287, 1506-	1893-2131	NA
Halpin and Selley, 2010	Lupoto, DRC	RAT, Lower Roan Group	Sandstone	NA	LA-ICP-MS	15	1092	2039	NA	1062	1769-2039	NA
Halpin and Selley, 2010	Kipushi, DRC	RGS, Upper Roan Group	Siltstone/Sandst	NA	LA-ICP-MS	24	1053	2640	NA	1053	1774-2031	2640
Liu et al., 2019	Chambishi, Zambia	Mindola Fm., Lower Roa	Conglomerate	CW-23	LA-ICP-MS	118	1042	2716	NA	1042	1889, 1960	2716
Liu et al., 2019	Chambishi, Zambia	Mindola Fm., Lower Roa	Argillaceous San	CW-22	LA-ICP-MS	63	1057	2451	NA	1057, 1506	1900	2451
Liu et al., 2019	Chambishi, Zambia	Mindola Fm., Lower Roa	Argillaceous San	CW-21	LA-ICP-MS	66	1879	2692	NA	NA	1879-1945	2692
Liu et al., 2019	Chambishi, Zambia	Kitwe Fm., Lower Roan G	Quartz Arenite	CW-20	LA-ICP-MS	59	1617	2012	NA	NA	1898-1970	NA
Liu et al., 2019	Chambishi, Zambia	Kitwe Fm., Lower Roan G	Quartz Arenite	CW-19	LA-ICP-MS	60	1784	2184	NA	NA	1963-2040	NA
Liu et al., 2019	Chambishi, Zambia	Kitwe Fm., Lower Roan G	Arkose	CW-11	LA-ICP-MS	97	1750	2095	NA	NA	1902	NA
Liu et al., 2019	Chambishi, Zambia	Kitwe Fm., Lower Roan G	Quartz Arenite	CW-10	LA-ICP-MS	99	1743	2147	NA	NA	1903	NA

Table 1.

Reference	Basement	Location	Sample Name	Rock Type	Age (Ma)	Method	Grains Analysed
De Waele et al., 2003	Irumide belt	Irumide belt, Zambia	ML2	granite gneiss	1468-1528	SHRIMP	7
De Waele et al., 2003	Irumide belt	Irumide belt, Zambia	SER62	granite gneiss	1616-1697	SHRIMP	11
De Waele et al., 2003	Irumide belt	Irumide belt, Zambia	SER63	granite gneiss	1609-1660	SHRIMP	10
De Waele et al., 2003	Irumide belt	Irumide belt, Zambia	SER12	granite gneiss	1604-1652	SHRIMP	7
De Waele et al., 2003	Irumide belt	Irumide belt, Zambia	MTGG1	granite gneiss	979-1053*t	SHRIMP	14
De Waele et al., 2003	Irumide belt	Irumide belt, Zambia	MTGG2	granite gneiss	997-1062*	SHRIMP	6
De Waele et al., 2003	Irumide belt	Irumide belt, Zambia	LW2	syenite gneiss	800-991	SHRIMP	8
De Waele et al., 2003	Irumide belt	Irumide belt, Zambia	SER64	porphyritic granite	841-1074*	SHRIMP	10
De Waele et al., 2003	Irumide belt	Irumide belt, Zambia	SER53	porphyritic granite	933-1067	SHRIMP	10
De Waele et al., 2003	Irumide belt	Irumide belt, Zambia	ZM36	porphyritic granite	919-1219	SHRIMP	10
De Waele et al., 2003	Irumide belt	Irumide belt, Zambia	SASA2	foliated granite	906-1109	SHRIMP	12
De Waele et al., 2003	Irumide belt	Irumide belt, Zambia	SQG	granite	990-1099	SHRIMP	14
De Waele et al., 2003	Irumide belt	Irumide belt, Zambia	MTG4	granite	957-1032*x	SHRIMP	13
De Waele et al., 2003	Irumide belt	Irumide belt, Zambia	LW1	granite	1005-1538	SHRIMP	6
De Waele et al., 2003	Irumide belt	Irumide belt, Zambia	SER66	migmatite	977-1012*s	SHRIMP	12
De Waele et al., 2003	Irumide belt	Irumide belt, Zambia	SER67	migmatite	994-1181*x	SHRIMP	16
Kokonyangi et al., 2004	Kibaran belt	Mitwaba, DRC	K2	Granitic gneiss	1377	SHRIMP	12
Kokonyangi et al., 2004	Kibaran belt	Mitwaba, DRC	K12	Granitic gneiss	1370	SHRIMP	15
Kokonyangi et al., 2004	Kibaran belt	Mitwaba, DRC	K23	foliated granite	1370	SHRIMP	16
Kokonyangi et al., 2004	Kibaran belt	Mitwaba, DRC	K15	monzogranite	1370	SHRIMP	15
Kokonyangi et al., 2004	Kibaran belt	Mitwaba, DRC	K30	monzogranite	1370	SHRIMP	16
Armstrong et al., 2005	Nchanga granite	Nchanga (west side Kafue anticline), Zambia	Nchanga	Granite	883	SHRIMP	13
De Waele and Fitzsimons, 2007	Bangweulu block	Zambia	MA1	Granite	1860	SHRIMP	4
De Waele and Fitzsimons, 2007	Bangweulu block	Zambia	MA2	Granite	1862	SHRIMP	9
De Waele and Fitzsimons, 2007	Bangweulu block	Zambia	MA3	Granite	1868	SHRIMP	9
De Waele and Fitzsimons, 2007	Bangweulu block	Zambia	MA5	Rhyolite	1862	SHRIMP	4
De Waele and Fitzsimons, 2007	Bangweulu block	Zambia	MA9	Granite	1866	SHRIMP	9
De Waele and Fitzsimons, 2007	Irumide belt	Irumide belt, Zambia	IS20	Tuff intercalated Manshya F	1856	SHRIMP	7
De Waele and Fitzsimons, 2007	Irumide belt	Irumide belt, Zambia	ZM31	Rhyolite intercalated with M	1879	SHRIMP	10
De Waele and Fitzsimons, 2007	Irumide belt	Irumide belt, Zambia	KB5	Basalt	1871	SHRIMP	6
De Waele et al., 2009	Irumide belt	Irumide belt, Zambia	KMP1	granite gneiss	2685-3104	SHRIMP	6
De Waele et al., 2009	Irumide belt	Irumide belt, Zambia	MK3	gneiss	2015-2049	SHRIMP	5
De Waele et al., 2009	Irumide belt	Irumide belt, Zambia	MK5	gneiss	1973-2052	SHRIMP	7
De Waele et al., 2009	Irumide belt	Irumide belt, Zambia	CC10	gneiss	1881-1964	SHRIMP	6
De Waele et al., 2009	Irumide belt	Irumide belt, Zambia	KN1	gneiss	2031-2089	SHRIMP	6
De Waele et al., 2009	Irumide belt	Irumide belt, Zambia	ISK1	granite gneiss	1892-1957	SHRIMP	9
De Waele et al., 2009	Irumide belt	Irumide belt, Zambia	ISK2	granite gneiss	1905-1945	SHRIMP	5
De Waele et al., 2009	Irumide belt	Irumide belt, Zambia	ND2	porphyritic granite gneiss	1622-1644	SHRIMP	4
De Waele et al., 2009	Irumide belt	Irumide belt, Zambia	LW10	gneiss	1409-1661	SHRIMP	13
De Waele et al., 2009	Irumide belt	Irumide belt, Zambia	KK1	porphyritic granite	954-1052	SHRIMP	6
De Waele et al., 2009	Irumide belt	Irumide belt, Zambia	MH4	porphyritic granite	974-1066	SHRIMP	6
De Waele et al., 2009	Irumide belt	Irumide belt, Zambia	MH9	porphyritic granite	986-1077	SHRIMP	8
De Waele et al., 2009	Irumide belt	Irumide belt, Zambia	CC5	porphyritic granite	995-1113	SHRIMP	6
De Waele et al., 2009	Irumide belt	Irumide belt, Zambia	CC8	porphyritic granite	983-1047	SHRIMP	6
De Waele et al., 2009	Irumide belt	Irumide belt, Zambia	MK7	porphyritic granite	890-1166*o	SHRIMP	6
De Waele et al., 2009	Irumide belt	Irumide belt, Zambia	ND1	porphyritic granite	1017-1151*	SHRIMP	10
De Waele et al., 2009	Irumide belt	Irumide belt, Zambia	ND4	granodiorite	1029-1053	SHRIMP	4
De Waele et al., 2009	Irumide belt	Irumide belt, Zambia	ND5	syeno-granite	1012-1117	SHRIMP	4
De Waele et al., 2009	Irumide belt	Irumide belt, Zambia	FW1	porphyritic granite	948-1058	SHRIMP	7
De Waele et al., 2009	Irumide belt	Irumide belt, Zambia	FW2	aplite in porphyritic granite	1258-2483	SHRIMP	13
De Waele et al., 2009	Irumide belt	Irumide belt, Zambia	KN2	porphyritic granite	1035-1339	SHRIMP	8
De Waele et al., 2009	Irumide belt	Irumide belt, Zambia	KN5	porphyritic granite	1058-1216	SHRIMP	9
De Waele et al., 2009	Irumide belt	Irumide belt, Zambia	KN7	porphyritic granite	1047-2792	SHRIMP	8
De Waele et al., 2009	Irumide belt	Irumide belt, Zambia	KN8	porphyritic granite	1060-2074	SHRIMP	13
De Waele et al., 2009	Irumide belt	Irumide belt, Zambia	CHT6	porphyritic granite	792-1034	SHRIMP	9
De Waele et al., 2009	Irumide belt	Irumide belt, Zambia	CHL5	porphyritic granite	985-1145	SHRIMP	8
De Waele et al., 2009	Irumide belt	Irumide belt, Zambia	ZM32	granite	853-2036	SHRIMP	6
Rainaud et al., 2005b	LMC	Kafue Anticline, Zambia	LUFMUF	lufubu schist	1954-2174	SHRIMP	14
Rainaud et al., 2005b	LMC	Kafue Anticline, Zambia	KNS1	trachyandesite	1843-1893	SHRIMP	15
Rainaud et al., 2005b	LMC	Kafue Anticline, Zambia	NB53/1	trachyandesite	1976-2023	SHRIMP	10
Rainaud et al., 2005b	LMC	Kafue Anticline, Zambia	CT169	felsic metavolcanic schist	1909-2392	SHRIMP	16
Rainaud et al., 2005b	LMC	Kafue Anticline, Zambia	MGn	gneiss	2019-2078	SHRIMP	12
Rainaud et al., 2005b	LMC	Kafue Anticline, Zambia	APL1	aplite	2009-2072	SHRIMP	14
Rainaud et al., 2005b	LMC	Kafue Anticline, Zambia	APL2	aplite	692-2730	SHRIMP	30
Rainaud et al., 2005b	LMC	Kafue Anticline, Zambia	MPG-1	granite	1954-2002	SHRIMP	10
Rainaud et al., 2005b	LMC	Kafue Anticline, Zambia	NN75/1	granite	1996-2013	SHRIMP	15
Rainaud et al., 2005b	LMC	Kafue Anticline, Zambia	MFG-1	gneiss	1969-1991	SHRIMP	12
Key et al., 2001	Kasai block	Kasai, DRC	3DA	gneiss	2525-2553	SHRIMP	12
Key et al., 2001	Kasai block	Kasai, DRC	3DA 101	foliated granite	2242-3154	SHRIMP	14
Key et al., 2001	Kasai block	Kasai, DRC	3DA57	granite	2133-2555	SHRIMP	15
Key et al., 2001	Kasai block	Kasai, DRC	3DA 150	porphyritic granite	1981-2076	SHRIMP	12

Table 2.

Sample Name	**Drill hole #**	**Pyrite Float**	**Processing Method**
Phyllite basement	DKMC072	No	SelFrag
Lower Dipeta	DMAK009	No	SelFrag
Middle Dipeta	DMAK009	No	EPD
Upper Dipeta	DMAK009	No	EPD
Lower Mwashya	DMAK009	No	EPD
Upper Mwashya	DMAK009	No	EPD
Basal Diamictite Lower Package	DKMC749W3	Yes	EPD
Basal Diamictite Siltstone Interbed	DKMC749W3	Yes	EPD
Basal Diamictite Upper Package	DKMC749W3	Yes	SelFrag
Lower KPS	DKLE6	Yes	EPD
Middle Diamictite	DKLE6	Yes	SelFrag
Upper Diamictite	DKMC12	No	EPD

Table 3.

Stratigraphic Unit	Provenance Source Area	Interpretation
Dipeta and Mwashya subgroups	Dominant mid-Paleoproterozoic population with a peak ~1930 Ma = Recycling from Kibaran Supergroup and earlier strata of the Katanga Supergroup Dominant Mesoproterozoic population with a peak ~1370 Ma = Kibaran intrusives and metasedimentary rocks of the Kibaran Supergroup Minor amounts of Archean to early-Paleoproterozoic grains = reworked from Kibaran Supergroup	Locally derived from locally exposed quartzite of the Kibaran Supergroup with direct sourcing from intrusions associated with the Kibaran magmatic event located in the Kamoa area.
Basal Diamictite	Dominant mid-Paleoproterozoic population with a peak ~1960 Ma = recycling of Kibaran Supergroup with minor influence from Dipeta and Mwashya subgroups Subordinate Mesoproterozoic population with a peak ~1500 Ma = unknown Mesoproterozoic source area Subordinate early-Paleoproterozoic population with a peak ~2470 and a Neoarchean population ~2710 Ma = Kasai block	Locally derived from recycling of Kibaran Supergroup with broader distally sourced provenance from primary source areas (i.e., Kasai block) on the northern margin of the Katangan basin.
Lower KPS	Dominant mid-Paleoproterozoic population with a peak at ~1890 Ma = Recycling of underlying Katangan strata or from the Kibaran Supergroup Subordinate Mesoproterozoic population at ~1380 Ma = Kibaran Supergroup and Kibaran intrusives Minor Mesoproterozoic population with a peak ~1070 Ma = post-Kibaran intrusives Minor amounts of early-Paleoproterozoic to Archean grains = Recycling from underlying Katangan strata or from the Kibaran Supergroup	Predominantly reworked from Kibaran Supergroup with additional direct sourcing from Kibaran intrusives and post-Kibaran intrusives. Mid-Neoproterozoic grains are derived from locally intercalated mafic volcanic rocks.

	Mid-Neoproterozoic grains ~700 Ma = rift-related volcanic rocks	
Middle Diamictite	Dominant mid-Paleoproterozoic population ~2000 Ma = Recycling of underlying Katangan strata or from the Kibaran Supergroup Subordinate early Paleoproterozoic to Neoarchean population ~2510 Ma = Kasai block Minor amounts of Mesoproterozoic grains around 1290 Ma = unknown Mesoproterozoic source area	Similar provenance as the basal diamictite with a local recycling but broader provenance indicated by presence of Neoarchean to early-Paleoproterozoic population.
Upper Diamictite	Dominant Mesoproterozoic population with a peak ~1350 Ma = Kibaran intrusives. Subordinate mid-Paleoproterozoic population with peaks ~1750 Ma, 1830 Ma, and 2020 Ma = Recycling of underlying Katangan strata or from the Kibaran Supergroup Minor amounts of early-Paleoproterozoic and Archean grains = Recycling of underlying Katangan strata or from the Kibaran Supergroup	Dominantly local recycling with decrease in mid-Paleoproterozoic population and increase in Mesoproterozoic population due to an increase in contribution to the sediment supply from primary Mesoproterozoic source areas (i.e., Kibaran magmatic rocks). The lack of the Neoarchean to early-Paleoproterozoic population indicates distal primary source areas (i.e., Kasai block) was not a significant source area.

Table 4.

Figures

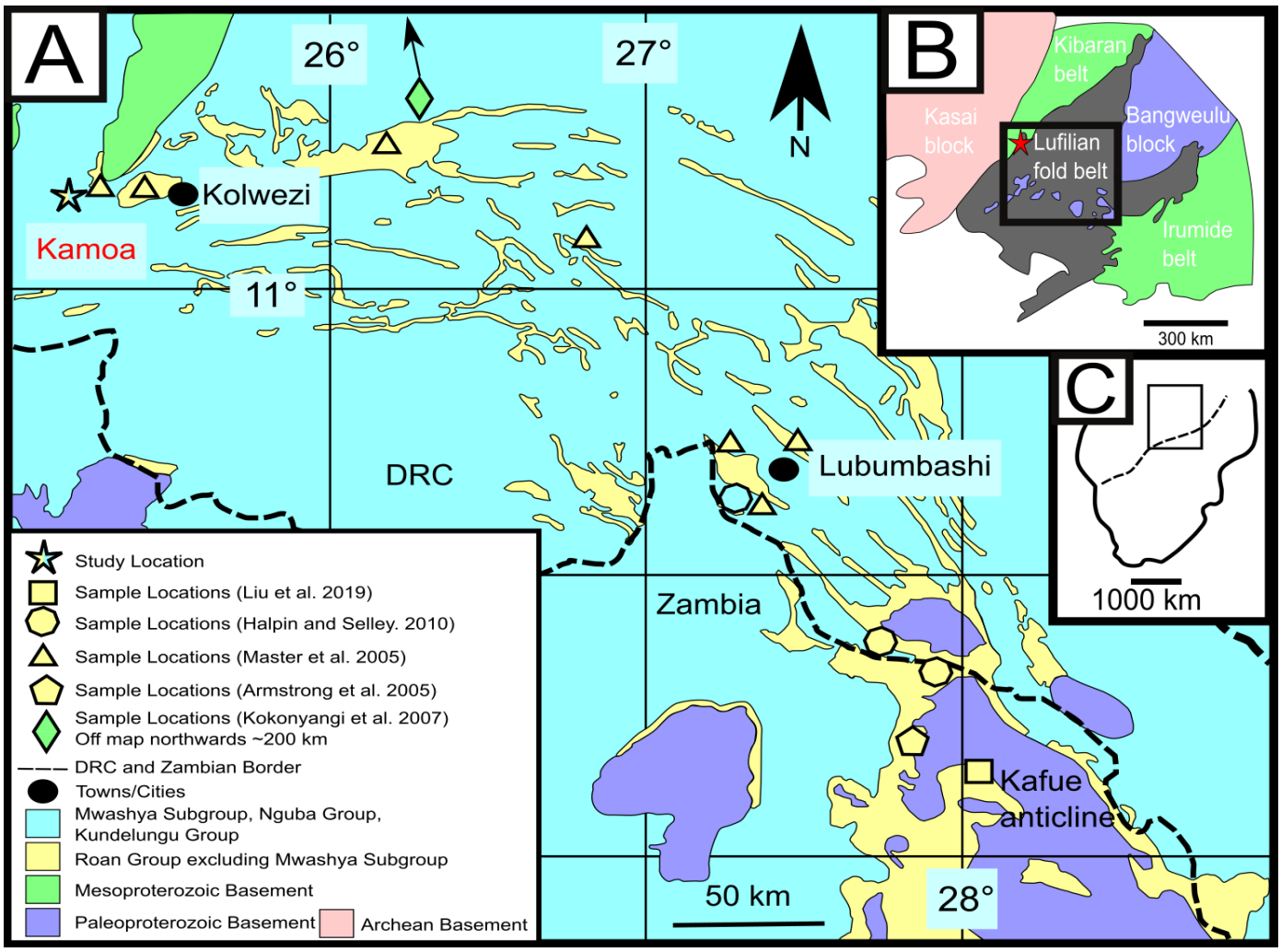

Figure 1.

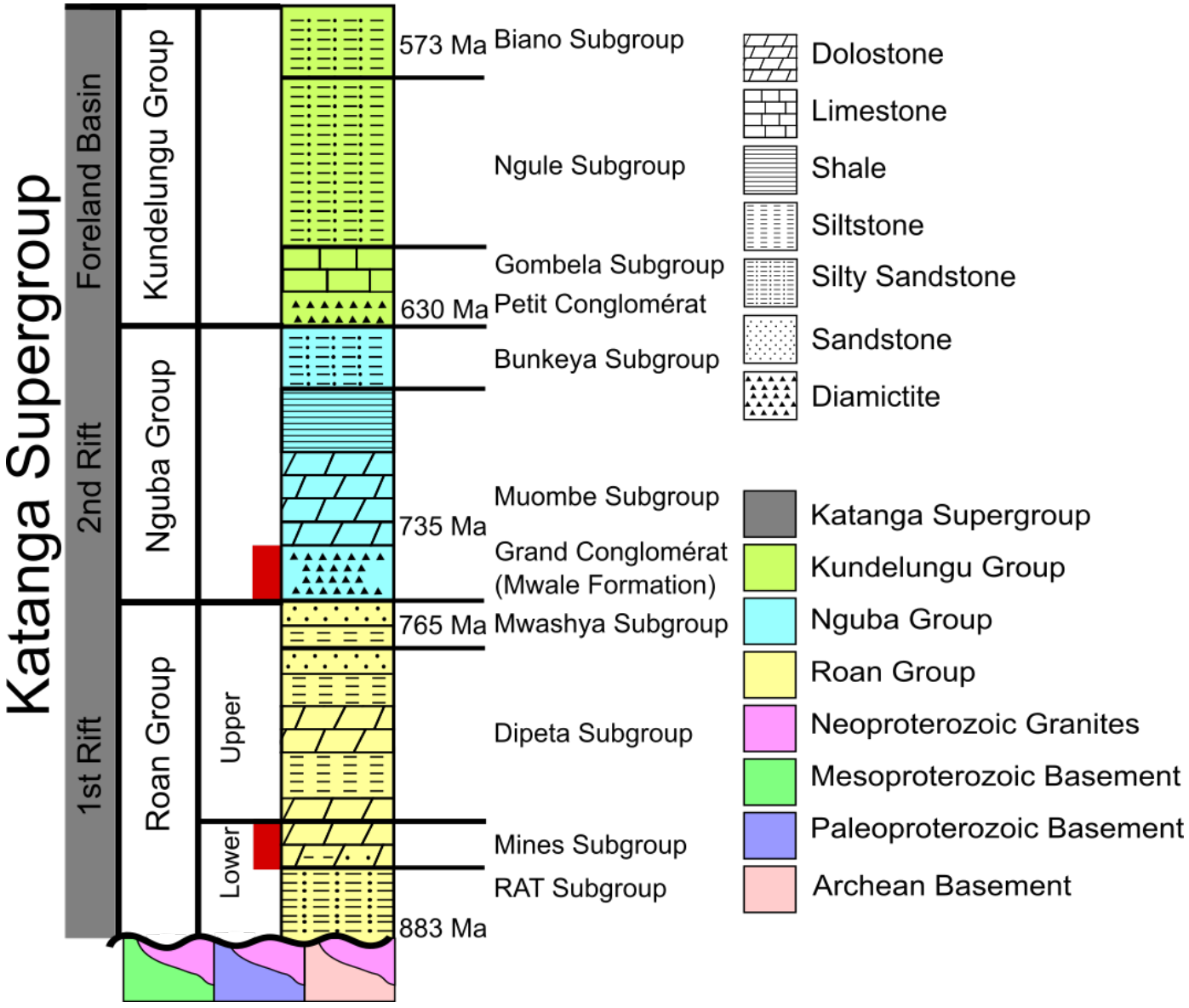
Katanga Supergroup
Foreland Basin
2nd Rift
1st Rift
Kundelungu Group
Nguba Group
Roan Group
Upper
Lower
573 Ma
Biano Subgroup
Ngule Subgroup
Gombela Subgroup
630 Ma
Petit Conglomérat
Bunkeya Subgroup
Muombe Subgroup
735 Ma
Grand Conglomérat
(Mwale Formation)
765 Ma
Mwashya Subgroup
Dipeta Subgroup
Mines Subgroup
RAT Subgroup
883 Ma
Dolostone
Limestone
Shale
Siltstone
Silty Sandstone
Sandstone
Diamictite
Katanga Supergroup
Kundelungu Group
Nguba Group
Roan Group
Neoproterozoic Granites
Mesoproterozoic Basement
Paleoproterozoic Basement
Archean Basement

Figure 2.

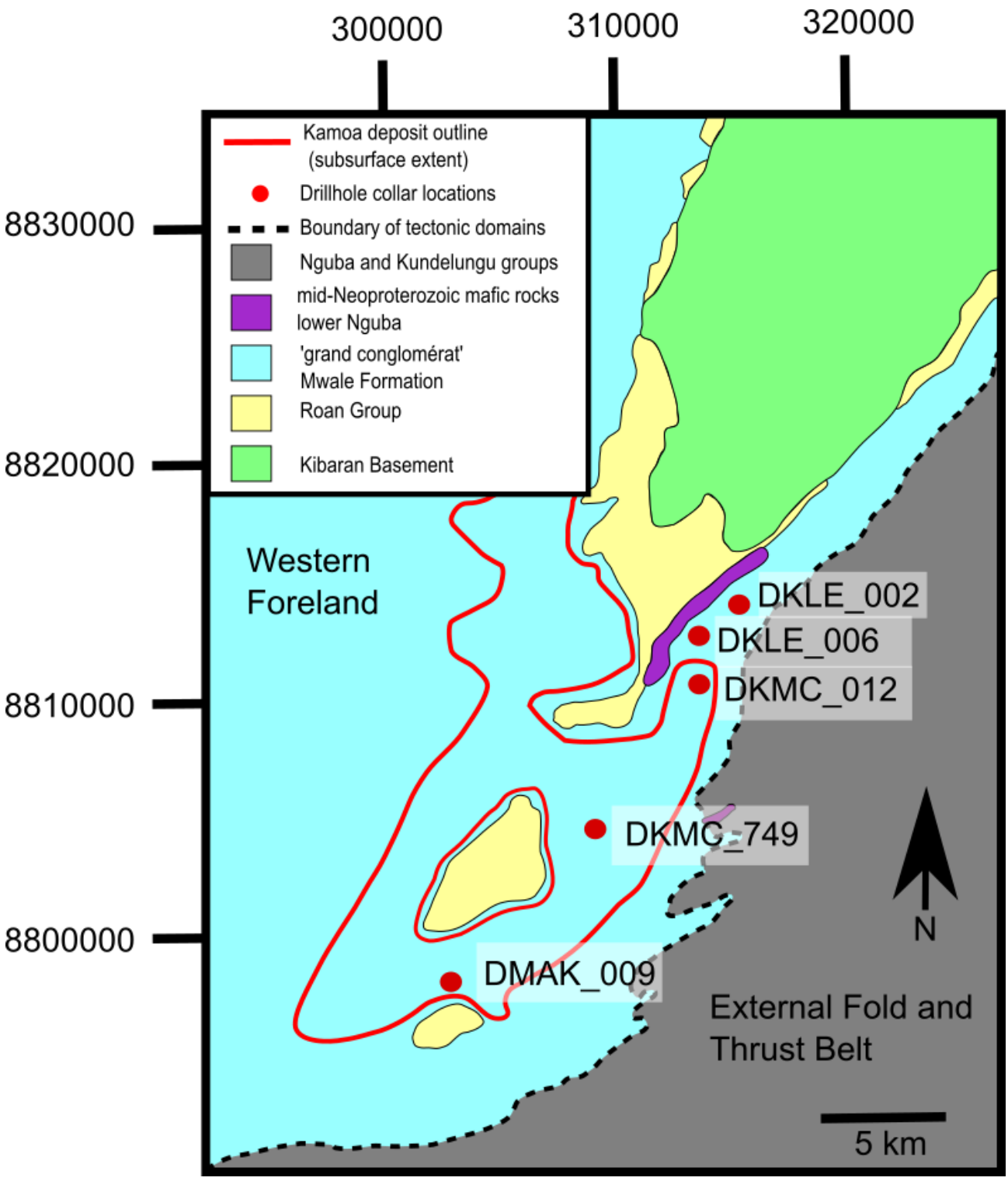
300000
310000
320000
8830000
8820000
8810000
8800000
Kamoa deposit outline
(subsurface extent)
Drillhole collar locations
Boundary of tectonic domains
Nguba and Kundelungu groups
mid-Neoproterozoic mafic rocks
lower Nguba
'grand conglomérat'
Mwale Formation
Roan Group
Kibaran Basement
Western
Foreland
DKLE_002
DKLE_006
DKMC_012
DKMC_749
DMAK_009
N
External Fold and
Thrust Belt
5 km

Figure 3.

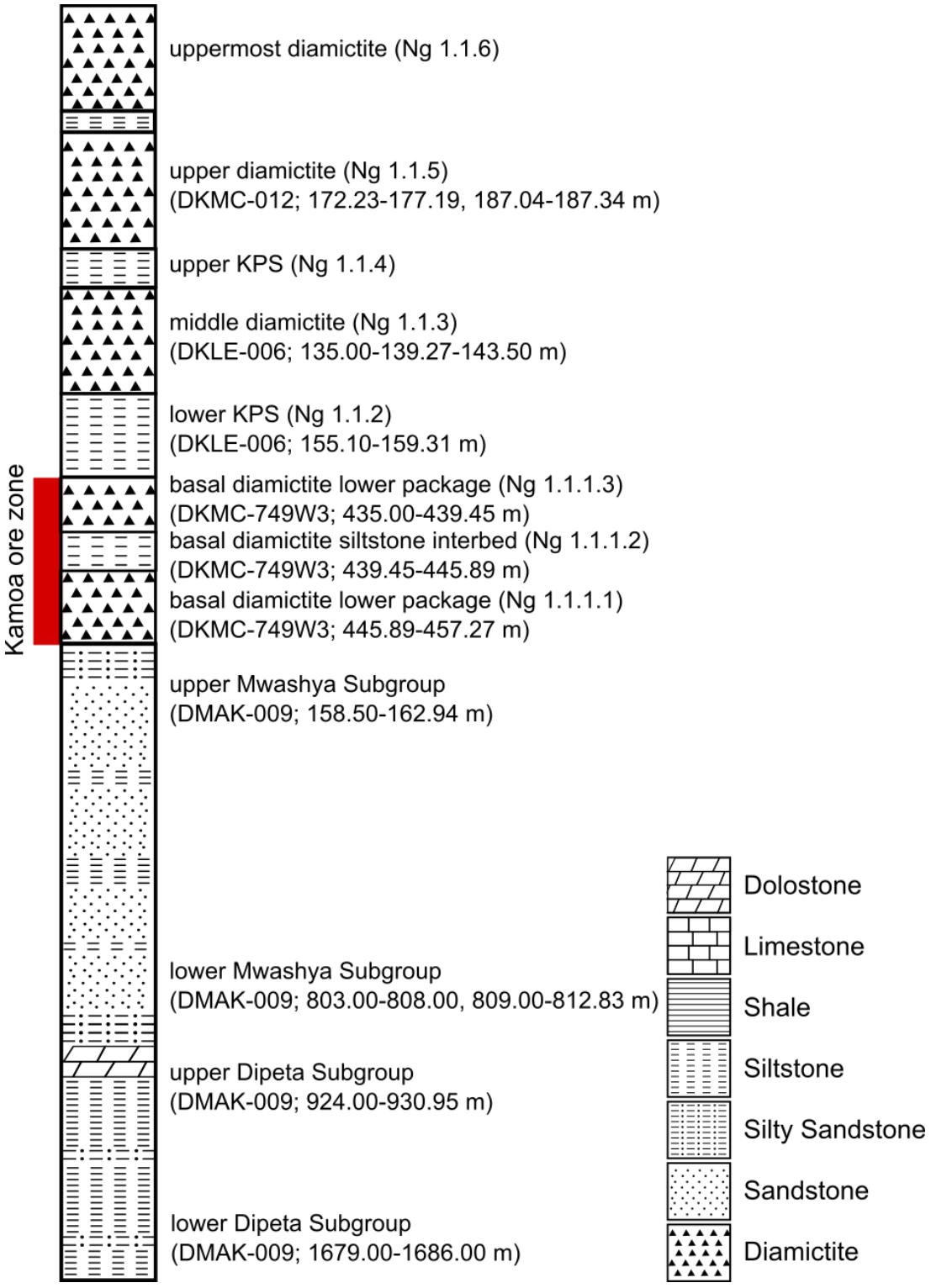
uppermost diamictite (Ng 1.1.6)
upper diamictite (Ng 1.1.5)
(DKMC-012; 172.23-177.19, 187.04-187.34 m)
upper KPS (Ng 1.1.4)
middle diamictite (Ng 1.1.3)
(DKLE-006; 135.00-139.27-143.50 m)
lower KPS (Ng 1.1.2)
(DKLE-006; 155.10-159.31 m)
Kamoa ore zone
basal diamictite lower package (Ng 1.1.1.3)
(DKMC-749W3; 435.00-439.45 m)
basal diamictite siltstone interbed (Ng 1.1.1.2)
(DKMC-749W3; 439.45-445.89 m)
basal diamictite lower package (Ng 1.1.1.1)
(DKMC-749W3; 445.89-457.27 m)
upper Mwashya Subgroup
(DMAK-009; 158.50-162.94 m)
lower Mwashya Subgroup
(DMAK-009; 803.00-808.00, 809.00-812.83 m)
upper Dipeta Subgroup
(DMAK-009; 924.00-930.95 m)
lower Dipeta Subgroup
(DMAK-009; 1679.00-1686.00 m)
Dolostone
Limestone
Shale
Siltstone
Silty Sandstone
Sandstone
Diamictite

Figure 4.

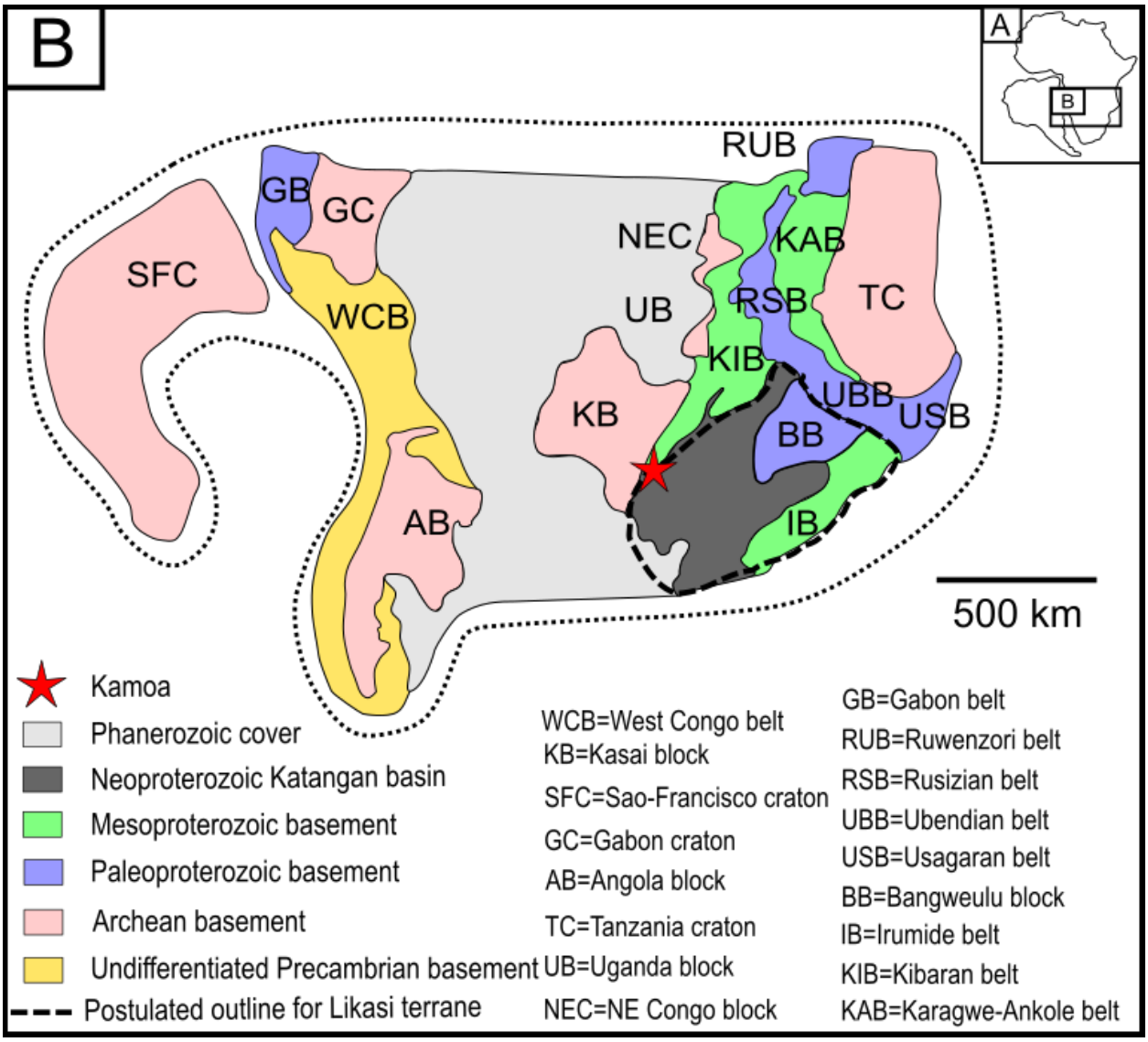
B
A
B
RUB
GB
GC
NEC
KAB
SFC
WCB
UB
RSB
TC
KIB
KB
UBB
USB
BB
AB
IB
500 km
Kamoa
Phanerozoic cover
Neoproterozoic Katangan basin
Mesoproterozoic basement
Paleoproterozoic basement
Archean basement
Undifferentiated Precambrian basement
Postulated outline for Likasi terrane
WCB=West Congo belt
KB=Kasai block
SFC=Sao-Francisco craton
GC=Gabon craton
AB=Angola block
TC=Tanzania craton
UB=Uganda block
NEC=NE Congo block
GB=Gabon belt
RUB=Ruwenzori belt
RSB=Rusizian belt
UBB=Ubendian belt
USB=Usagaran belt
BB=Bangweulu block
IB=Irumide belt
KIB=Kibaran belt
KAB=Karagwe-Ankole belt

Figure 5.

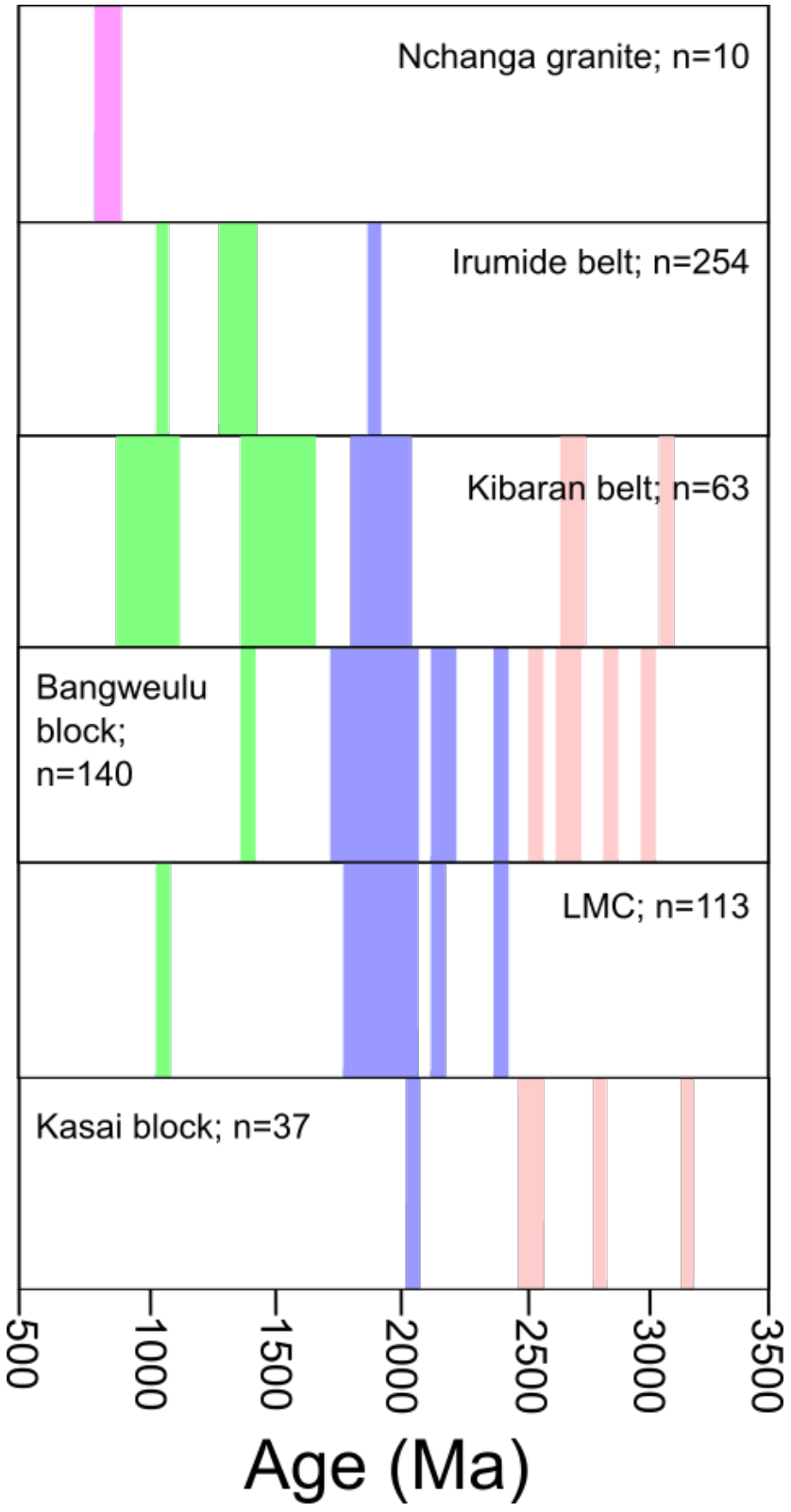
Nchanga granite; n=10
Irumide belt; n=254
Kibaran belt; n=63
Bangweulu block; n=140
LMC; n=113
Kasai block; n=37
500
1000
1500
2000
2500
3000
3500
Age (Ma)

Figure 6.

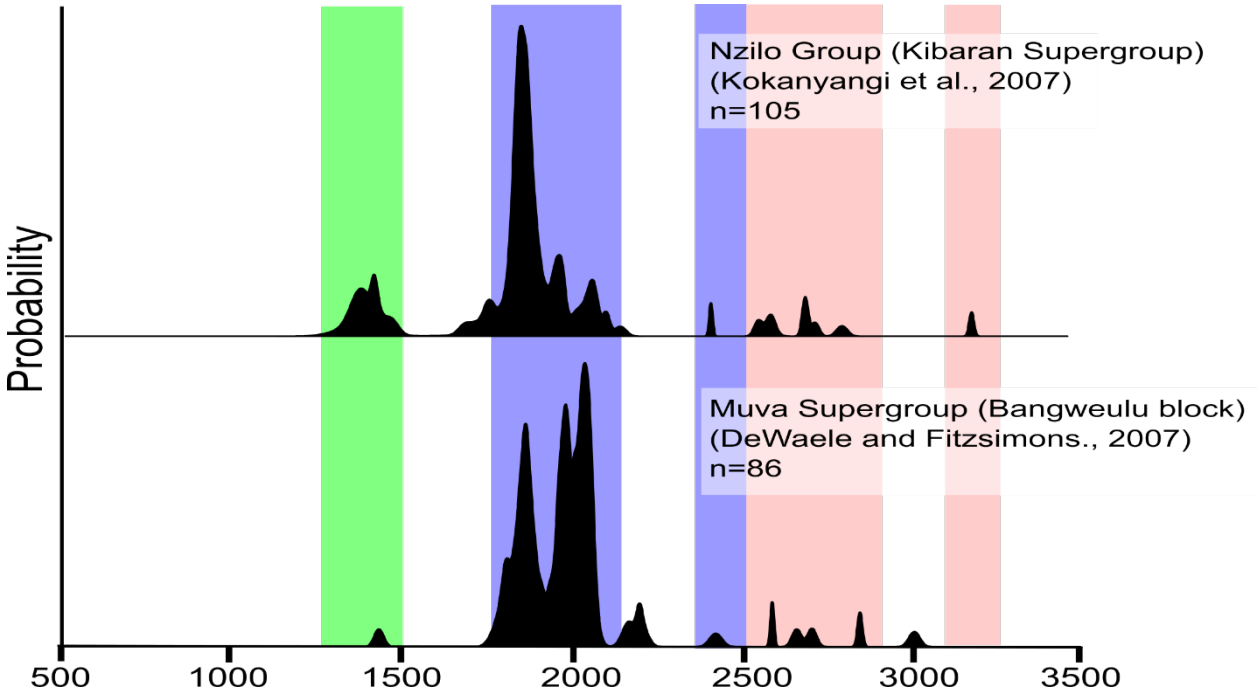
Nzilo Group (Kibaran Supergroup)
(Kokanyangi et al., 2007)
n=105
Muva Supergroup (Bangweulu block)
(DeWaele and Fitzsimons., 2007)
n=86
Probability
500
1000
1500
2000
2500
3000
3500

Figure 7.

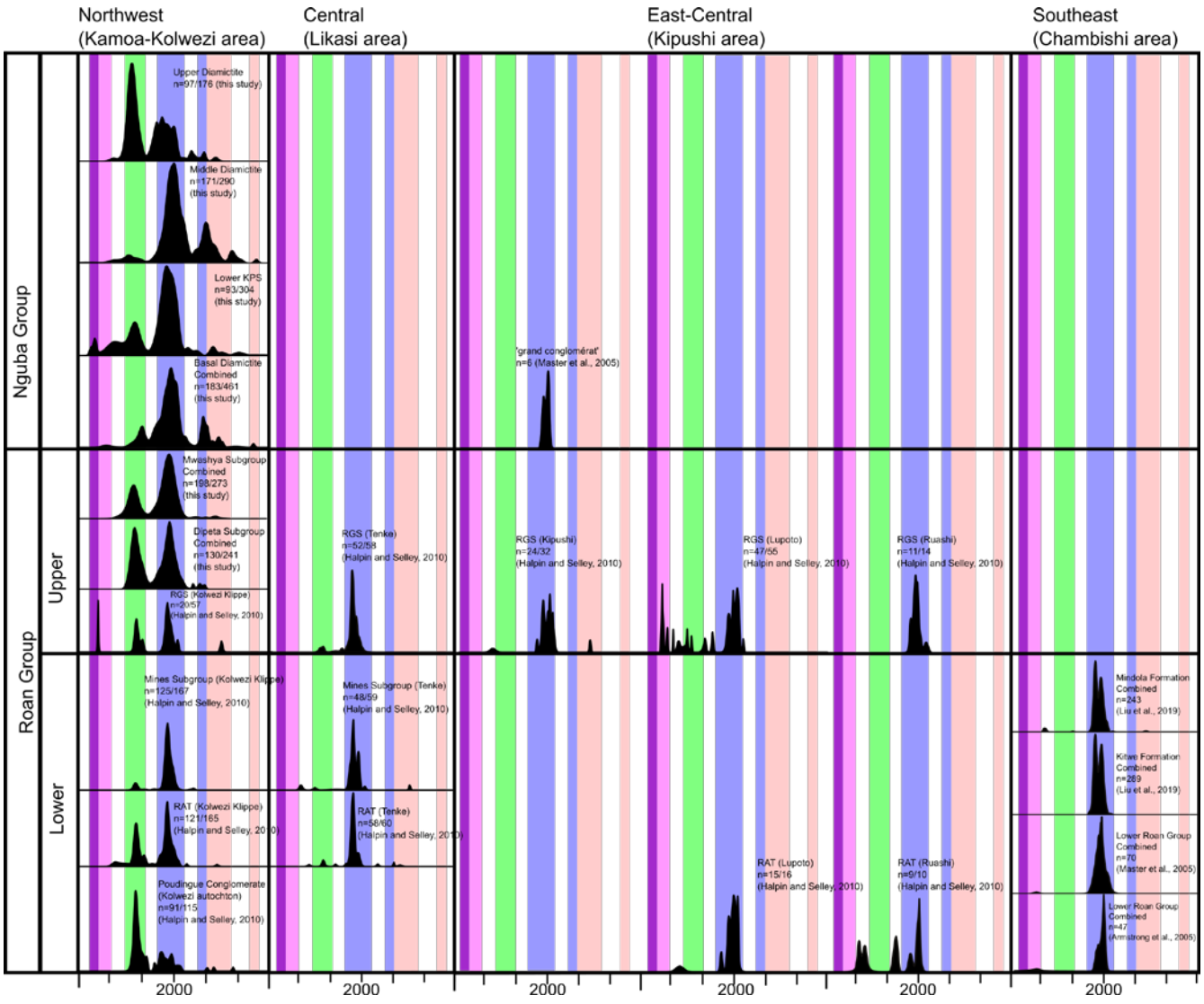
Northwest
(Kamoa-Kolwezi area)
Central
(Likasi area)
East-Central
(Kipushi area)
Southeast
(Chambishi area)
Nguba Group
Roan Group
Upper
Lower
Upper Diamictite
n=97/176 (this study)
Middle Diamictite
n=171/290
(this study)
Lower KPS
n=93/304
(this study)
Basal Diamictite
Combined
n=183/461
(this study)
'grand conglomérat'
n=6 (Master et al., 2005)
Mwashya Subgroup
Combined
n=198/273
(this study)
Dipeta Subgroup
Combined
n=130/241
(this study)
RGS (Kolwezi Klippe)
n=20/57
(Halpin and Selley, 2010)
RGS (Tenke)
n=52/58
(Halpin and Selley, 2010)
RGS (Kipushi)
n=24/32
(Halpin and Selley, 2010)
RGS (Lupoto)
n=47/55
(Halpin and Selley, 2010)
RGS (Ruashi)
n=11/14
(Halpin and Selley, 2010)
Mines Subgroup (Kolwezi Klippe)
n=125/167
(Halpin and Selley, 2010)
RAT (Kolwezi Klippe)
n=121/165
(Halpin and Selley, 2010)
Poudingue Conglomerate
(Kolwezi autochton)
n=91/115
(Halpin and Selley, 2010)
Mines Subgroup (Tenke)
n=48/59
(Halpin and Selley, 2010)
RAT (Tenke)
n=58/60
(Halpin and Selley, 2010)
RAT (Lupoto)
n=15/16
(Halpin and Selley, 2010)
RAT (Ruashi)
n=9/10
(Halpin and Selley, 2010)
Mindola Formation
Combined
n=243
(Liu et al., 2019)
Kitwe Formation
Combined
n=289
(Liu et al., 2019)
Lower Roan Group
Combined
n=70
(Master et al., 2005)
Lower Roan Group
Combined
n=47
(Armstrong et al., 2005)
2000
2000
2000
2000
2000
2000

Figure 8.

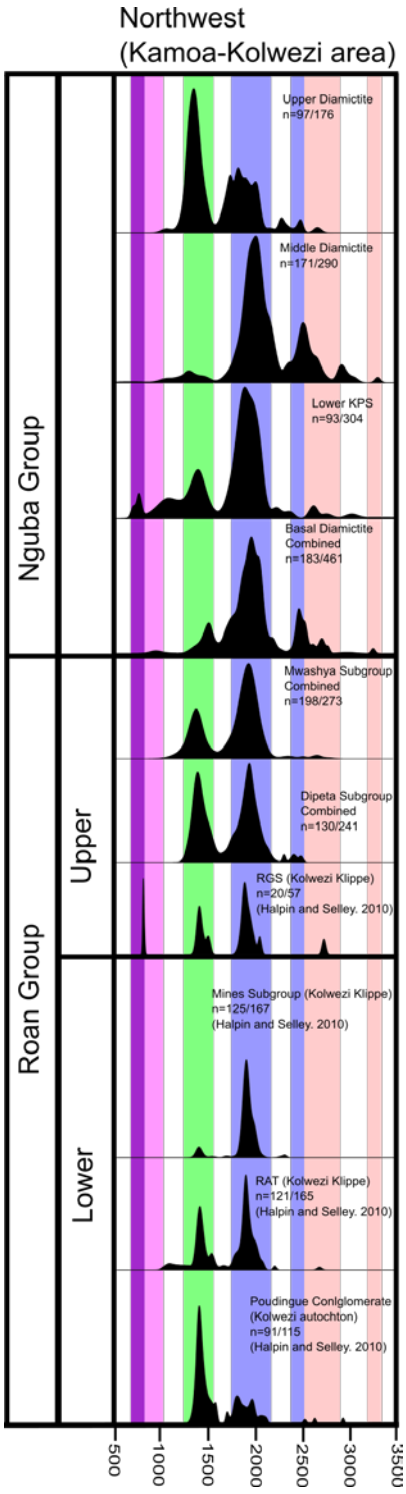
Northwest
(Kamoa-Kolwezi area)
Nguba Group
Roan Group
Upper
Lower
Upper Diamictite
n=97/176
Middle Diamictite
n=171/290
Lower KPS
n=93/304
Basal Diamictite
Combined
n=183/461
Mwashya Subgroup
Combined
n=198/273
Dipeta Subgroup
Combined
n=130/241
RGS (Kolwezi Klippe)
n=20/57
(Halpin and Selley. 2010)
Mines Subgroup (Kolwezi Klippe)
n=125/167
(Halpin and Selley. 2010)
RAT (Kolwezi Klippe)
n=121/165
(Halpin and Selley. 2010)
Poudingue Conlglomerate
(Kolwezi autochton)
n=91/115
(Halpin and Selley. 2010)
500
1000
1500
2000
2500
3000
3500

Figure 9.

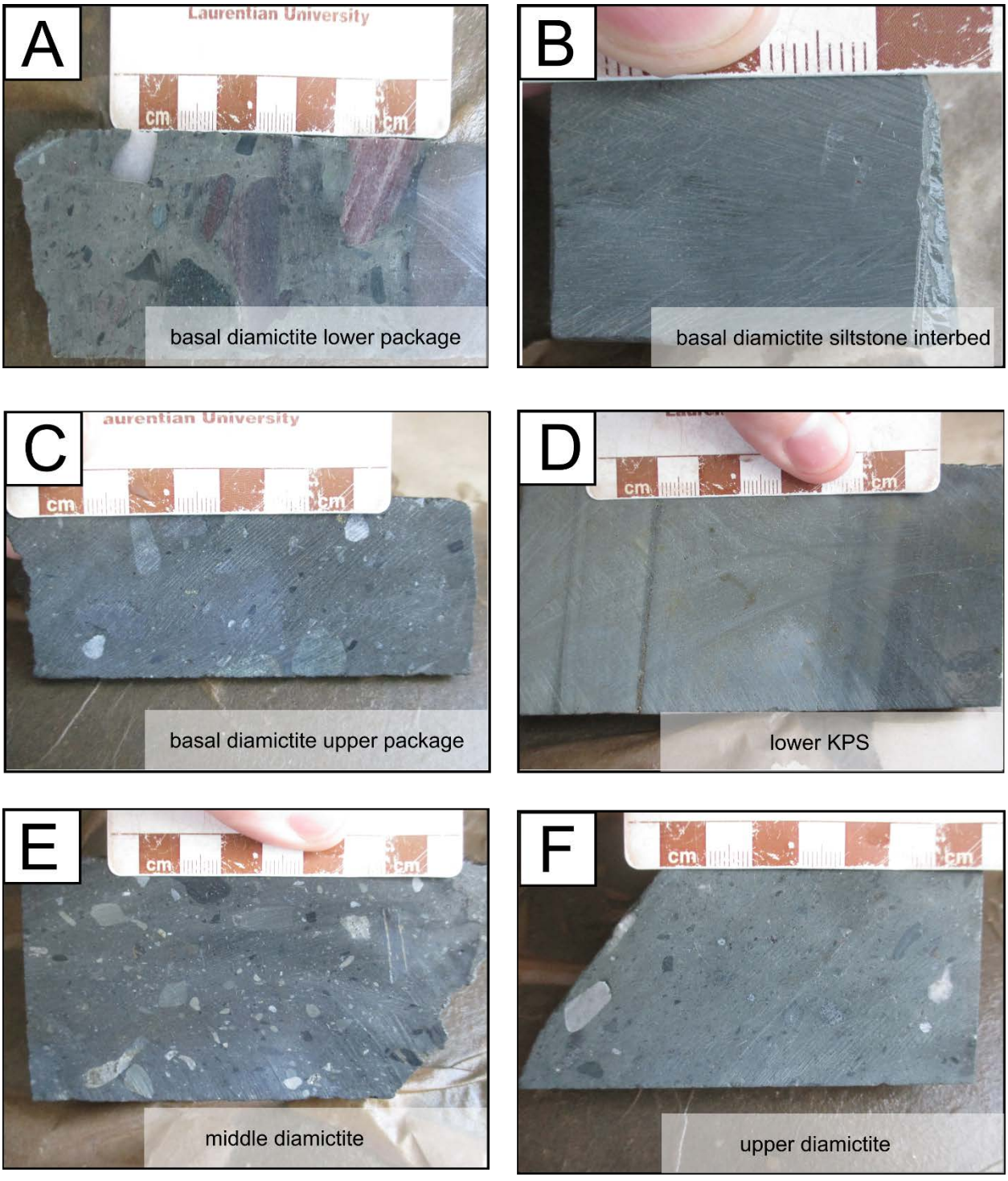
A
Laurentian University
cm
cm
basal diamictite lower package
B
basal diamictite siltstone interbed
C
aurentian University
cm
cm
basal diamictite upper package
D
cm
cm
lower KPS
E
cm
cm
middle diamictite
F
cm
cm
upper diamictite

Figure 10.

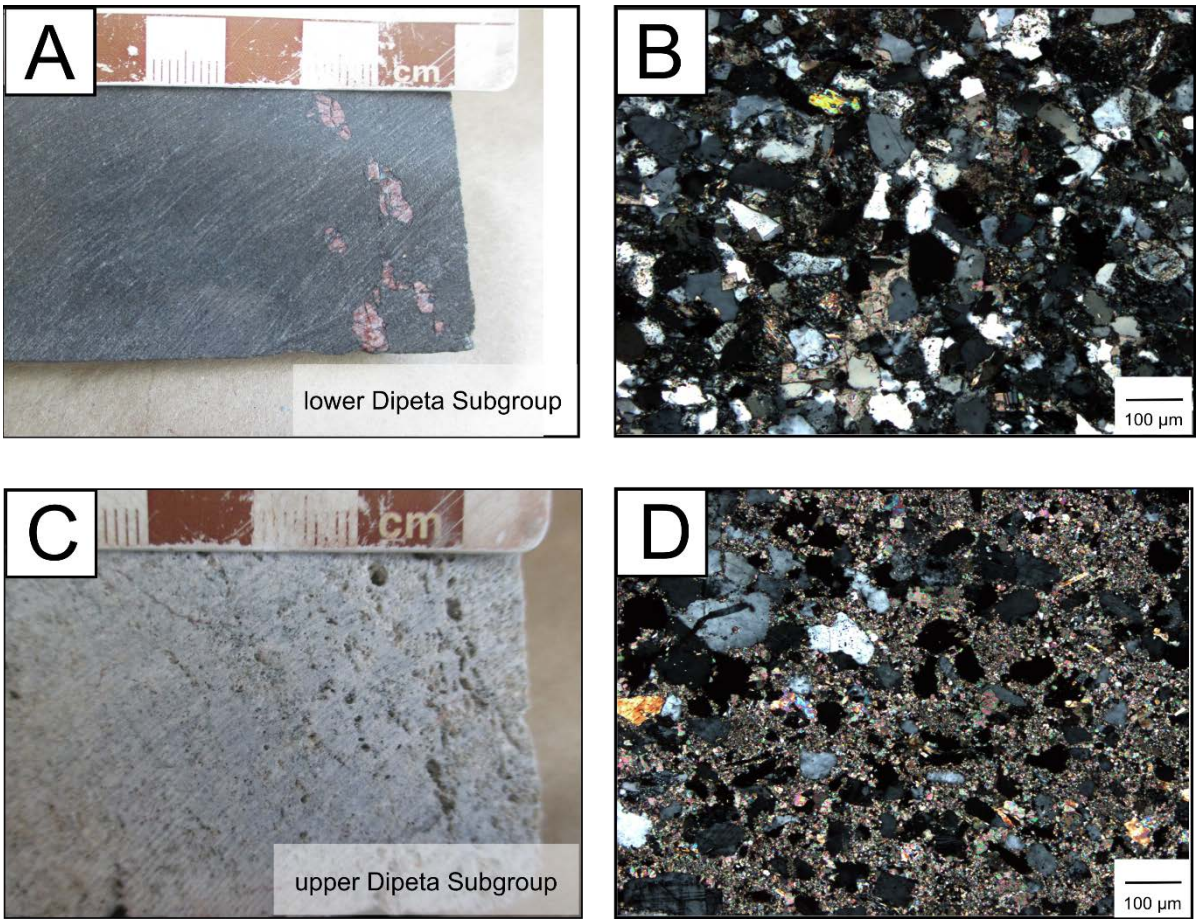
A
cm
lower Dipeta Subgroup
B
100 µm
C
cm
upper Dipeta Subgroup
D
100 µm

Figure 11.

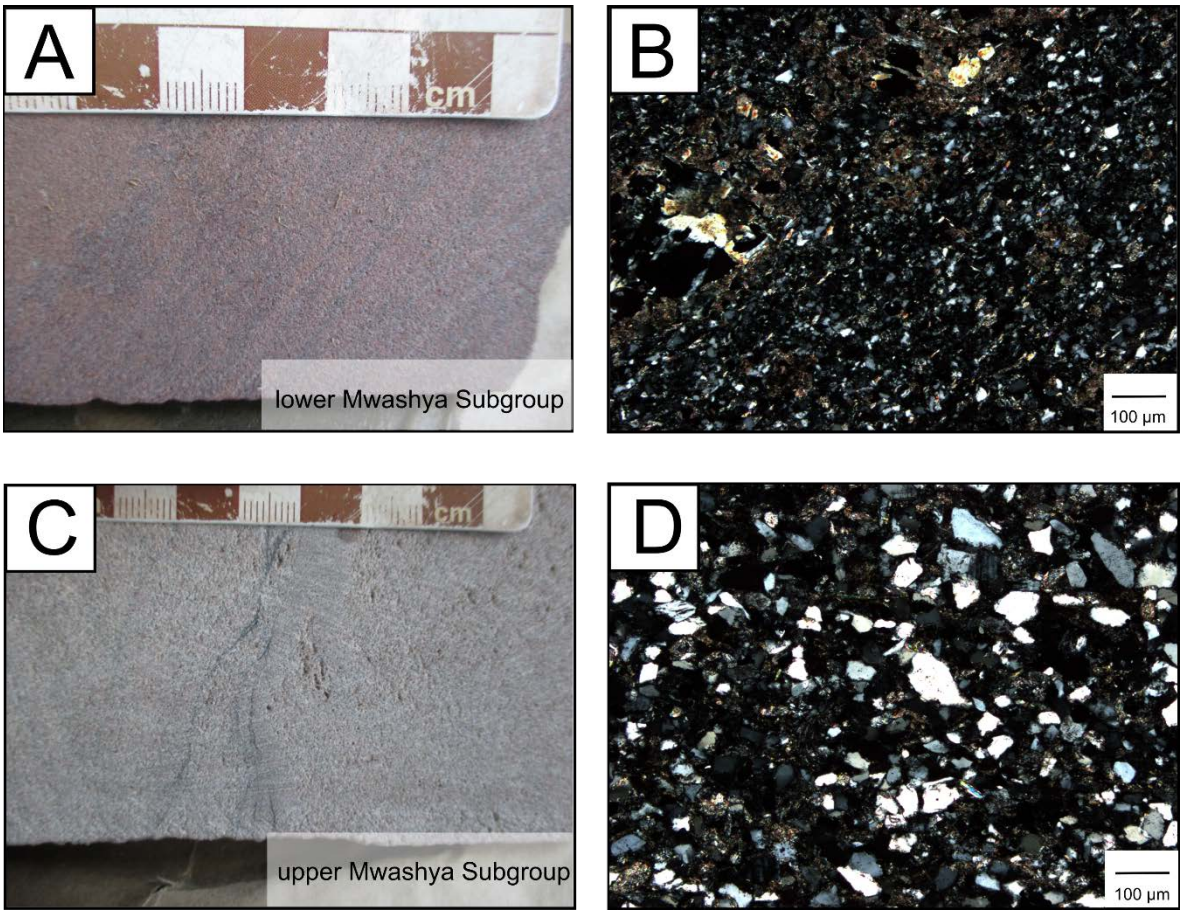
A
cm
lower Mwashya Subgroup
B
100 µm
C
cm
upper Mwashya Subgroup
D
100 µm

Figure 12.

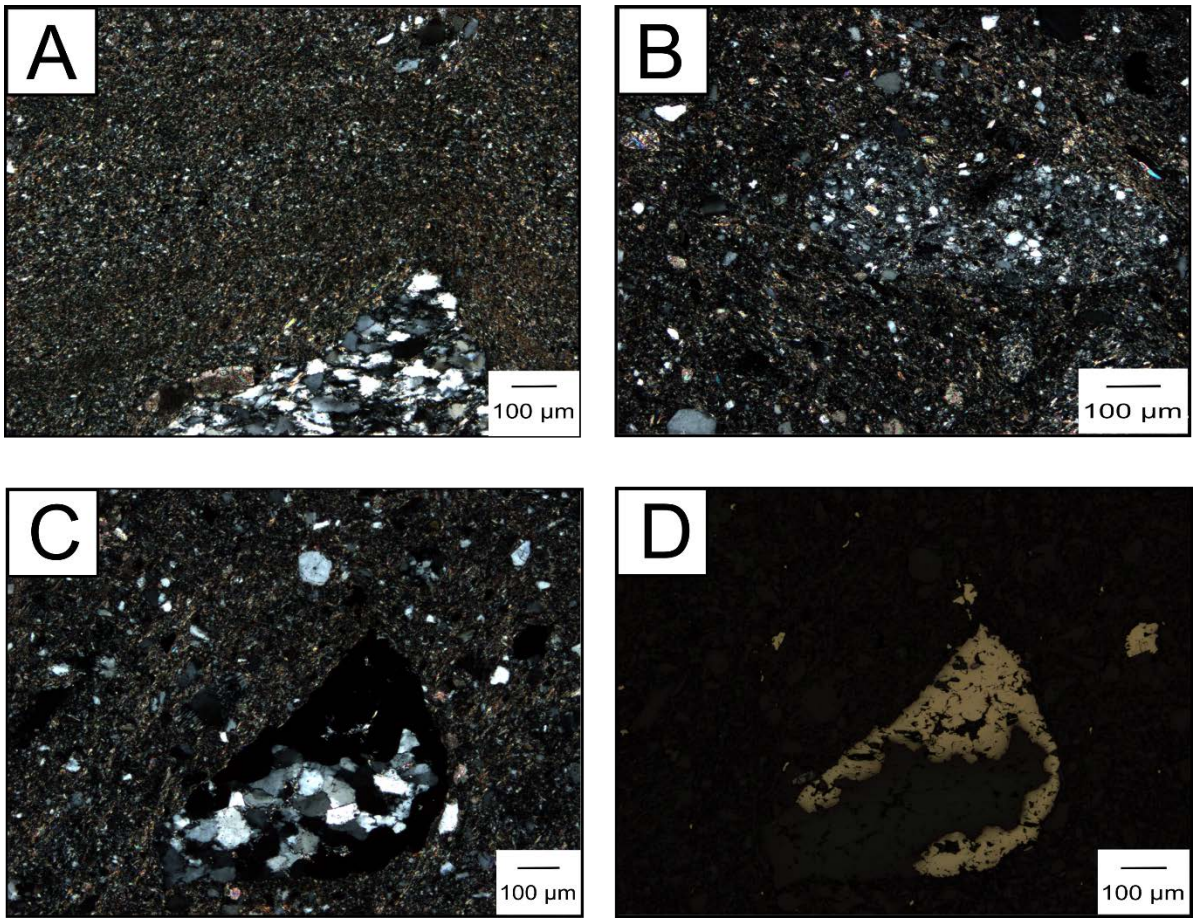

Figure 13.

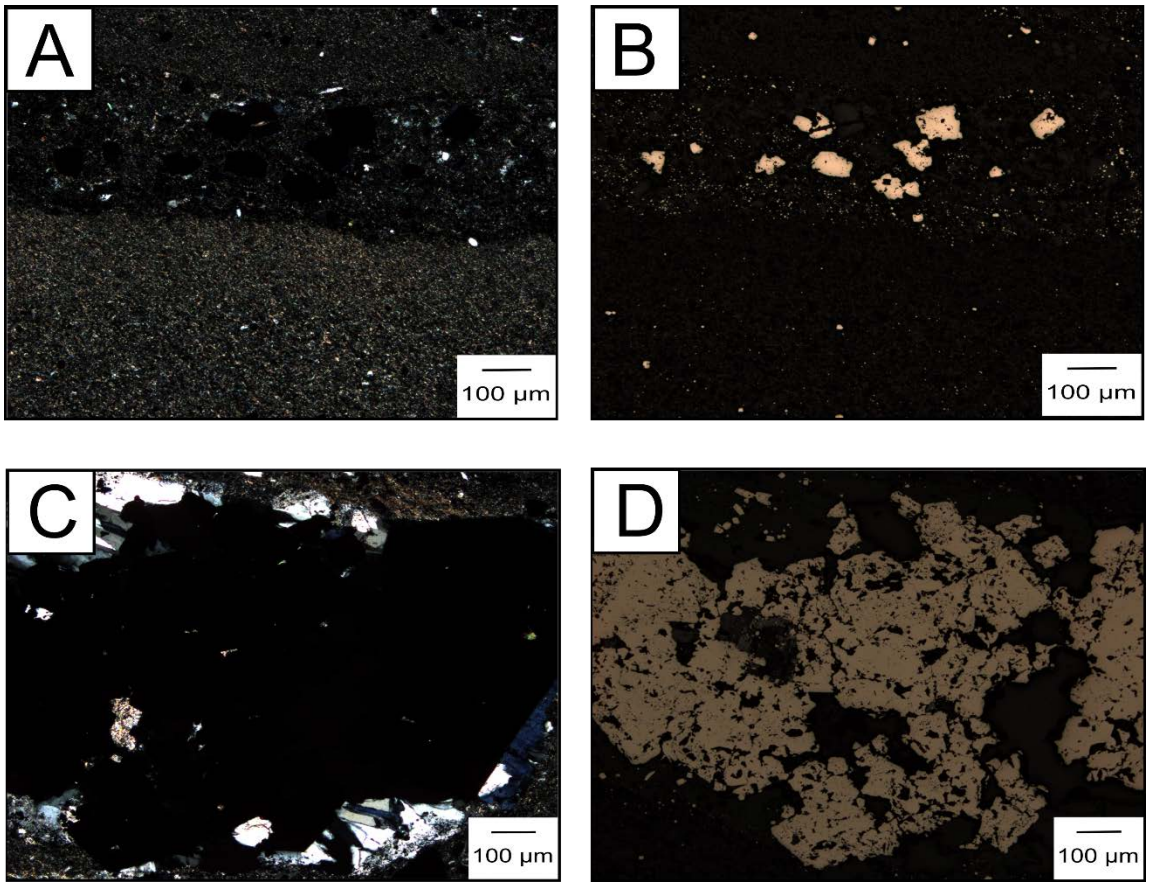

Figure 14.

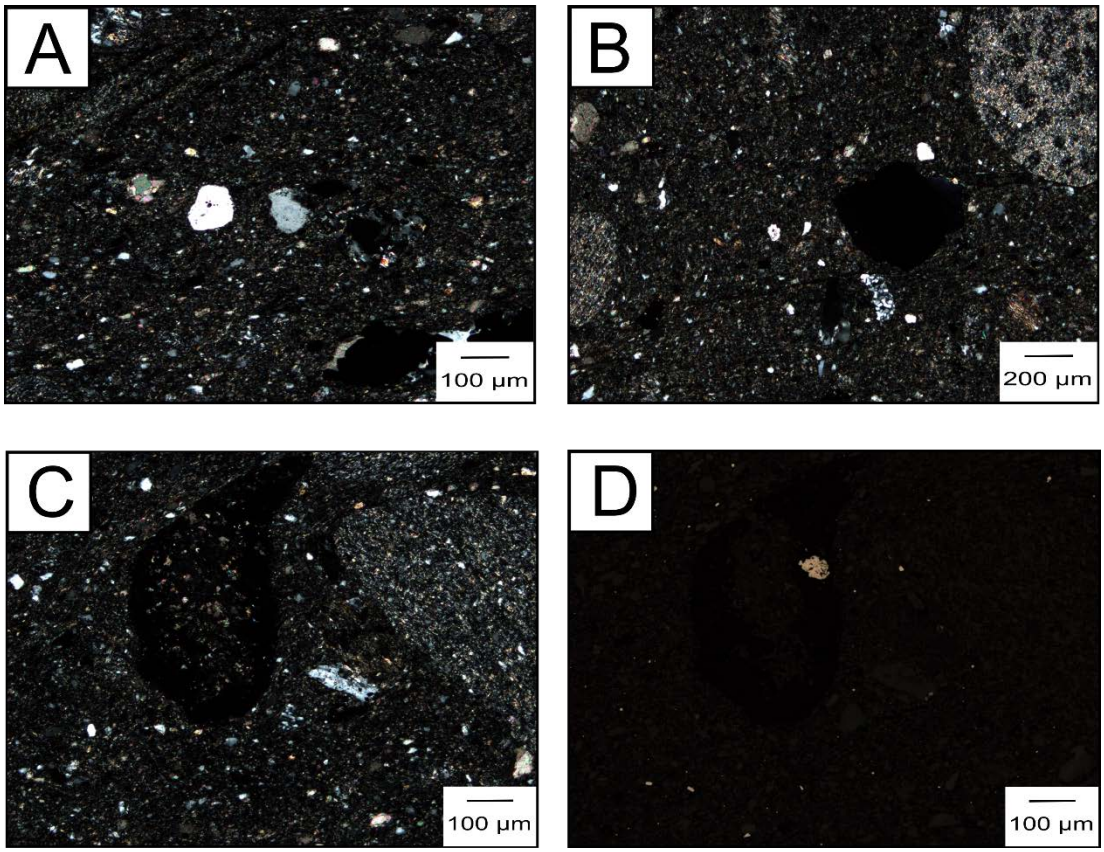

Figure 15.

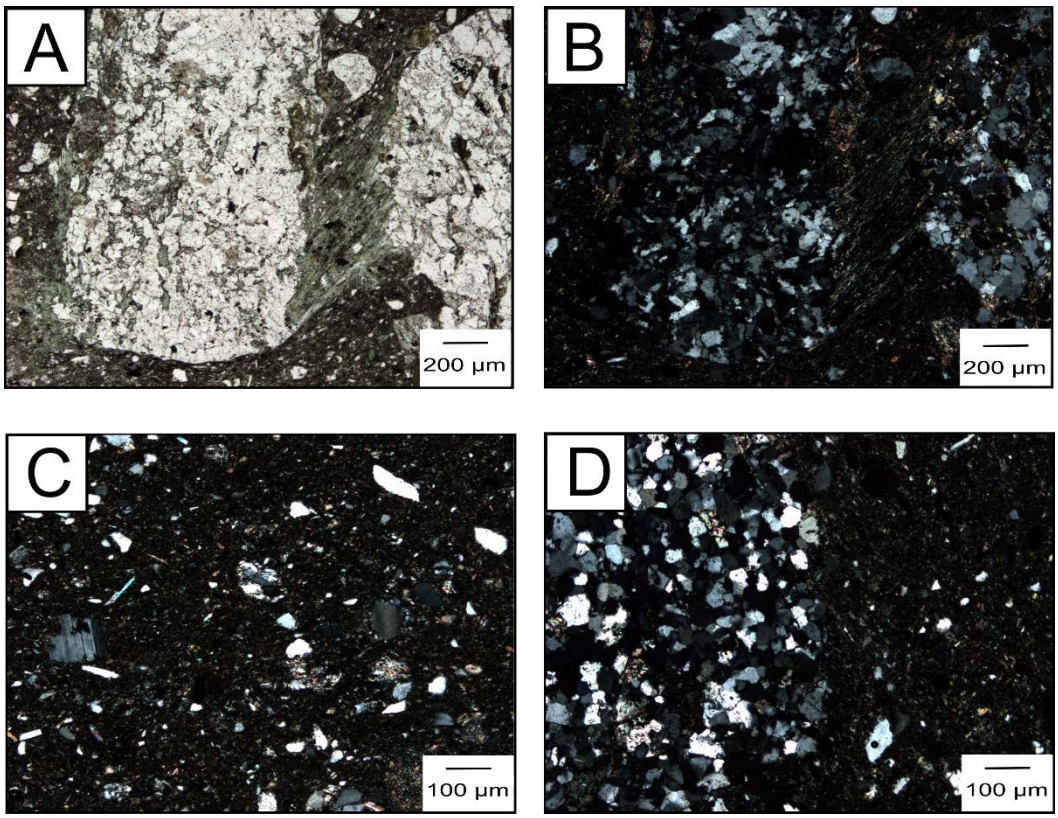

Figure 16.

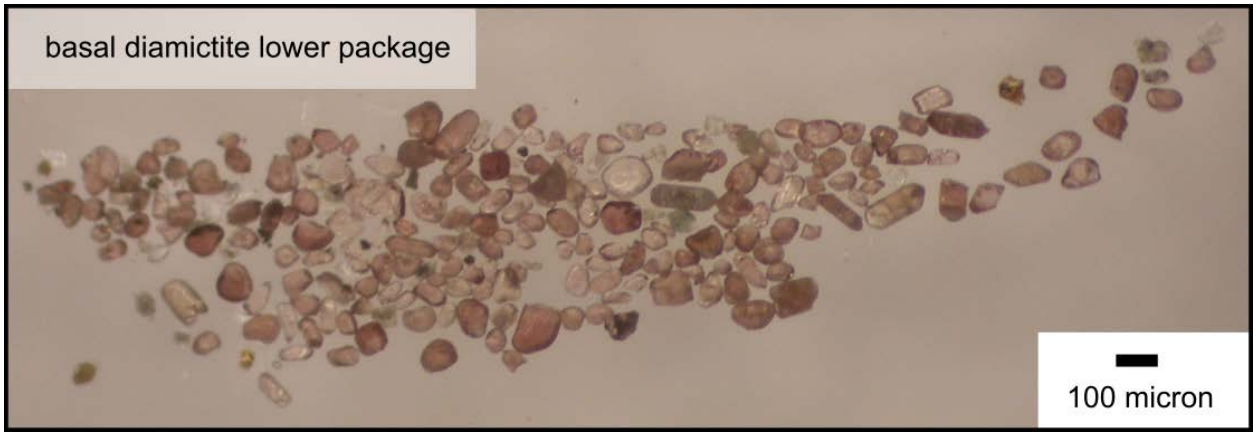

Figure 17.

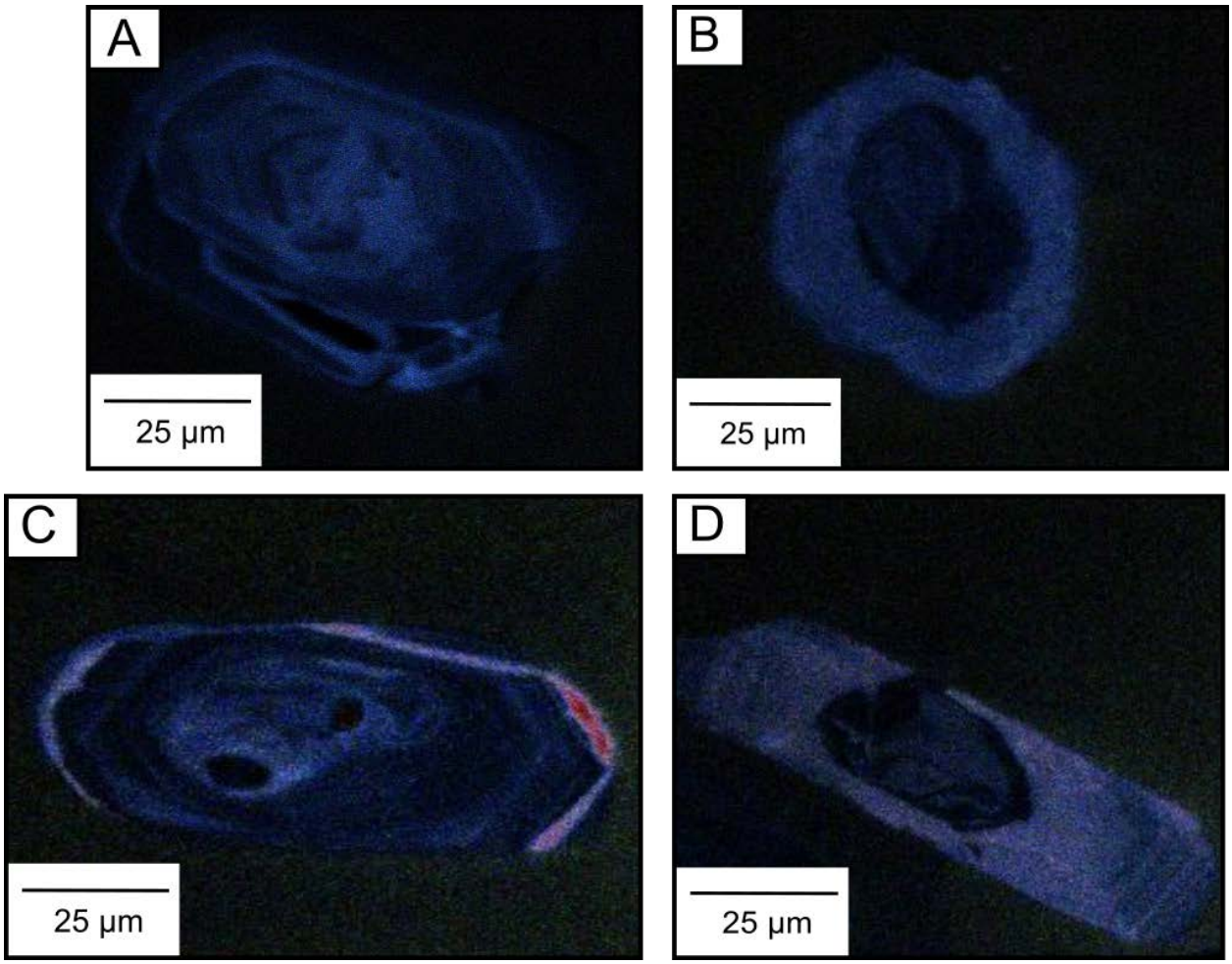

Figure 18.

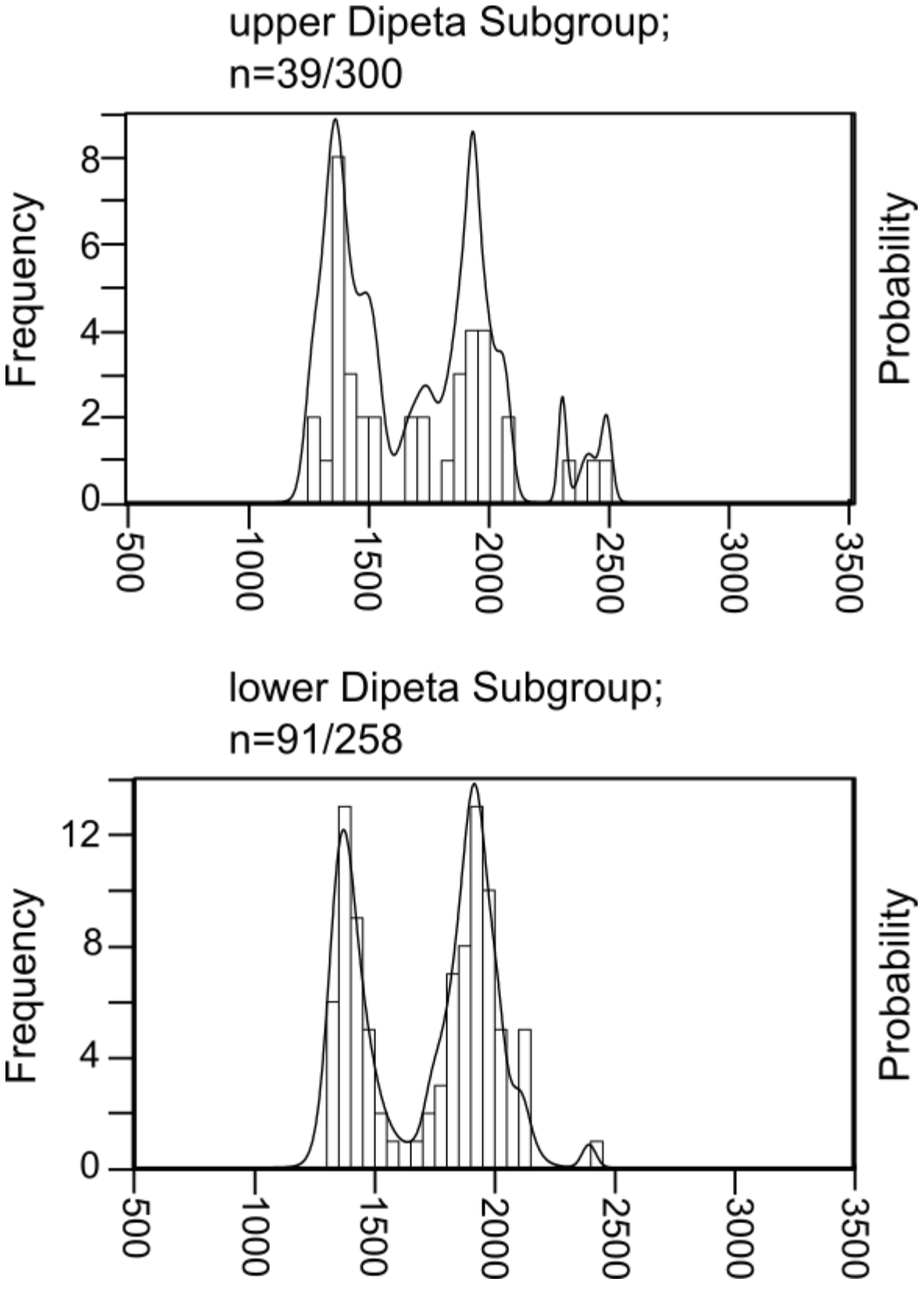
upper Dipeta Subgroup;
n=39/300
Frequency
Probability
0
2
4
6
8
500
1000
1500
2000
2500
3000
3500
lower Dipeta Subgroup;
n=91/258
Frequency
Probability
0
4
8
12
500
1000
1500
2000
2500
3000
3500

Figure 19.

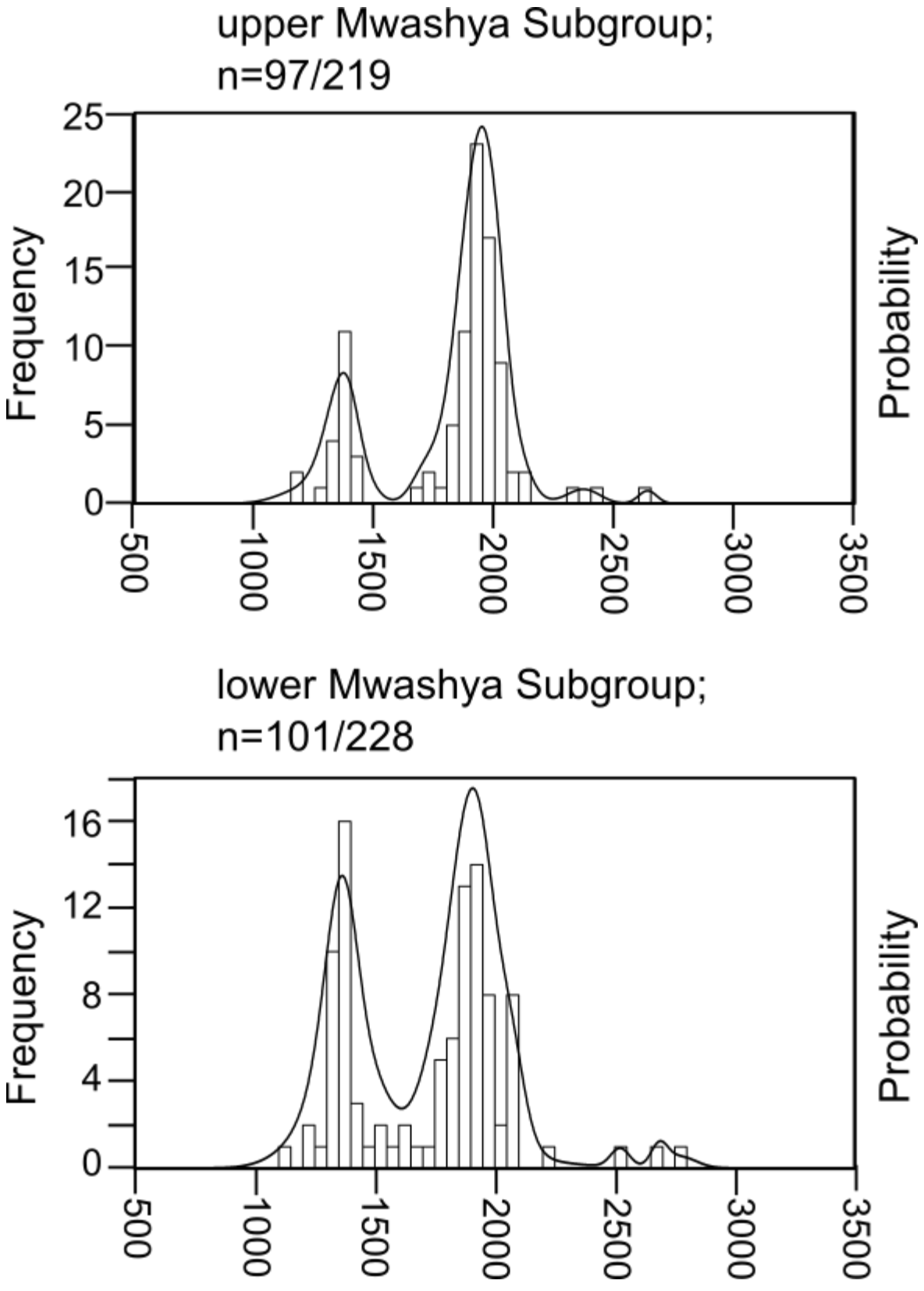
upper Mwashya Subgroup;
n=97/219
Frequency
Probability
25
20
15
10
5
0
500
1000
1500
2000
2500
3000
3500
lower Mwashya Subgroup;
n=101/228
Frequency
Probability
16
12
8
4
0
500
1000
1500
2000
2500
3000
3500

Figure 20.

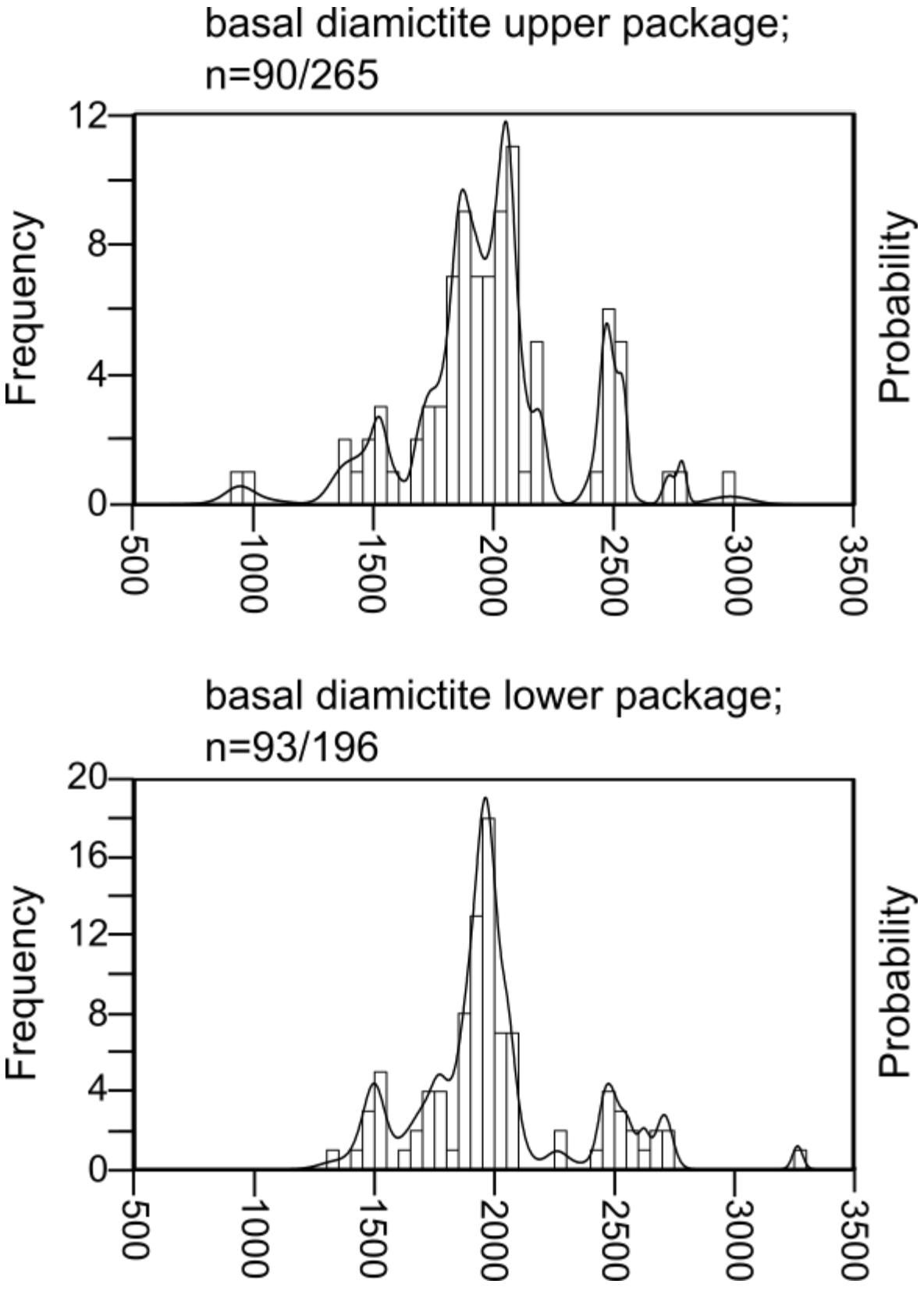
basal diamictite upper package;
n=90/265
Frequency
Probability
0
4
8
12
500
1000
1500
2000
2500
3000
3500
basal diamictite lower package;
n=93/196
Frequency
Probability
0
4
8
12
16
20
500
1000
1500
2000
2500
3000
3500

Figure 21.

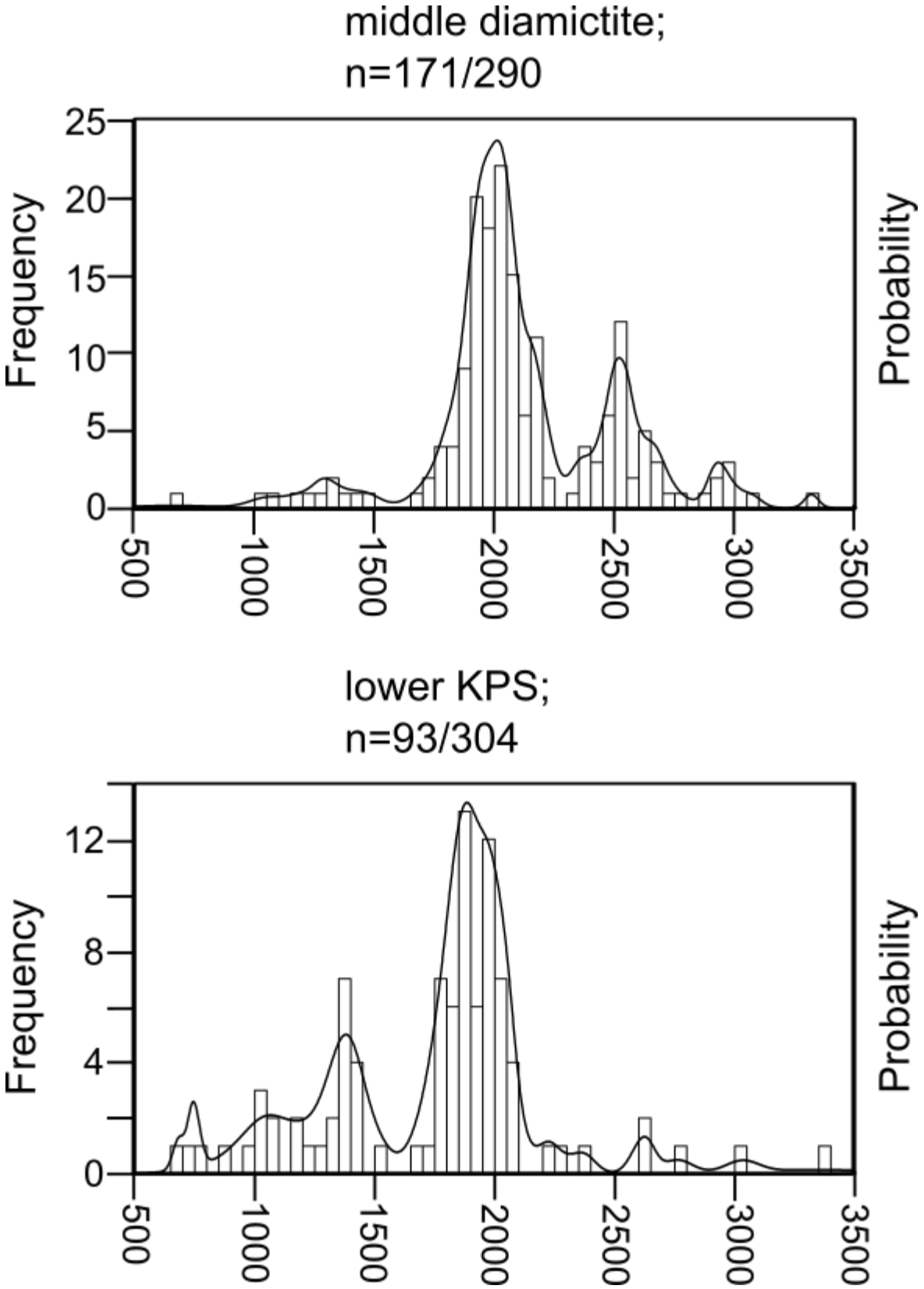
middle diamictite;
n=171/290
Frequency
Probability
25
20
15
10
5
0
500
1000
1500
2000
2500
3000
3500
lower KPS;
n=93/304
Frequency
Probability
12
8
4
0
500
1000
1500
2000
2500
3000
3500

Figure 22.

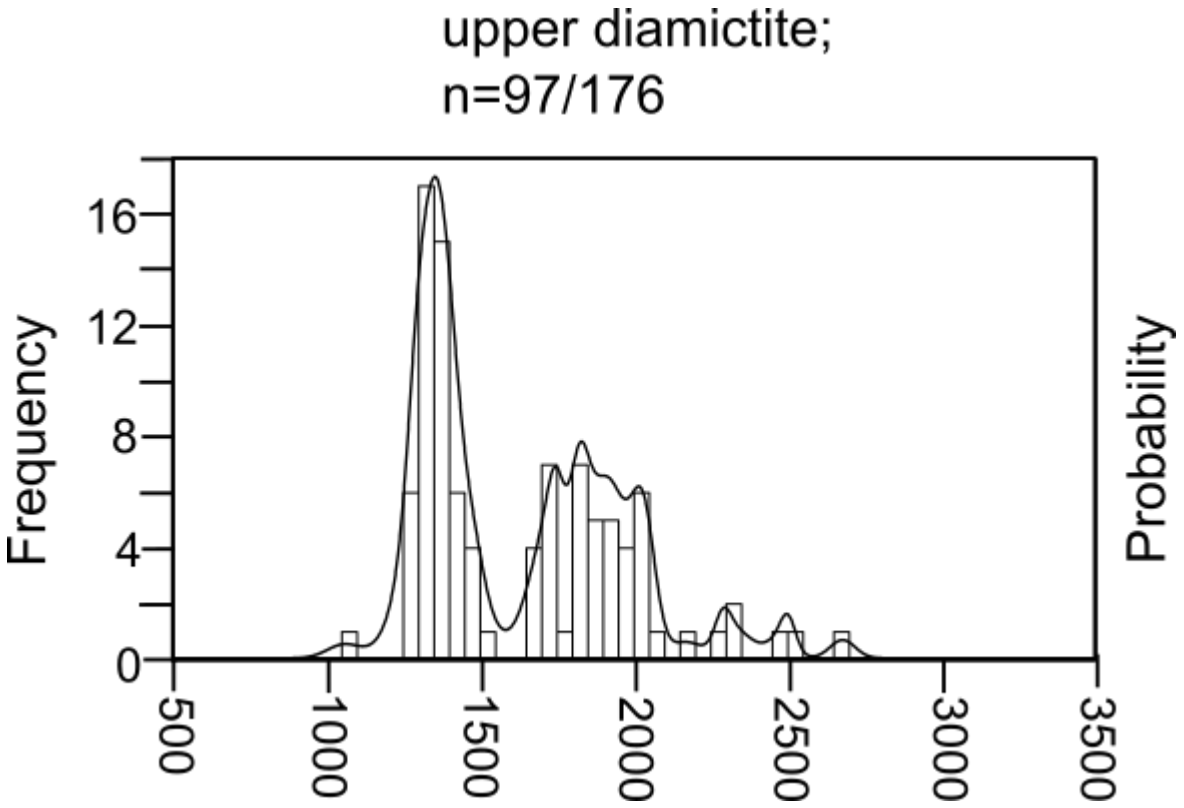
upper diamictite;
n=97/176
Frequency
Probability
0
4
8
12
16
500
1000
1500
2000
2500
3000
3500

Figure 23.

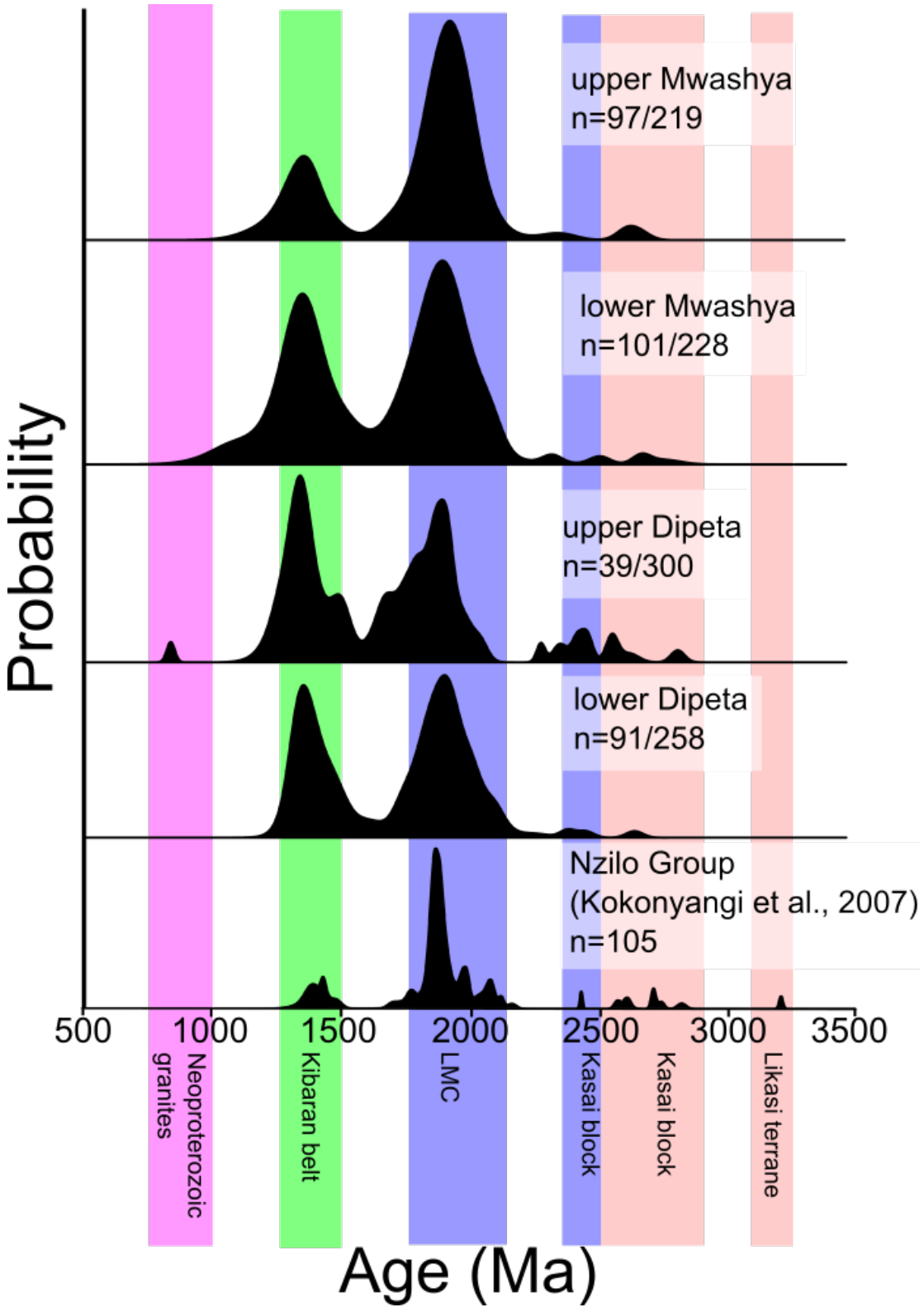
upper Mwashya
n=97/219
lower Mwashya
n=101/228
upper Dipeta
n=39/300
lower Dipeta
n=91/258
Nzilo Group
(Kokonyangi et al., 2007)
n=105
Probability
500
1000
1500
2000
2500
3000
3500
Age (Ma)
Neoproterozoic granites
Kibaran belt
LMC
Kasai block
Kasai block
Likasi terrane

Figure 24.

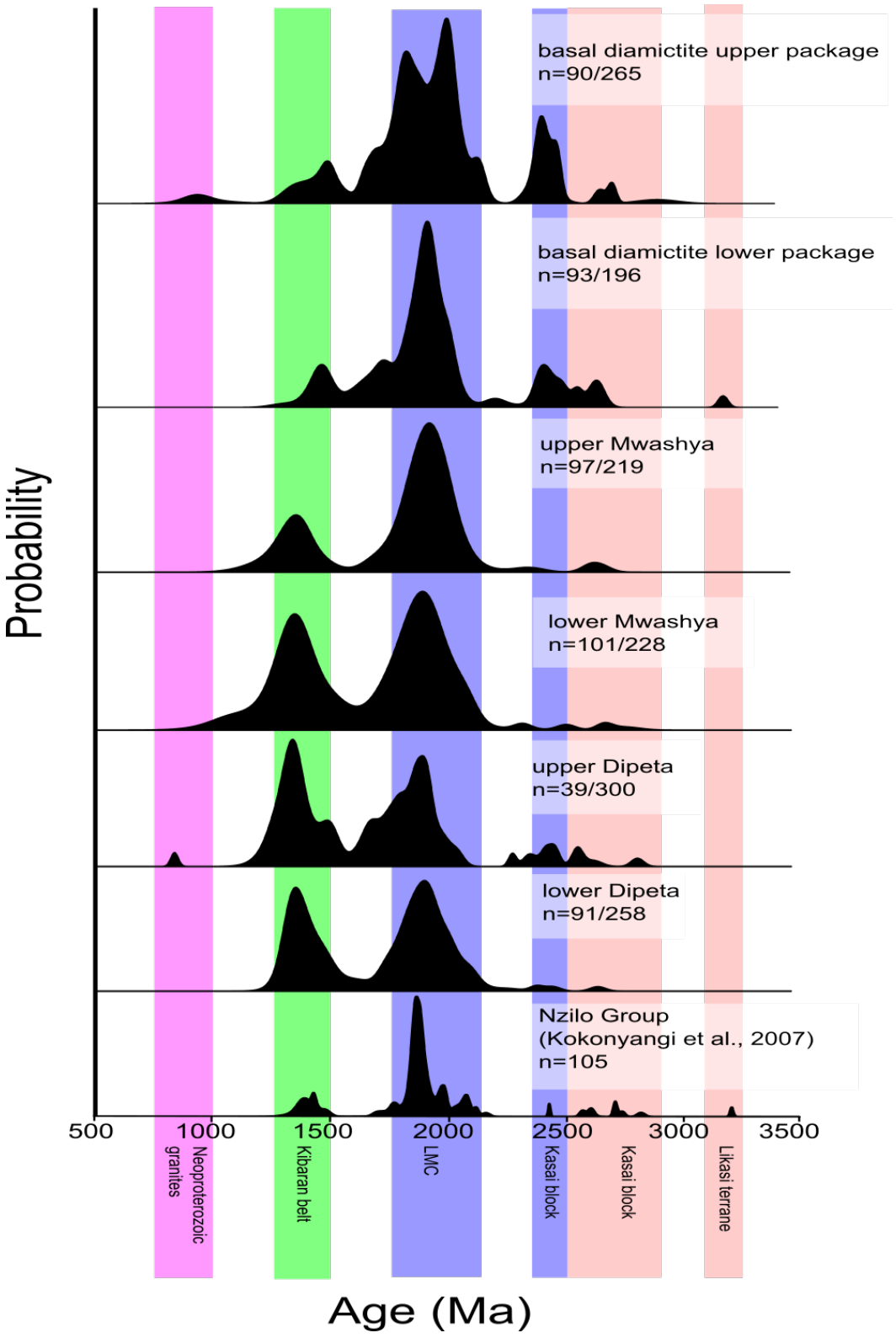
basal diamictite upper package
n=90/265
basal diamictite lower package
n=93/196
upper Mwashya
n=97/219
lower Mwashya
n=101/228
upper Dipeta
n=39/300
lower Dipeta
n=91/258
Nzilo Group
(Kokonyangi et al., 2007)
n=105
Probability
500
1000
1500
2000
2500
3000
3500
Age (Ma)
Neoproterozoic granites
Kibaran belt
LMC
Kasai block
Kasai block
Likasi terrane

Figure 25.

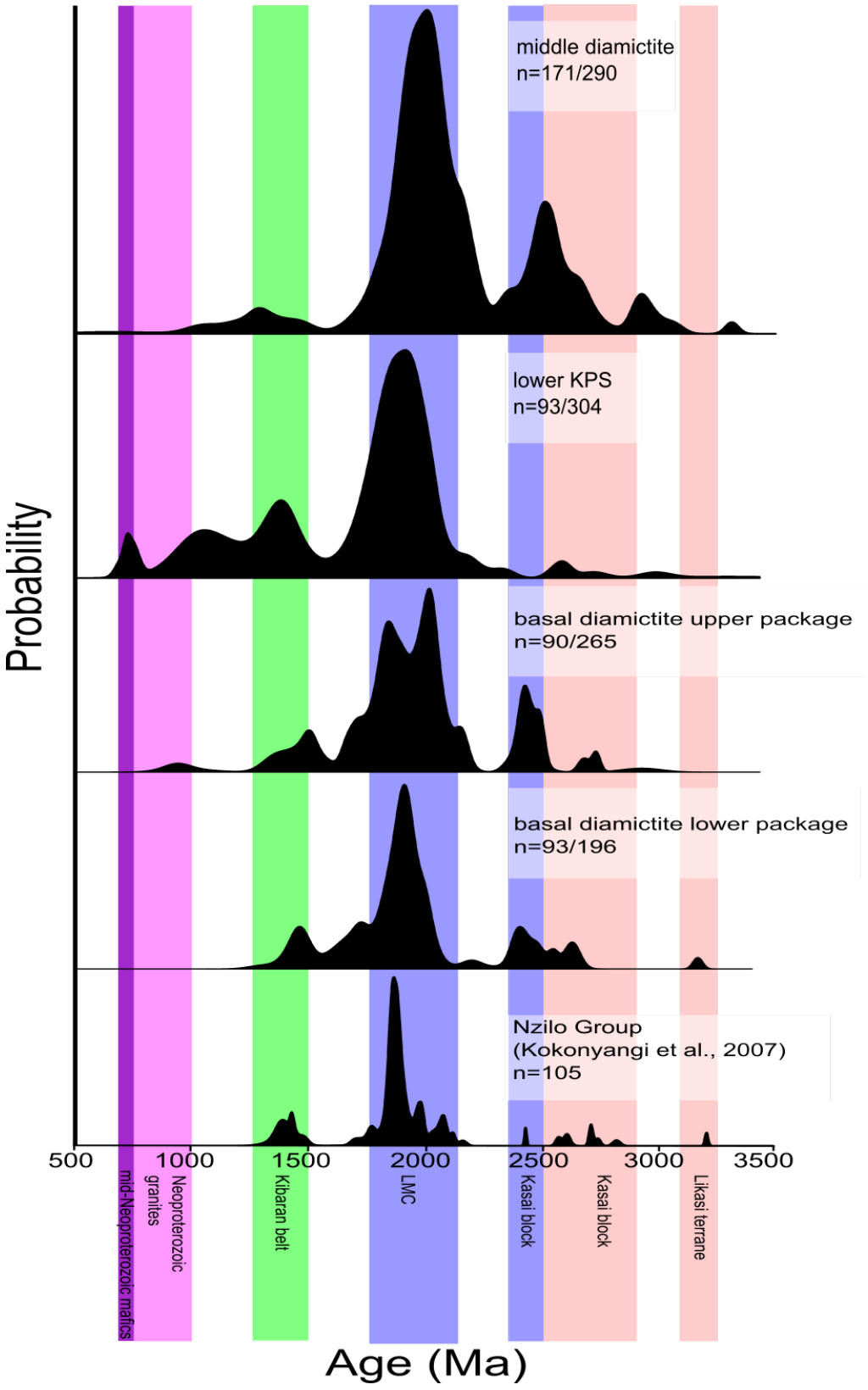
middle diamictite
n=171/290
lower KPS
n=93/304
basal diamictite upper package
n=90/265
basal diamictite lower package
n=93/196
Nzilo Group
(Kokonyangi et al., 2007)
n=105
Probability
500
1000
1500
2000
2500
3000
3500
Age (Ma)
mid-Neoproterozoic mafics
Neoproterozoic granites
Kibaran belt
LMC
Kasai block
Kasai block
Likasi terrane

Figure 26.

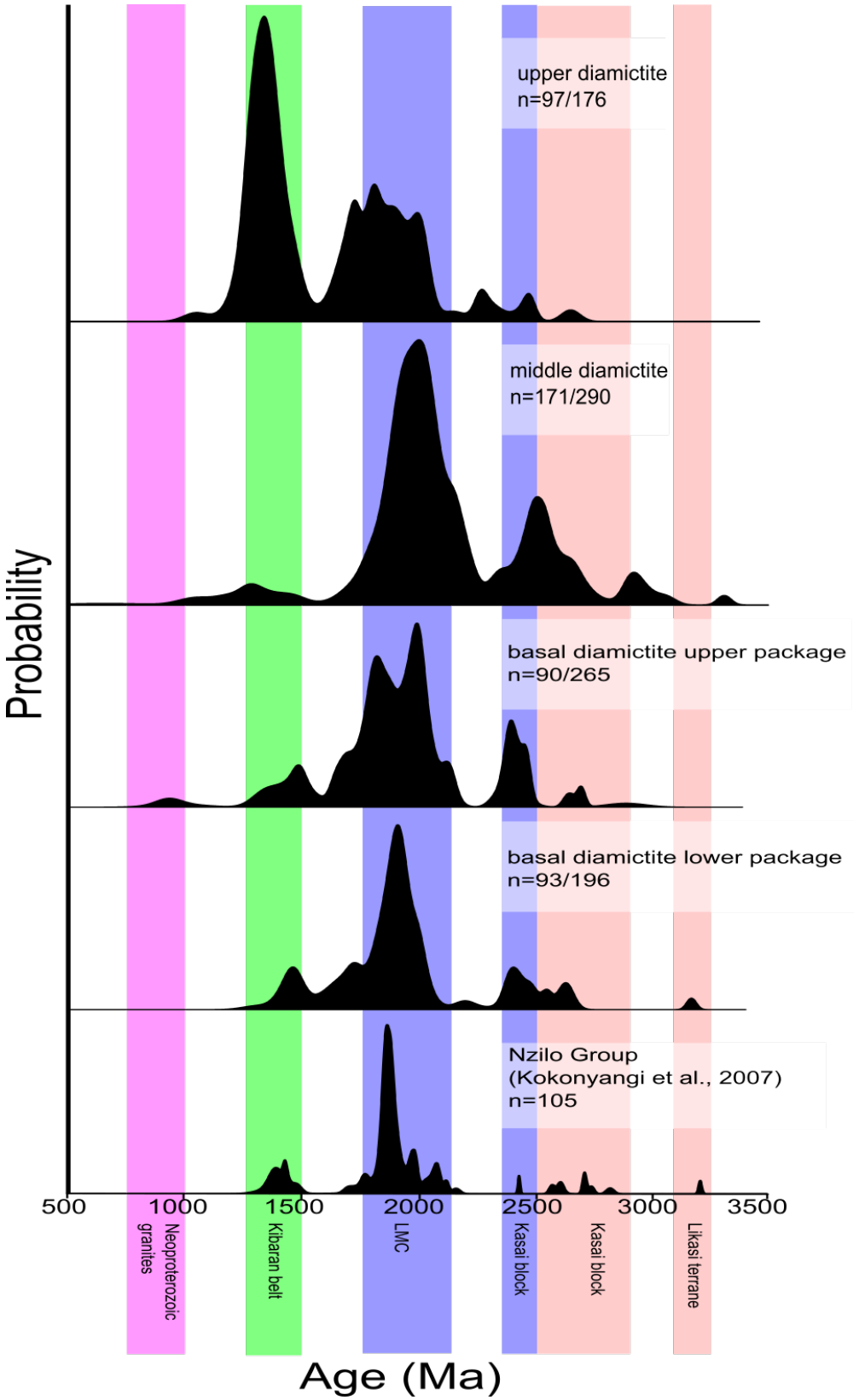
upper diamictite
n=97/176
middle diamictite
n=171/290
basal diamictite upper package
n=90/265
basal diamictite lower package
n=93/196
Nzilo Group
(Kokonyangi et al., 2007)
n=105
Probability
500
1000
1500
2000
2500
3000
3500
Age (Ma)
Neoproterozoic granites
Kibaran belt
LMC
Kasai block
Kasai block
Likasi terrane

Figure 27.

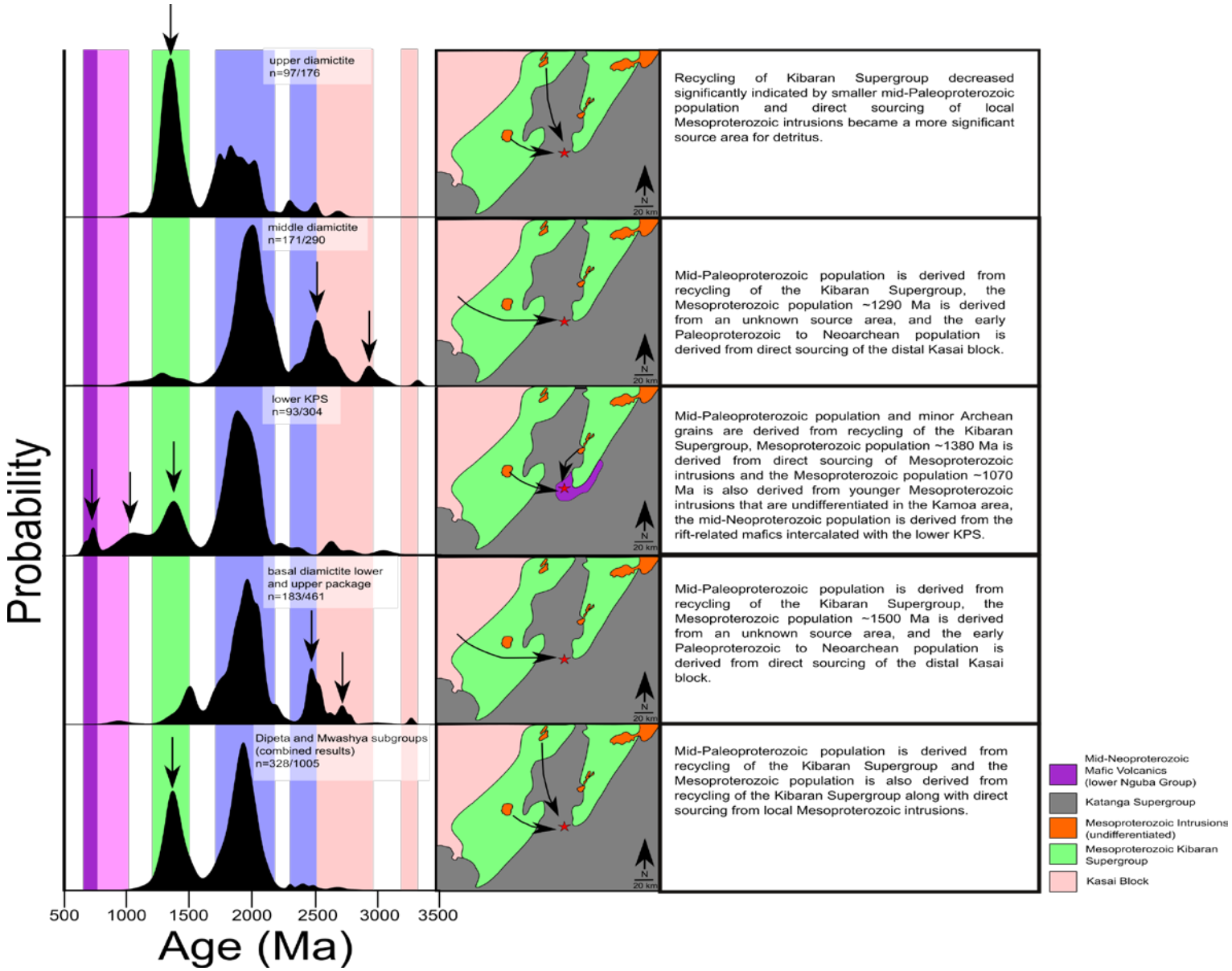
upper diamictite
n=97/176
middle diamictite
n=171/290
lower KPS
n=93/304
basal diamictite lower
and upper package
n=183/461
Dipeta and Mwashya subgroups
(combined results)
n=328/1005
Probability
500
1000
1500
2000
2500
3000
3500
Age (Ma)
Recycling of Kibaran Supergroup decreased significantly indicated by smaller mid-Paleoproterozoic population and direct sourcing of local Mesoproterozoic intrusions became a more significant source area for detritus.
Mid-Paleoproterozoic population is derived from recycling of the Kibaran Supergroup, the Mesoproterozoic population ~1290 Ma is derived from an unknown source area, and the early Paleoproterozoic to Neoarchean population is derived from direct sourcing of the distal Kasai block.
Mid-Paleoproterozoic population and minor Archean grains are derived from recycling of the Kibaran Supergroup, Mesoproterozoic population ~1380 Ma is derived from direct sourcing of Mesoproterozoic intrusions and the Mesoproterozoic population ~1070 Ma is also derived from younger Mesoproterozoic intrusions that are undifferentiated in the Kamoa area, the mid-Neoproterozoic population is derived from the rift-related mafics intercalated with the lower KPS.
Mid-Paleoproterozoic population is derived from recycling of the Kibaran Supergroup, the Mesoproterozoic population ~1500 Ma is derived from an unknown source area, and the early Paleoproterozoic to Neoarchean population is derived from direct sourcing of the distal Kasai block.
Mid-Paleoproterozoic population is derived from recycling of the Kibaran Supergroup and the Mesoproterozoic population is also derived from recycling of the Kibaran Supergroup along with direct sourcing from local Mesoproterozoic intrusions.
N
20 km
Mid-Neoproterozoic Mafic Volcanics (lower Nguba Group)
Katanga Supergroup
Mesoproterozoic Intrusions (undifferentiated)
Mesoproterozoic Kibaran Supergroup
Kasai Block

Figure 28.

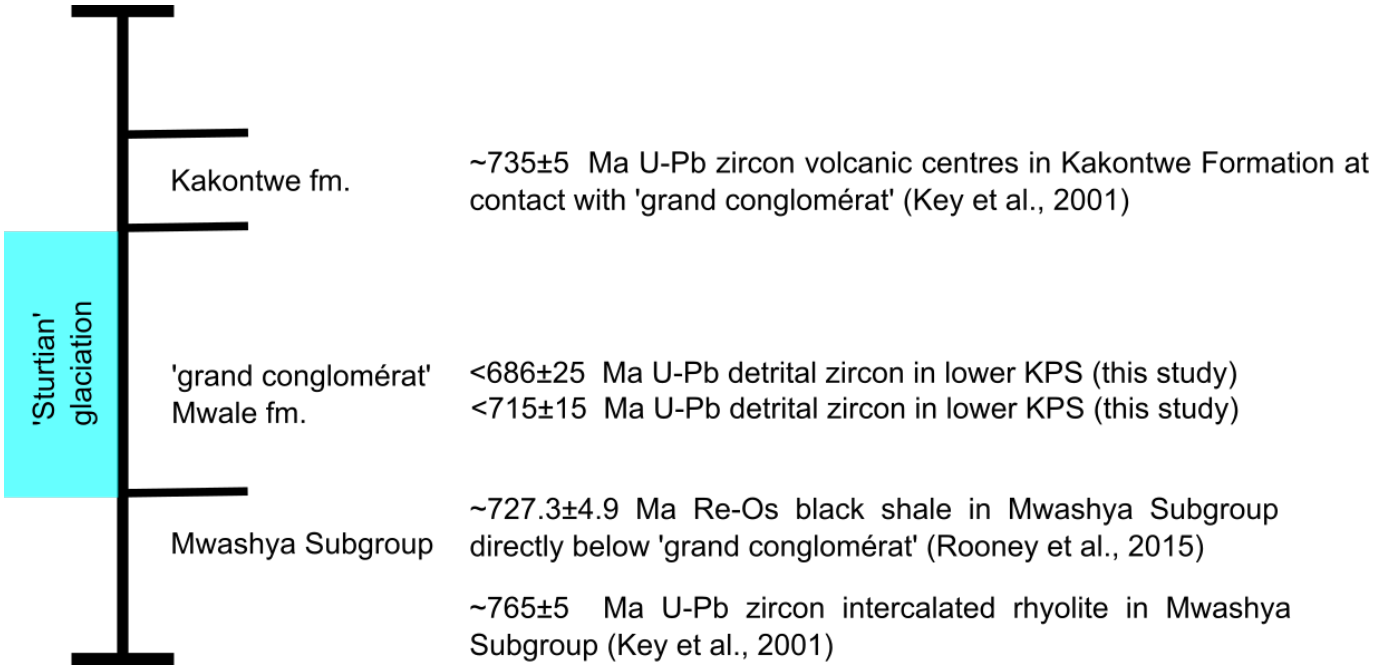
'Sturtian' glaciation
Kakontwe fm.
'grand conglomérat'
Mwale fm.
Mwashya Subgroup
~735±5 Ma U-Pb zircon volcanic centres in Kakontwe Formation at contact with 'grand conglomérat' (Key et al., 2001)
<686±25 Ma U-Pb detrital zircon in lower KPS (this study)
<715±15 Ma U-Pb detrital zircon in lower KPS (this study)
~727.3±4.9 Ma Re-Os black shale in Mwashya Subgroup directly below 'grand conglomérat' (Rooney et al., 2015)
~765±5 Ma U-Pb zircon intercalated rhyolite in Mwashya Subgroup (Key et al., 2001)

Figure 29.

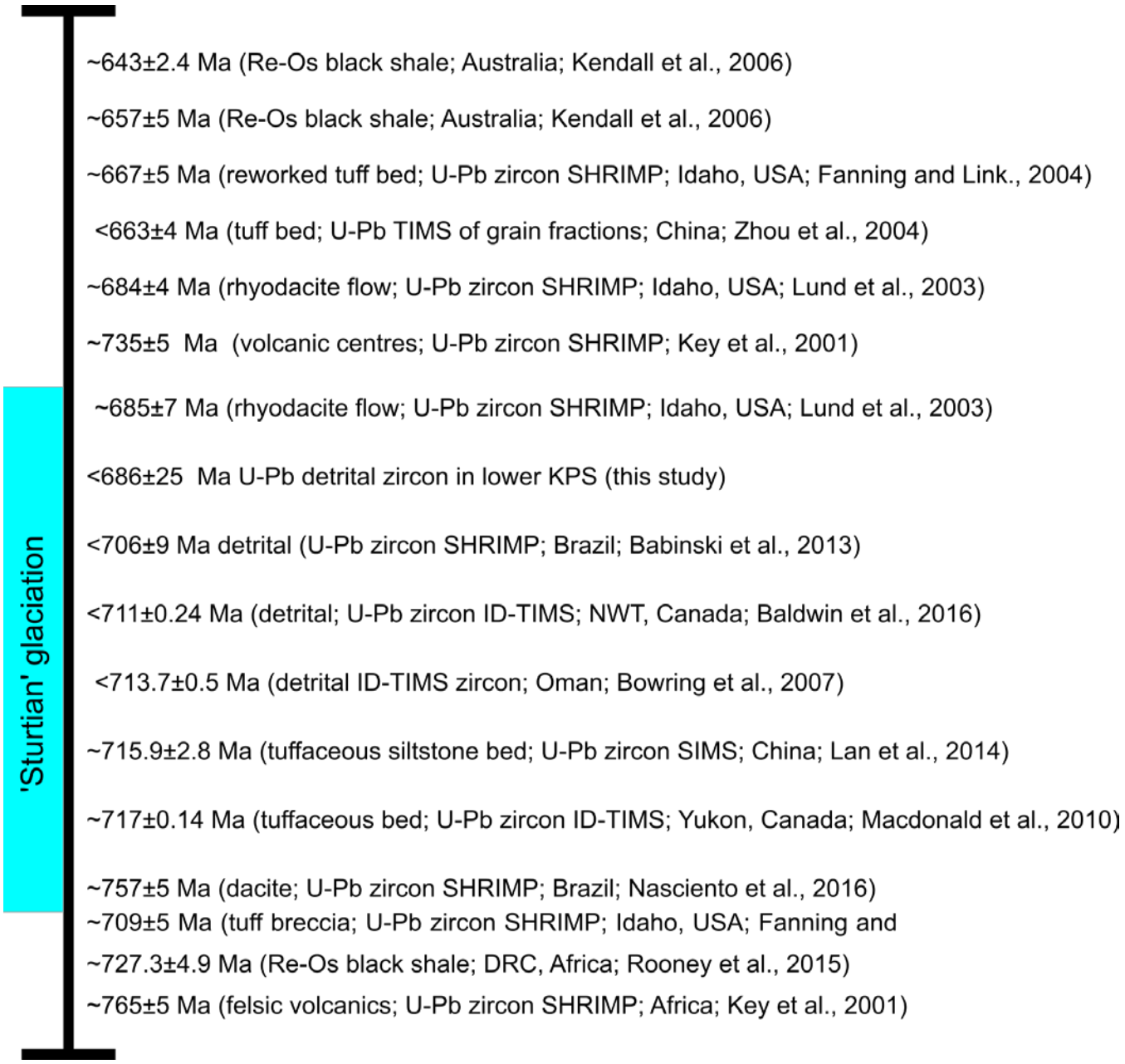
'Sturtian' glaciation
~643±2.4 Ma (Re-Os black shale; Australia; Kendall et al., 2006)
~657±5 Ma (Re-Os black shale; Australia; Kendall et al., 2006)
~667±5 Ma (reworked tuff bed; U-Pb zircon SHRIMP; Idaho, USA; Fanning and Link., 2004)
<663±4 Ma (tuff bed; U-Pb TIMS of grain fractions; China; Zhou et al., 2004)
~684±4 Ma (rhyodacite flow; U-Pb zircon SHRIMP; Idaho, USA; Lund et al., 2003)
~735±5 Ma (volcanic centres; U-Pb zircon SHRIMP; Key et al., 2001)
~685±7 Ma (rhyodacite flow; U-Pb zircon SHRIMP; Idaho, USA; Lund et al., 2003)
<686±25 Ma U-Pb detrital zircon in lower KPS (this study)
<706±9 Ma detrital (U-Pb zircon SHRIMP; Brazil; Babinski et al., 2013)
<711±0.24 Ma (detrital; U-Pb zircon ID-TIMS; NWT, Canada; Baldwin et al., 2016)
<713.7±0.5 Ma (detrital ID-TIMS zircon; Oman; Bowring et al., 2007)
~715.9±2.8 Ma (tuffaceous siltstone bed; U-Pb zircon SIMS; China; Lan et al., 2014)
~717±0.14 Ma (tuffaceous bed; U-Pb zircon ID-TIMS; Yukon, Canada; Macdonald et al., 2010)
~757±5 Ma (dacite; U-Pb zircon SHRIMP; Brazil; Nasciento et al., 2016)
~709±5 Ma (tuff breccia; U-Pb zircon SHRIMP; Idaho, USA; Fanning and
~727.3±4.9 Ma (Re-Os black shale; DRC, Africa; Rooney et al., 2015)
~765±5 Ma (felsic volcanics; U-Pb zircon SHRIMP; Africa; Key et al., 2001)

Figure 30.

Appendices

Spot #	Compositional Data				Isotope Ratios						Apparent Ages (Ma)						Discordance
	U (ppm)	Th (ppm)	U Th	Pb (ppm)	207Pb 235U	±207Pb 235U	206Pb 238U	±206Pb 238U	207Pb 206Pb	±207Pb 206Pb	207Pb 235U	±207Pb 235U	206Pb 238U	±206Pb 238U	207Pb 206Pb	±207Pb 206Pb	(%)
4	380	171	2.07	149.8	5.5	0.3	0.34	0.017	0.12	0.003	1852	58	1887	84	1871	42	-0.9
7	365	172.8	2.14	115.2	3.1	0.1	0.24	0.004	0.09	0.003	1412	25	1392	23	1459	58	4.6
8	533	281.9	1.973	182	2.8	0.055	0.23	0.005	0.09	0.002	1341	15	1343	26	1351	34	0.6
10	1521	803	1.92	452	2.8	0.072	0.24	0.005	0.09	0.002	1339	19	1365	26	1346	37	-1.4
11	586	103.8	6.75	62.5	2.7	0.059	0.24	0.004	0.09	0.002	1339	16	1368	21	1318	43	-3.8
15	462	171	2.727	113.5	3.3	0.12	0.25	0.006	0.09	0.003	1459	27	1455	28	1479	55	1.6
16	982	591	1.81	518	9.4	0.22	0.45	0.009	0.16	0.003	2377	20	2377	41	2403	29	1.1
17	313	340	1.014	283	5.7	0.13	0.35	0.007	0.12	0.002	1922	20	1919	33	1946	35	1.4
18	260	187	1.503	159.1	5.1	0.18	0.33	0.014	0.12	0.003	1834	31	1827	68	1879	50	2.8
19	150	345	0.4505	291	5.3	0.13	0.34	0.006	0.11	0.003	1861	21	1890	31	1846	45	-2.4
23	848	538	1.599	393	4.2	0.08	0.29	0.005	0.11	0.002	1680	15	1661	26	1738	31	4.4
26	1323	601	2.263	561	6.5	0.1	0.39	0.007	0.13	0.002	2046	14	2098	31	2026	27	-3.6
30	712	1320	0.557	921	5.3	0.16	0.34	0.010	0.12	0.002	1855	24	1855	49	1903	34	2.5
31	120.4	137	0.887	108.2	4.4	0.2	0.30	0.006	0.11	0.004	1683	28	1686	30	1701	61	0.9
32	390	204	2.26	125	3.0	0.1	0.24	0.005	0.09	0.002	1383	23	1386	26	1406	51	1.4
37	830	206.4	3.76	173	4.9	0.15	0.32	0.009	0.11	0.003	1799	27	1802	46	1838	43	2.0
39	252	201	1.279	205	6.9	0.27	0.38	0.016	0.13	0.004	2092	34	2074	74	2128	48	2.5
40	1175	580	2.085	464	6.0	0.12	0.36	0.007	0.12	0.002	1966	18	1967	35	1996	31	1.5
43	544	203	2.73	149.1	2.8	0.069	0.24	0.006	0.09	0.002	1366	18	1373	29	1371	46	-0.1
46	941	353	2.62	268	4.5	0.11	0.30	0.006	0.11	0.002	1721	20	1698	30	1771	34	4.1
47	350	206	1.824	155	3.1	0.078	0.25	0.005	0.09	0.002	1435	19	1428	23	1441	45	0.9
48	1153	440	2.601	275	2.8	0.064	0.23	0.004	0.09	0.002	1361	17	1354	23	1389	36	2.5
50	1330	626	2.111	370	2.9	0.063	0.23	0.005	0.09	0.002	1375	17	1355	26	1406	38	3.6
55	300	151.2	2.027	124.9	4.8	0.16	0.32	0.008	0.11	0.004	1782	24	1795	38	1795	65	0.0
57	675	447	1.496	296	2.9	0.093	0.24	0.007	0.09	0.003	1381	24	1374	34	1419	68	3.2
60	218.3	234.6	0.942	187.1	5.9	0.17	0.36	0.009	0.12	0.003	1949	26	1970	42	1938	43	-1.7
61	431	711	0.592	619	5.8	0.18	0.35	0.008	0.12	0.003	1935	27	1949	37	1911	49	-2.0
63	1096	425	2.546	256.1	2.8	0.094	0.24	0.007	0.09	0.003	1358	25	1365	35	1362	55	-0.2
66	451	323	1.402	310.1	6.0	0.11	0.36	0.007	0.12	0.002	1976	16	1999	31	1940	33	-3.0
69	164.7	157.7	1.085	153.1	5.3	0.12	0.33	0.005	0.11	0.003	1856	20	1855	25	1835	43	-1.1
70	623	334	1.868	220.4	3.0	0.076	0.24	0.005	0.09	0.002	1391	20	1395	24	1360	41	-2.6
73	234	240	1.073	222	5.7	0.15	0.35	0.009	0.12	0.002	1931	22	1941	42	1893	36	-2.5
74	195	203.4	0.953	200.9	6.3	0.14	0.37	0.006	0.12	0.003	2013	20	2043	28	1954	40	-4.6
80	327	300	1.115	341	6.4	0.17	0.37	0.008	0.12	0.003	2031	22	2018	36	1994	42	-1.2
89	592	237.4	2.47	206	5.3	0.13	0.34	0.008	0.11	0.003	1866	21	1885	36	1820	49	-3.6
91	568	216	2.687	160	3.1	0.071	0.25	0.005	0.09	0.002	1423	18	1426	26	1367	42	-4.3
96	378	121.8	3.098	79	2.9	0.08	0.24	0.005	0.09	0.003	1371	21	1379	27	1318	57	-4.6
97	302	160	1.924	116.2	3.1	0.11	0.24	0.006	0.09	0.003	1434	29	1372	32	1442	58	4.9
99	199.1	148.3	1.387	134	6.2	0.16	0.36	0.008	0.12	0.003	1992	23	1961	39	1971	43	0.5
100	105	83	1.53	82	7.7	0.69	0.40	0.016	0.13	0.008	2162	74	2172	74	2100	100	-3.4
104	1000	349	2.857	256	3.7	0.5	0.26	0.007	0.10	0.011	1490	32	1467	35	1450	130	-1.2
106	886	527	1.655	308	2.8	0.093	0.23	0.006	0.09	0.002	1357	24	1336	29	1349	54	1.0
118	525	385	1.372	369	6.3	0.17	0.37	0.007	0.12	0.003	2019	24	2043	35	1975	39	-3.4
122	771	242	3.171	140.8	3.1	0.13	0.25	0.007	0.09	0.003	1417	32	1426	35	1396	69	-2.1
124	1106	384	2.878	240.7	3.0	0.07	0.24	0.007	0.09	0.002	1420	19	1408	33	1418	52	0.7
130	709	405	1.73	258.1	3.0	0.062	0.24	0.005	0.09	0.002	1395	16	1383	26	1362	46	-1.5
143	365	317	1.177	258	5.4	0.18	0.34	0.010	0.11	0.003	1880	28	1883	47	1876	48	-0.4
144	1000	270	3.15	359	7.2	0.41	0.39	0.023	0.13	0.002	2094	57	2110	110	2122	30	0.6
146	206.8	87.1	2.365	80.9	5.7	0.15	0.35	0.008	0.12	0.003	1919	24	1920	40	1912	40	-0.4
148	435.6	285	1.94	234	5.4	0.11	0.34	0.006	0.12	0.002	1877	18	1868	28	1886	36	1.0
155	1006	165.3	6.37	115.8	3.0	0.057	0.25	0.005	0.09	0.002	1410	15	1414	24	1400	32	-1.0
161	269	170	1.77	122.4	5.3	0.14	0.34	0.010	0.12	0.003	1869	23	1864	47	1871	50	0.4
163	1069	908	1.209	762	5.9	0.11	0.37	0.008	0.12	0.002	1960	17	2011	40	1928	35	-4.3
168	498	565	0.944	471	5.2	0.14	0.33	0.008	0.12	0.003	1854	25	1837	38	1884	49	2.5
170	191.6	65.7	3.012	60.3	3.9	0.18	0.28	0.008	0.10	0.004	1593	31	1589	37	1565	71	-1.5
171	735	298	2.54	236	3.3	0.082	0.26	0.006	0.09	0.003	1489	20	1493	31	1451	53	-2.9
173	246	197.3	1.239	177	5.8	0.22	0.35	0.008	0.12	0.005	1932	30	1951	39	1888	68	-3.3
176	915	570	1.638	291	2.8	0.084	0.23	0.005	0.09	0.002	1361	22	1356	25	1391	48	2.5
177	116.5	127.4	0.909	137.1	6.9	0.28	0.39	0.013	0.13	0.005	2106	37	2113	59	2105	71	-0.4
181	474	218	2.26	152	3.3	0.22	0.25	0.009	0.10	0.007	1465	48	1425	46	1500	110	5.0
182	394	1060	0.464	790	5.9	0.23	0.35	0.010	0.12	0.005	1942	30	1937	49	1954	59	0.9
183	532	282	2.05	180	2.8	0.086	0.24	0.006	0.09	0.002	1360	23	1378	32	1347	38	-2.3
189	445	527	0.839	478.8	6.0	0.11	0.36	0.006	0.12	0.002	1975	16	1985	28	1950	31	-1.8
190	561	381	1.53	364	6.4	0.17	0.38	0.015	0.13	0.004	2023	23	2067	71	2037	59	-1.5
192	487	410	1.243	377	6.6	0.13	0.39	0.008	0.13	0.003	2056	18	2104	36	2020	34	-4.2
193	876	108.1	8.11	157.6	5.6	0.13	0.33	0.007	0.12	0.003	1912	19	1860	33	1947	38	4.5
197	293	124.1	2.375	118.4	5.8	0.15	0.36	0.009	0.12	0.003	1936	22	1973	41	1914	50	-3.1
199	191.3	249	0.777	260	5.0	0.16	0.32	0.007	0.11	0.004	1818	27	1792	35	1829	61	2.0
201	470	256.2	1.838	345	7.1	0.2	0.39	0.007	0.13	0.004	2125	24	2108	28	2115	49	0.3
207	264	213.8	1.251	197.6	6.1	0.21	0.37	0.012	0.12	0.005	1992	32	2029	55	1975	68	-2.7
208	438	201	2.22	137.8	3.1	0.11	0.25	0.006	0.09	0.004	1427	28	1436	32	1448	69	0.8
210	1054	144	13.6	64	5.7	0.2	0.35	0.012	0.12	0.003	1933	29	1941	60	1947	44	0.3
217	386.4	781	0.531	616	4.9	0.15	0.32	0.008	0.11	0.003	1793	26	1778	39	1836	48	3.2
223	143.4	138.4	1.084	152.8	6.7	0.23	0.38	0.007	0.13	0.004	2051	30	2056	35	2040	46	-0.8
224	487	242	2.055	165.6	3.5	0.11	0.27	0.007	0.10	0.003	1527	23	1527	37	1531	55	0.3
225	144.7	104	1.414	74.8	3.5	0.12	0.27	0.006	0.09	0.003	1519	28	1538	31	1489	69	-3.3
226	278	131	1.87	90	4.0	0.21	0.29	0.018	0.11	0.008	1610	44	1608	91	1680	130	4.3
232	1337	423	3.18	349	5.5	0.17	0.34	0.009	0.12	0.003	1897	28	1886	44	1923	41	1.9
235	804	436	1.851	480	6.1	0.18	0.35	0.009	0.13	0.003	1985	26	1928	42	2018	47	4.5
239	436	150	3.1	106	3.0	0.081	0.24	0.005	0.09	0.002	1392	20	1397	23	1344	48	-3.9
241	355	139.1	2.53	93.6	2.8	0.077	0.23	0.006	0.09	0.003	1353	21	1326	29	1387	56	4.4
243	446	178	2.42	161	5.9	0.15	0.35	0.007	0.12	0.003	1951	22	1951	31	1934	42	-0.9
244	340	197.7	1.727	126.1	3.1	0.08	0.25	0.004	0.09	0.002	1416	20	1420	21	1386	51	-2.5
245	482	217.6	2.238	146.7	3.0	0.062	0.24	0.004	0.09	0.002	1402	16	1400	22	1376	39	-1.7
246	257.3	124.3	2.094	87	3.1	0.1	0.25	0.006	0.09	0.003	1426	25	1423	31	1367	54	-4.1
247	620	906	0.706	815	6.2	0.16	0.37	0.011	0.12	0.004	2003	23	2011	50	1990	53	-1.1
251	150.2	108.4	1.361	100.9	6.4	0.4	0.37	0.007	0.13	0.007	1997	35	2029	32	1955	56	-3.8
253	298.6	153.5	1.979	89.9	3.2	0.094	0.25	0.006	0.09	0.002	1447	21	1442	33	1449	47	0.5
257	667	316	2.136	319	5.9	0.11	0.36	0.007	0.12	0.002	1965	16	1986	32	1912	29	-3.9
259	714	577	1.38	284	5.0	0.47	0.32	0.023	0.11	0.004	1767	87	1770	110	1804	67	1.9
265	342	168	2.036	146	5.0	0.12	0.33	0.007	0.11	0.003	1809	21	1837	31	1772	43	-3.7

Lower Dipeta Subgroup

Spot #	Compositional Data				Isotope Ratios						Apparent Ages (Ma)						Discordance
	U (ppm)	Th (ppm)	U Th	Pb (ppm)	207Pb 235U	±207Pb 235U	206Pb 238U	±206Pb 238U	207Pb 206Pb	±207Pb 206Pb	207Pb 235U	±207Pb 235U	206Pb 238U	±206Pb 238U	207Pb 206Pb	±207Pb 206Pb	(%)
24	754	317	2.497	198	3.06	0.07	0.24	0.003	0.09	0.002	1419	18	1363	17	1365	44	0.15
26	951	229.5	4.191	227.7	6.21	0.08	0.37	0.004	0.12	0.001	2005	11	2012	20	1932	20	-4.14
28	1087	625	1.793	651	7.42	0.12	0.40	0.005	0.13	0.002	2162	15	2155	23	2063	28	-4.46
35	326	216.3	1.498	215.5	6.37	0.13	0.37	0.005	0.12	0.002	2024	18	2020	23	1941	36	-4.07
40	188.3	120.1	1.577	121.6	6.34	0.14	0.37	0.005	0.12	0.003	2020	19	2041	24	1952	42	-4.56
42	495	190	2.694	129	2.96	0.08	0.24	0.004	0.09	0.002	1392	20	1383	21	1353	48	-2.22
45	166.6	101.6	4.4	94	6.00	0.12	0.36	0.005	0.12	0.003	1973	17	1978	22	1920	38	-3.02
55	162.4	188.3	0.858	154.5	4.99	0.11	0.33	0.005	0.11	0.002	1813	19	1823	22	1822	35	-0.05
61	441	122.5	3.567	84.8	3.16	0.09	0.25	0.005	0.09	0.002	1442	21	1452	25	1490	42	2.55
67	63.2	28.9	2.252	21.5	4.82	0.12	0.32	0.005	0.12	0.003	1784	21	1803	23	1879	43	4.04
87	483	225	2.05	312	10.67	0.55	0.47	0.025	0.16	0.002	2440	67	2440	120	2484	22	1.77
88	141	204.4	0.753	231.6	5.80	0.24	0.34	0.015	0.12	0.004	1930	38	1883	74	1965	57	4.17
90	589.1	80.4	7.61	57.6	2.54	0.06	0.21	0.003	0.08	0.002	1285	16	1240	16	1286	42	3.58
99	227	242.1	0.952	227.5	5.51	0.28	0.34	0.017	0.11	0.003	1893	47	1857	86	1863	50	0.32
108	230	63.8	3.55	42	2.95	0.15	0.24	0.011	0.09	0.003	1395	39	1390	61	1352	59	-2.81
113	544	400	1.5	253	3.23	0.09	0.24	0.007	0.09	0.002	1459	22	1400	37	1442	50	2.91
120	479	137.1	3.339	105	2.99	0.08	0.24	0.006	0.09	0.002	1406	23	1401	32	1388	47	-0.94
125	585	411	2.89	232	2.98	0.06	0.24	0.003	0.09	0.002	1401	15	1402	15	1356	36	-3.39
130	293	124.6	2.344	130.2	5.36	0.18	0.34	0.011	0.12	0.002	1868	29	1869	52	1881	33	0.64
133	617	241	2.646	177.5	2.72	0.06	0.23	0.003	0.09	0.002	1331	15	1316	18	1350	40	2.52
139	664	278	2.405	200.6	2.84	0.06	0.24	0.003	0.09	0.002	1361	17	1362	16	1363	33	0.07
149	636	156.9	4.09	155.1	3.43	0.11	0.25	0.008	0.09	0.002	1501	25	1440	43	1498	38	3.87
162	567	691	0.837	545	4.85	0.09	0.33	0.005	0.11	0.002	1794	16	1835	26	1748	34	-4.98
194	353	215.4	1.63	173.4	4.83	0.44	0.31	0.028	0.11	0.003	1744	89	1700	150	1713	56	0.76
196	440.9	310	1.481	247	3.85	0.08	0.28	0.006	0.09	0.002	1603	17	1571	29	1512	39	-3.90
221	726	260	2.89	167	2.71	0.09	0.24	0.008	0.09	0.002	1325	26	1360	41	1301	46	-4.53
225	109.3	112.6	1.017	95.7	4.23	0.18	0.30	0.008	0.11	0.004	1659	38	1676	41	1694	68	1.06
229	506	596	1.008	581	6.06	0.16	0.36	0.008	0.12	0.003	1979	23	1995	38	1997	44	0.10
240	704	135.7	5.32	85.3	2.44	0.06	0.21	0.005	0.08	0.001	1248	19	1249	24	1264	30	1.19
241	410	474	0.879	374	4.23	0.13	0.30	0.008	0.10	0.003	1680	27	1677	41	1666	48	-0.66
248	1093	453	2.425	368	2.94	0.05	0.24	0.006	0.09	0.002	1391	13	1384	30	1436	45	3.62
252	712	292	2.49	283.2	6.54	0.12	0.38	0.007	0.12	0.002	2052	16	2059	33	1986	32	-3.68
259	658	248.2	2.651	163.7	3.05	0.09	0.24	0.006	0.09	0.002	1415	23	1374	34	1360	53	-1.03
269	521	229	2.313	216	7.13	0.16	0.39	0.008	0.13	0.003	2124	20	2134	36	2054	34	-3.89
280	598	254.5	2.32	202	3.43	0.10	0.26	0.005	0.10	0.002	1507	22	1468	25	1539	37	4.61
281	230	378	0.635	467	9.79	0.27	0.45	0.010	0.16	0.003	2409	26	2379	47	2409	37	1.25
283	1860	588	3.263	682	9.00	0.11	0.44	0.006	0.15	0.001	2336	11	2359	27	2301	17	-2.52
292	256	289	0.913	278	5.96	0.12	0.36	0.006	0.12	0.002	1964	18	1999	26	1919	34	-4.17
296	251.6	127.6	2	98.3	3.05	0.08	0.25	0.005	0.09	0.003	1414	21	1436	27	1413	54	-1.63

Upper Dipeta Subgroup

Spot #	Compositional Data				Isotope Ratios						Apparent Ages (Ma)						Discordance
	U (ppm)	Th (ppm)	U Th	Pb (ppm)	207Pb 235U	±207Pb 235U	206Pb 238U	±206Pb 238U	207Pb 206Pb	±207Pb 206Pb	207Pb 235U	±207Pb 235U	206Pb 238U	±206Pb 238U	207Pb 206Pb	±207Pb 206Pb	(%)
1	339	439	0.79	377	5.8	0.19	0.35	0.010	0.12	0.004	1938	28	1929	44	1949	54	1.03
4	156	187	0.81	152	5.8	0.24	0.36	0.012	0.12	0.005	1923	36	1968	58	1886	69	-4.35
5	257	124	2.40	66	2.4	0.10	0.21	0.007	0.08	0.003	1222	29	1224	35	1211	76	-1.07
13	107.7	69.7	1.61	52	3.0	0.23	0.24	0.012	0.09	0.006	1377	62	1381	64	1330	150	-3.83
14	178	71.8	2.42	32	3.0	0.17	0.24	0.009	0.09	0.005	1406	43	1373	46	1430	100	3.99
15	135.4	139.6	0.98	137	6.2	0.28	0.36	0.013	0.12	0.006	1979	41	1974	61	1954	81	-1.02
17	81.4	138.7	0.59	120	5.4	0.31	0.33	0.011	0.12	0.007	1848	52	1817	53	1860	110	2.31
19	391	159.1	2.48	109	3.2	0.12	0.25	0.007	0.09	0.004	1439	29	1440	35	1388	80	-3.75
21	146.3	85.8	1.81	72	6.2	0.24	0.37	0.011	0.12	0.004	1984	35	2019	52	1929	56	-4.67
22	115.3	64.2	1.83	56	5.0	0.25	0.32	0.010	0.11	0.005	1791	42	1801	46	1752	84	-2.80
25	198.5	69.9	2.96	42	3.0	0.19	0.23	0.009	0.09	0.005	1376	48	1321	46	1390	110	4.96
26	115.2	45.2	2.61	28	2.6	0.15	0.22	0.007	0.09	0.005	1289	46	1280	38	1230	120	-4.07
29	296	132.9	2.25	82	2.8	0.09	0.23	0.006	0.09	0.003	1358	25	1354	34	1329	70	-1.88
33	229	61.6	3.86	44	3.7	0.12	0.27	0.006	0.10	0.003	1575	25	1563	32	1555	60	-0.51
34	262	214	1.30	187	5.3	0.16	0.33	0.006	0.12	0.003	1863	27	1831	29	1862	52	1.66
38	114.3	64.3	1.81	60	6.0	0.24	0.35	0.008	0.12	0.005	1960	37	1932	40	1941	78	0.46
41	164	82.2	2.02	54	3.2	0.17	0.25	0.007	0.09	0.005	1440	39	1441	36	1380	110	-4.42
42	155.4	130.7	1.20	120	5.9	0.21	0.35	0.010	0.12	0.004	1961	33	1925	47	1956	69	1.58
48	245	220	1.10	213	5.9	0.21	0.35	0.010	0.12	0.004	1946	31	1918	45	1945	64	1.39
55	366	212.5	1.69	128	2.8	0.13	0.23	0.011	0.09	0.004	1350	37	1338	55	1337	94	-0.07
56	85.1	72.1	1.20	70	5.6	0.35	0.35	0.017	0.12	0.007	1884	54	1897	81	1870	100	-1.44
57	169.8	216	0.80	208	5.8	0.38	0.35	0.020	0.12	0.006	1906	58	1907	92	1860	100	-2.53
59	60.6	47.6	1.27	47	7.0	0.54	0.38	0.027	0.14	0.011	2089	69	2050	120	2090	140	1.91
60	96.6	64.8	1.49	43	2.9	0.16	0.23	0.007	0.09	0.006	1365	43	1313	36	1360	130	3.46
61	285.8	106.8	2.68	70	3.0	0.12	0.24	0.007	0.09	0.003	1398	32	1392	36	1361	62	-2.28
62	155.7	89.6	1.75	93	7.2	0.27	0.39	0.010	0.13	0.005	2122	33	2120	46	2078	66	-2.02
63	498	68.3	6.97	79	11.3	0.32	0.48	0.013	0.17	0.004	2536	27	2532	58	2530	40	-0.08
64	137.4	140	0.97	142	6.2	0.21	0.37	0.009	0.12	0.004	1993	29	2013	41	1936	56	-3.98
65	131.9	113.2	1.22	106	5.6	0.18	0.35	0.009	0.12	0.004	1911	28	1925	39	1877	61	-2.56
66	267	63.8	4.56	39	3.0	0.09	0.24	0.005	0.09	0.003	1404	23	1400	28	1378	60	-1.60
67	71	94.8	0.76	63	3.4	0.18	0.25	0.009	0.09	0.006	1472	44	1452	49	1460	130	0.55
68	430	600	3.40	27	5.0	0.24	0.32	0.014	0.11	0.006	1817	40	1771	68	1841	90	3.80
69	411	126.9	3.33	72	2.7	0.13	0.22	0.007	0.09	0.004	1321	37	1301	36	1331	85	2.25
70	74	60.4	1.24	54	6.1	0.27	0.35	0.010	0.12	0.006	1967	39	1926	47	1977	83	2.58
72	186.2	231	0.80	228	6.2	0.18	0.37	0.008	0.12	0.004	1993	26	2015	37	1935	61	-4.13
73	245.1	95.6	2.56	124	13.6	0.33	0.52	0.012	0.19	0.004	2718	22	2699	49	2694	35	-0.19
74	370	83	6.63	53	3.0	0.10	0.24	0.006	0.09	0.003	1409	26	1403	31	1361	63	-3.09
77	275	141	2.25	116	4.6	0.12	0.30	0.006	0.11	0.003	1747	21	1689	28	1762	51	4.14
79	128	101.7	1.23	101	5.8	0.22	0.35	0.010	0.12	0.004	1933	32	1931	45	1901	66	-1.58
81	402	356	1.11	261	3.5	0.10	0.26	0.005	0.09	0.003	1525	22	1504	23	1503	51	-0.07
82	96.9	55.4	1.77	35	2.9	0.13	0.24	0.006	0.09	0.004	1371	35	1375	33	1320	93	-4.17
83	176.3	181	0.99	151	4.4	0.14	0.30	0.007	0.11	0.003	1709	27	1678	32	1697	59	1.12
85	157.9	104.4	1.48	88	5.9	0.23	0.35	0.012	0.12	0.005	1954	34	1956	60	1911	68	-2.35
86	171	129	1.56	127	6.2	0.22	0.37	0.011	0.12	0.004	1990	31	2008	54	1941	62	-3.45
87	275	195	1.54	197	6.4	0.19	0.37	0.010	0.12	0.004	2014	26	2008	48	2000	49	-0.40
89	88.9	50.1	2.27	44	5.6	0.28	0.34	0.011	0.12	0.005	1897	43	1892	50	1850	85	-2.27
90	123.8	113	1.07	83	5.0	0.24	0.32	0.011	0.11	0.005	1821	43	1767	53	1826	88	3.23
92	392	120	3.16	71	3.0	0.12	0.24	0.008	0.09	0.003	1380	31	1383	41	1342	67	-3.06
93	156.6	87.9	1.76	63	3.0	0.14	0.24	0.008	0.09	0.004	1384	38	1383	41	1322	90	-4.61
97	261	44.3	5.84	33	3.1	0.10	0.25	0.006	0.09	0.003	1425	25	1414	29	1386	63	-2.02
98	229	140.4	1.58	134	5.0	0.34	0.32	0.018	0.11	0.005	1800	60	1793	91	1786	77	-0.39
99	213	70.3	2.94	47	3.0	0.11	0.24	0.007	0.09	0.004	1405	29	1387	36	1374	80	-0.95
101	159.6	77.9	2.45	88	5.5	0.20	0.33	0.009	0.12	0.004	1888	31	1838	45	1910	65	3.77
102	166.9	128.8	1.26	136	6.1	0.20	0.36	0.009	0.12	0.004	1984	29	1977	43	1960	53	-0.87
103	225	87.1	2.51	57	3.0	0.12	0.24	0.006	0.09	0.003	1396	31	1391	30	1359	71	-2.35
106	299	165	1.73	89	2.1	0.11	0.18	0.005	0.08	0.004	1121	36	1088	27	1130	100	3.72
109	300	222	1.34	231	6.8	0.20	0.38	0.011	0.13	0.004	2084	26	2070	54	2053	55	-0.83
110	245	45.5	5.56	30	2.7	0.11	0.22	0.006	0.09	0.004	1319	30	1286	33	1343	82	4.24
114	269	113.1	2.39	76	3.9	0.15	0.27	0.008	0.10	0.004	1612	29	1559	39	1617	72	3.59
118	64.7	65.7	0.98	61	5.9	0.27	0.35	0.009	0.12	0.005	1949	42	1922	42	1918	80	-0.21
122	277.3	303	0.91	251	5.9	0.23	0.36	0.012	0.12	0.003	1956	33	1958	59	1919	57	-2.03
124	104.5	51	2.01	43	4.3	0.19	0.30	0.008	0.10	0.004	1671	39	1671	40	1607	83	-3.98
126	65.3	27.4	2.41	29	5.5	0.26	0.33	0.010	0.12	0.006	1876	44	1839	50	1875	93	1.92
127	99	38	2.69	27	3.2	0.16	0.25	0.009	0.09	0.005	1439	40	1441	46	1390	99	-3.67
130	269.3	131	3.32	83	3.3	0.14	0.25	0.010	0.09	0.003	1459	33	1456	49	1407	69	-3.48
132	167.5	116.9	1.41	114	5.1	0.25	0.32	0.010	0.11	0.005	1805	42	1773	50	1793	81	1.12
133	193	106.2	1.81	109	6.4	0.39	0.37	0.020	0.12	0.006	1996	56	2001	97	1977	87	-1.21
136	422	107.4	3.92	71	2.8	0.09	0.23	0.006	0.09	0.003	1361	24	1319	30	1368	64	3.58
137	157	213	0.72	195	5.2	0.21	0.32	0.010	0.12	0.004	1834	35	1781	50	1860	69	4.25
142	103.3	62.6	1.65	73	7.2	0.35	0.39	0.014	0.13	0.005	2118	44	2116	63	2077	80	-1.88
144	273	57.3	4.92	38	3.0	0.10	0.24	0.006	0.09	0.003	1399	24	1398	32	1343	60	-4.10
146	172.1	148.1	1.20	158	6.5	0.24	0.37	0.010	0.13	0.004	2036	32	2027	47	2031	58	0.20
149	243.4	90.2	2.73	67	3.1	0.09	0.25	0.005	0.09	0.003	1423	23	1419	25	1402	57	-1.21
151	220	208.1	1.05	206	6.9	0.27	0.38	0.010	0.13	0.004	2086	35	2071	45	2067	60	-0.19
154	143	151	0.97	139	5.6	0.22	0.35	0.008	0.12	0.005	1911	33	1912	39	1858	75	-2.91
160	250.6	101.3	2.47	71	2.9	0.09	0.24	0.006	0.09	0.003	1375	23	1369	31	1352	61	-1.26
161	269.9	150.4	1.80	161	6.7	0.20	0.37	0.008	0.13	0.003	2066	26	2025	35	2081	48	2.69
163	161.5	116.6	1.39	101	4.7	0.18	0.31	0.008	0.11	0.004	1750	33	1718	41	1762	69	2.50
164	233	207	1.12	193	5.4	0.17	0.33	0.007	0.11	0.003	1868	28	1858	32	1842	50	-0.87
170	279	159	1.91	145	5.2	0.27	0.32	0.010	0.11	0.004	1825	49	1804	49	1818	75	0.77
172	97.2	164	0.61	140	5.3	0.24	0.33	0.011	0.12	0.005	1861	42	1819	53	1869	90	2.68
177	181	116.2	1.36	108	6.2	0.33	0.36	0.014	0.12	0.006	1974	46	1962	63	1952	84	-0.51
180	437	316	1.39	205	2.8	0.12	0.23	0.007	0.09	0.003	1336	32	1314	39	1343	65	2.16
184	179.8	106.1	1.69	77	4.5	0.20	0.31	0.010	0.11	0.004	1732	35	1712	50	1721	67	0.52
189	185	101.9	1.82	63	2.7	0.12	0.23	0.006	0.09	0.003	1326	32	1323	33	1294	81	-2.24
191	386	583	0.65	569	5.5	0.27	0.34	0.013	0.12	0.004	1885	42	1881	63	1879	70	-0.11
196	46.5	97.1	0.53	92	5.7	0.33	0.35	0.013	0.12	0.008	1898	51	1920	64	1840	120	-4.35
199	202	135	1.76	129	6.2	0.24	0.37	0.012	0.12	0.004	1986	35	2002	55	1951	63	-2.61
200	131.3	68.4	1.87	67	6.1	0.23	0.37	0.010	0.12	0.004	1983	33	2007	45	1932	61	-3.88
206	193.8	130.5	1.53	79	2.9	0.13	0.24	0.008	0.09	0.003	1369	35	1370	42	1373	71	0.22
207	194.8	156.5	1.23	151	5.9	0.22	0.35	0.011	0.12	0.004	1949	33	1934	54	1952	63	0.92
208	255	137	1.95	138	6.7	0.24	0.37	0.011	0.13	0.004	2065	32	2045	50	2077	48	1.54
209	276	119.8	2.29	87	3.1	0.14	0.25	0.009	0.09	0.003	1432	35	1449	44	1397	69	-3.72
211	421	118.1	3.50	77	3.6	0.14	0.27	0.009	0.10	0.003	1532	32	1534	44	1520	68	-0.92
212	274	161.4	1.79	224	14.1	0.77	0.51	0.026	0.20	0.008	2728	53	2670	110	2781	67	3.99
216	381	198	1.90	178	6.5	0.27	0.36	0.012	0.13	0.005	2040	34	1989	56	2088	62	4.74
220	188.2	147.3	1.24	136	5.2	0.18	0.33	0.010	0.11	0.003	1833	30	1853	46	1823	53	-1.65
222	354	98.9	3.58	66	3.0	0.11	0.25	0.007	0.09	0.003	1404	27	1419	36	1385	57	-2.45
226	34.4	11.1	3.31	17	8.0	1.20	0.41	0.032	0.14	0.014	2180	120	2210	150	2210	190	0.00
227	173.6	207	0.84	194	5.6	0.29	0.34	0.013	0.12	0.006	1906	43	1875	63	1938	93	3.25
228	365	180.6	2.09	151	5.4	0.22	0.34	0.012	0.12	0.003	1868	34	1871	58	1860	52	-0.59

Lower Mwashya Subgroup

Spot #	Compositional Data				Isotope Ratios						Apparent Ages (Ma)						Discordance
	U (ppm)	Th (ppm)	U Th	Pb (ppm)	207Pb 235U	±207Pb 235U	206Pb 238U	±206Pb 238U	207Pb 206Pb	±207Pb 206Pb	207Pb 235U	±207Pb 235U	206Pb 238U	±206Pb 238U	207Pb 206Pb	±207Pb 206Pb	(%)
2	96.6	70.9	1.416	67.7	5.78	0.19	0.35	0.01	0.12	0.004	1933	29	1916	42	1969	61	2.69
3	63.4	110.3	0.6	99	5.28	0.22	0.33	0.01	0.12	0.005	1855	37	1858	43	1848	78	-0.54
4	105.5	137.9	0.788	128.7	5.51	0.22	0.34	0.01	0.11	0.004	1895	36	1872	43	1841	71	-1.68
5	238	164	1.526	176	6.39	0.20	0.36	0.01	0.12	0.004	2028	28	1996	40	1969	53	-1.37
7	216	96.5	2.285	65.4	3.19	0.11	0.25	0.01	0.09	0.003	1448	26	1415	34	1439	61	1.67
9	452	530	0.859	535	6.57	0.18	0.37	0.01	0.13	0.003	2047	24	2045	40	2014	42	-1.54
10	116.7	128	0.985	122.9	5.89	0.24	0.36	0.01	0.12	0.005	1941	36	1950	48	1915	72	-1.83
12	101	83.5	1.228	81.7	6.21	0.29	0.36	0.01	0.12	0.005	1986	42	1985	52	1907	82	-4.09
13	124.7	90	1.36	86.2	6.37	0.25	0.37	0.01	0.13	0.005	2026	34	2025	49	2001	69	-1.20
15	263	195	1.331	144	4.54	0.15	0.31	0.01	0.10	0.003	1732	26	1730	33	1690	46	-2.37
16	327.4	279	1.182	278	6.49	0.24	0.36	0.01	0.12	0.004	2042	31	1987	53	1992	54	0.25
18	239.7	80.6	3.08	50.8	2.70	0.09	0.23	0.00	0.09	0.003	1322	23	1325	25	1313	67	-0.91
21	139.8	162.1	0.839	163.5	6.50	0.21	0.37	0.01	0.12	0.004	2036	29	2040	43	1976	60	-3.24
23	320	61.4	4.79	15.5	5.47	0.17	0.33	0.01	0.12	0.004	1889	26	1811	40	1905	53	4.93
24	466	248	1.802	164	3.02	0.09	0.24	0.00	0.09	0.002	1408	22	1376	25	1367	53	-0.66
26	439	178.5	2.369	124.4	3.16	0.09	0.25	0.00	0.09	0.002	1443	21	1454	25	1391	41	-4.53
28	179.9	257	0.673	235	5.51	0.21	0.34	0.01	0.12	0.004	1892	33	1894	44	1859	71	-1.88
29	144	63	2.17	60.6	5.16	0.24	0.31	0.01	0.11	0.005	1832	39	1756	44	1819	76	3.46
30	97.4	81.9	1.143	84.1	6.15	0.25	0.36	0.01	0.12	0.004	1979	36	1986	47	1936	64	-2.58
34	103.4	98.2	1.091	90.5	5.73	0.33	0.34	0.02	0.12	0.005	1913	48	1883	78	1925	77	2.18
35	71.4	55.7	1.225	54.3	6.04	0.24	0.35	0.01	0.12	0.005	1960	35	1958	47	1944	71	-0.72
36	231	253	0.894	238	5.34	0.17	0.34	0.01	0.11	0.003	1866	27	1869	36	1808	54	-3.37
41	228	191	1.153	171.2	5.57	0.19	0.33	0.01	0.12	0.004	1909	28	1854	39	1938	66	4.33
42	257.3	303	0.919	256	5.32	0.15	0.33	0.01	0.11	0.003	1865	25	1821	40	1849	49	1.51
43	188	135	1.278	77.5	2.86	0.15	0.23	0.01	0.09	0.005	1357	40	1347	36	1350	110	0.22
46	95.4	86.5	1.12	82	6.06	0.21	0.36	0.01	0.12	0.004	1973	29	1974	42	1936	58	-1.96
49	174.7	121	2.14	117	6.33	0.26	0.37	0.01	0.12	0.003	2012	36	2016	52	1981	44	-1.77
50	80.4	72.6	1.122	70	6.61	0.26	0.37	0.01	0.13	0.004	2045	36	2046	43	2016	62	-1.49
51	289	207.1	1.368	169.6	5.44	0.17	0.33	0.01	0.12	0.003	1882	26	1838	36	1870	50	1.71
52	284	227	1.239	211	5.48	0.21	0.33	0.01	0.12	0.004	1888	33	1846	50	1896	65	2.64
53	82.7	71.6	1.154	74.6	6.56	0.35	0.36	0.01	0.13	0.006	2031	46	1994	52	1989	89	-0.25
54	73.2	73.8	1.001	73.8	6.22	0.24	0.36	0.01	0.12	0.005	1994	35	1990	48	1953	69	-1.89
55	365	105.6	3.49	48.6	5.76	0.23	0.35	0.01	0.12	0.004	1928	34	1927	59	1946	62	0.98
57	510	372	1.357	380	6.13	0.24	0.36	0.01	0.12	0.004	1980	35	1983	58	1915	58	-3.55
58	132.2	99.8	1.312	97.2	5.99	0.22	0.36	0.01	0.12	0.004	1969	32	1959	48	1930	63	-1.50
59	170.7	72.4	2.343	48.2	2.99	0.12	0.24	0.01	0.09	0.003	1396	32	1402	35	1357	67	-3.32
61	78.5	46	1.68	44.3	9.14	0.43	0.44	0.01	0.15	0.005	2331	41	2325	52	2340	61	0.64
62	165	56.9	3.44	29.2	2.80	0.11	0.23	0.01	0.09	0.003	1348	31	1313	33	1334	79	1.57
65	348	361	0.971	294	5.64	0.19	0.34	0.01	0.12	0.004	1915	30	1889	47	1974	56	4.31
66	102	80.6	1.243	71.9	6.22	0.24	0.37	0.01	0.12	0.004	1990	33	2005	45	1977	62	-1.42
69	140.9	128	1.11	124.9	6.25	0.18	0.37	0.01	0.12	0.003	2004	24	2028	37	1945	50	-4.27
72	269	232	1.228	206	6.23	0.19	0.36	0.01	0.12	0.004	2002	26	1959	41	1966	51	0.36
75	92	82.4	1.18	81.7	6.23	0.21	0.37	0.01	0.12	0.004	1999	31	2027	39	1935	60	-4.75
79	402	291	1.396	106.2	4.23	0.16	0.30	0.01	0.11	0.004	1674	32	1676	53	1706	62	1.76
80	89.2	185.3	0.484	174.8	5.70	0.22	0.34	0.01	0.12	0.005	1916	34	1900	41	1881	73	-1.01
83	58.4	49.3	1.199	50.4	6.11	0.26	0.36	0.01	0.12	0.005	1976	39	1961	47	1938	78	-1.19
86	59.8	76.5	0.815	69.5	5.93	0.24	0.35	0.01	0.12	0.006	1952	37	1946	53	1898	85	-2.53
90	211	162.1	1.274	109.7	5.55	0.19	0.34	0.01	0.12	0.004	1900	30	1880	48	1965	57	4.33
100	369	188.9	1.915	184.2	6.77	0.15	0.39	0.01	0.13	0.003	2076	20	2103	36	2024	35	-3.90
101	122.4	109.9	1.096	113	6.42	0.20	0.37	0.01	0.12	0.004	2029	28	2033	41	1965	52	-3.46
103	426	155	2.709	141.5	5.84	0.15	0.35	0.01	0.12	0.003	1945	22	1939	40	1938	43	-0.05
105	124.9	115.1	1.103	97	5.98	0.33	0.35	0.01	0.12	0.006	1953	47	1931	58	1973	85	2.13
106	65	56.9	1.136	50.9	6.31	0.30	0.35	0.01	0.13	0.006	1998	42	1946	71	2021	76	3.71
107	296	197.7	1.45	190.8	6.60	0.17	0.38	0.01	0.13	0.003	2055	23	2058	35	2030	40	-1.38
112	392	272	1.606	228	5.46	0.16	0.34	0.01	0.11	0.002	1882	25	1887	36	1867	35	-1.07
114	118	71.7	2.59	54.9	5.45	0.39	0.34	0.03	0.12	0.004	1858	55	1850	110	1936	64	4.44
141	166	109.1	1.573	99.5	5.89	0.17	0.35	0.01	0.12	0.003	1954	26	1916	40	1945	44	1.49
145	84.3	69	1.22	67.4	5.89	0.26	0.34	0.01	0.12	0.005	1946	39	1877	45	1964	76	4.43
146	112	59.7	1.85	56.6	5.58	0.19	0.34	0.01	0.12	0.004	1901	30	1903	40	1888	59	-0.79
150	84.5	76.2	1.16	74.9	6.21	0.29	0.35	0.01	0.13	0.005	1994	39	1933	62	2005	76	3.59
152	172	68.7	3.09	58.8	4.66	0.14	0.31	0.01	0.11	0.003	1753	26	1752	36	1741	50	-0.63
160	46.6	56.6	0.833	57	6.06	0.25	0.36	0.01	0.12	0.005	1969	37	1977	45	1919	74	-3.02
161	191	90	2.57	49.3	3.05	0.16	0.24	0.01	0.09	0.003	1398	41	1370	48	1399	74	2.07
162	93.4	48	1.991	29.4	2.42	0.13	0.21	0.01	0.08	0.004	1224	37	1221	28	1170	110	-4.36
165	130	183.6	0.711	177.8	5.77	0.20	0.34	0.01	0.12	0.004	1930	30	1905	39	1894	66	-0.58
166	68.9	87	1.01	75.8	5.60	0.29	0.34	0.01	0.12	0.006	1896	44	1862	63	1932	92	3.62
169	103.6	79.4	1.336	77.3	5.97	0.23	0.36	0.01	0.12	0.005	1957	35	1959	56	1940	69	-0.98
170	75.9	69.6	1.063	65.6	5.60	0.28	0.34	0.01	0.12	0.005	1901	45	1856	60	1932	74	3.93
171	116.9	57.3	2.04	49.5	5.42	0.27	0.34	0.01	0.11	0.005	1869	43	1881	64	1850	78	-1.68
173	226	107.5	2.152	76.2	3.20	0.14	0.25	0.01	0.09	0.003	1441	33	1437	43	1437	61	0.00
175	181	132	1.489	49.7	2.49	0.10	0.21	0.01	0.09	0.003	1255	29	1231	29	1289	68	4.50
176	111.2	232	0.494	229	6.09	0.20	0.35	0.01	0.13	0.004	1976	29	1925	39	2002	61	3.85
178	122.5	97.8	1.251	86.4	6.43	0.34	0.36	0.02	0.12	0.005	2014	45	1990	73	1985	62	-0.25
185	92.5	87.1	1.076	81.1	5.33	0.18	0.33	0.01	0.12	0.005	1861	30	1832	40	1902	71	3.68
186	140	173	0.804	142.6	4.71	0.18	0.30	0.01	0.11	0.004	1755	33	1723	52	1750	68	1.54
187	313	90.5	3.464	59.7	2.87	0.09	0.23	0.00	0.09	0.003	1369	23	1323	25	1363	63	2.93
188	56.2	72.9	0.764	86.7	9.68	0.34	0.45	0.01	0.16	0.005	2392	33	2389	58	2400	59	0.46
189	225.4	92.6	2.47	86.4	5.14	0.17	0.33	0.01	0.12	0.004	1833	28	1818	41	1863	57	2.42
192	451	65.2	7.06	31.6	3.03	0.07	0.24	0.00	0.09	0.002	1411	18	1392	22	1409	41	1.21
194	180.3	75.6	2.361	54.4	2.87	0.10	0.24	0.00	0.09	0.003	1368	26	1362	25	1327	67	-2.64
195	445	163	2.684	116	2.97	0.07	0.24	0.00	0.09	0.002	1399	17	1382	26	1364	51	-1.32
196	215.6	149.7	1.446	83.7	2.17	0.09	0.19	0.01	0.08	0.003	1161	28	1126	31	1171	78	3.84

Upper Mwashya Subgroup

Spot #	Compositional Data				Isotope Ratios						Apparent Ages (Ma)						Discordance
	U	Th	U	Pb	207Pb	±207Pb	206Pb	±206Pb	207Pb	±207Pb	207Pb	±207Pb	206Pb	±206Pb	207Pb	±207Pb	(%)
	(ppm)	(ppm)	Th	(ppm)	235U	235U	238U	238U	206Pb	206Pb	235U	235U	238U	238U	206Pb	206Pb	
197	64.5	61.9	1.095	60	6.25	0.30	0.37	0.010	0.12	0.005	1995	43	2015	46	1938	83	-3.97
198	272	98.5	2.65	66.9	2.90	0.08	0.24	0.005	0.09	0.003	1378	21	1385	27	1336	55	-3.67
201	363.7	71.2	5.34	42.6	2.94	0.08	0.24	0.004	0.09	0.002	1385	21	1385	23	1350	52	-2.59
203	250	167	1.688	182	6.58	0.56	0.36	0.011	0.13	0.008	1999	54	1969	53	2051	94	4.00
204	164	83	1.81	55.5	2.95	0.12	0.24	0.006	0.09	0.003	1377	32	1378	32	1354	73	-1.77
205	179.6	100.8	1.812	85.3	6.28	0.22	0.36	0.010	0.13	0.003	2003	30	1999	46	2033	49	1.67
206	291	156.2	1.823	195.3	12.18	0.39	0.49	0.014	0.18	0.004	2605	31	2573	62	2639	38	2.50
207	264	122	2.056	122.3	6.83	0.20	0.38	0.009	0.13	0.004	2088	24	2076	42	2102	48	1.24
210	387	195	1.971	131.9	3.01	0.09	0.24	0.006	0.09	0.002	1410	23	1406	30	1376	51	-2.18
211	218	145	1.401	138	7.31	0.25	0.39	0.010	0.13	0.004	2137	32	2133	46	2120	51	-0.61
212	75	53.6	1.369	57.1	6.15	0.26	0.35	0.008	0.12	0.005	1989	38	1954	40	1966	76	0.61
213	122.1	183.1	0.631	183.7	5.57	0.21	0.34	0.008	0.12	0.004	1908	32	1884	40	1869	68	-0.80
214	166.8	65.3	2.75	42	3.01	0.11	0.24	0.006	0.09	0.003	1402	27	1401	30	1364	74	-2.71
217	66.7	52.5	1.242	56.5	6.15	0.26	0.36	0.010	0.12	0.005	1988	36	1990	45	1952	71	-1.95
218	81	36.3	1.85	36.1	6.77	0.57	0.37	0.022	0.13	0.006	2009	80	1980	100	2056	93	3.70

Upper Mwashya Subgroup

Spot #	Compositional Data				Isotope Ratios						Apparent Ages (Ma)						Discordance
	U (ppm)	Th (ppm)	U Th	Pb (ppm)	207Pb 235U	±207Pb 235U	206Pb 238U	±206Pb 238U	207Pb 206Pb	±207Pb 206Pb	207Pb 235U	±207Pb 235U	206Pb 238U	±206Pb 238U	207Pb 206Pb	±207Pb 206Pb	(%)
1	379	201	1.91	190.1	4.6	0.120	0.307	0.008	0.108	0.002	1742	21	1725	40	1764	28	2.21
3	323.1	179.9	1.77	139.1	4.6	0.120	0.307	0.007	0.107	0.003	1739	22	1723	35	1738	53	0.86
4	233.4	168.4	1.37	156.2	4.5	0.160	0.310	0.007	0.105	0.003	1735	30	1739	37	1716	47	-1.34
8	288	154.4	1.83	127	5.5	0.100	0.340	0.006	0.115	0.002	1900	18	1885	29	1878	30	-0.37
12	94.3	142.1	0.65	200.2	13.1	0.230	0.502	0.007	0.187	0.003	2685	16	2621	31	2709	28	3.25
13	134.4	106.7	1.23	83.4	4.7	0.110	0.307	0.006	0.109	0.003	1768	20	1725	30	1771	46	2.60
14	432	372	1.16	344	5.3	0.120	0.326	0.008	0.117	0.002	1859	20	1817	38	1902	32	4.47
17	283.5	148.9	1.92	106.4	3.3	0.071	0.259	0.005	0.093	0.002	1481	18	1483	27	1481	41	-0.14
18	79.5	42.7	1.86	69.5	23.7	0.370	0.657	0.010	0.263	0.004	3252	15	3251	39	3261	21	0.31
21	134.3	67.5	2.04	57	4.8	0.090	0.315	0.004	0.110	0.002	1774	16	1764	20	1790	32	1.45
23	333	86	4.59	94	3.9	0.180	0.285	0.012	0.100	0.002	1613	36	1611	61	1620	41	0.56
24	56.9	49.2	1.18	54	5.6	0.160	0.343	0.009	0.120	0.004	1911	25	1898	41	1933	64	1.81
26	587	298	2.00	207	3.3	0.087	0.252	0.006	0.094	0.002	1480	21	1448	31	1498	32	3.34
27	102.4	86.5	1.19	74.9	6.5	0.210	0.363	0.008	0.128	0.004	2045	28	1995	40	2053	50	2.83
30	424	347	1.22	273	6.2	0.140	0.363	0.009	0.119	0.003	2000	20	1996	40	1941	44	-2.83
35	113.3	85.7	1.34	113.6	11.5	0.310	0.478	0.007	0.174	0.005	2562	24	2519	29	2591	42	2.78
36	206.3	83.8	2.45	128.6	12.1	0.220	0.496	0.007	0.177	0.002	2610	17	2595	30	2623	21	1.07
37	491	650	0.86	516	5.2	0.130	0.328	0.008	0.115	0.003	1852	21	1826	40	1865	44	2.09
38	343	90.7	3.92	94.4	5.6	0.130	0.336	0.007	0.120	0.003	1907	20	1865	31	1954	41	4.55
39	204	95.1	2.13	64.4	3.1	0.066	0.247	0.004	0.091	0.002	1423	17	1420	21	1439	42	1.32
41	242	236	1.03	213	5.7	0.160	0.348	0.008	0.121	0.003	1933	25	1922	38	1958	47	1.84
42	465.8	136.9	3.39	116	3.1	0.067	0.250	0.005	0.093	0.002	1441	17	1437	25	1482	37	3.04
44	184	88	2.10	108.8	6.2	0.190	0.366	0.010	0.124	0.003	2006	27	2008	48	2008	36	0.00
72	195	142	1.38	151.1	5.8	0.150	0.351	0.011	0.119	0.003	1940	23	1939	54	1940	47	0.05
76	180	117.6	1.52	122.3	5.9	0.140	0.355	0.006	0.120	0.003	1957	20	1956	30	1957	37	0.05
80	446	367.1	1.21	371	10.4	0.200	0.451	0.008	0.166	0.003	2465	18	2396	37	2512	31	4.62
82	373	183.4	1.98	161.3	6.4	0.110	0.369	0.007	0.127	0.002	2028	15	2024	32	2054	23	1.46
84	277	296	0.93	320	12.4	0.270	0.489	0.012	0.184	0.004	2630	20	2565	52	2679	38	4.26
85	313	230	1.52	222	6.5	0.300	0.372	0.019	0.129	0.003	2028	40	2029	90	2072	34	2.08
87	261	184	1.43	161.5	5.9	0.110	0.355	0.006	0.121	0.002	1955	16	1955	27	1975	28	1.01
91	244	266	0.88	229	5.7	0.098	0.349	0.005	0.120	0.002	1930	15	1930	23	1955	27	1.28
94	77	62.1	1.24	66.9	5.7	0.130	0.349	0.007	0.123	0.003	1933	21	1928	32	1988	42	3.02
1	159.6	194	0.82	198.1	6.1	0.110	0.359	0.005	0.123	0.002	1983	16	1978	21	1993	32	0.75
2	134.7	84.9	1.59	88.3	6.3	0.140	0.368	0.005	0.126	0.003	2017	20	2018	22	2020	42	0.10
3	141.6	103.8	1.35	109.7	6.2	0.140	0.361	0.005	0.127	0.003	2006	21	1986	24	2047	37	2.98
4	202.5	81.2	2.51	53.1	2.8	0.087	0.231	0.004	0.086	0.003	1336	24	1340	19	1308	64	-2.45
6	111	89	1.25	107.2	8.7	0.210	0.420	0.006	0.152	0.004	2305	22	2258	28	2357	41	4.20
8	164.5	83.7	1.99	67.3	3.5	0.089	0.270	0.004	0.095	0.002	1524	20	1540	18	1513	45	-1.78
10	125.6	106.6	1.13	109.3	5.8	0.120	0.358	0.005	0.118	0.003	1940	18	1971	23	1915	45	-2.92
11	160.1	90.7	1.77	117.8	10.9	0.180	0.474	0.006	0.168	0.003	2512	16	2501	24	2532	28	1.22
12	126.8	101.3	1.25	102	6.0	0.150	0.354	0.005	0.123	0.003	1963	22	1951	22	1975	44	1.22
13	40.6	38.5	1.05	38.7	6.0	0.250	0.354	0.007	0.124	0.005	1963	36	1956	34	1963	74	0.36
14	126.1	72.1	1.75	89.1	11.0	0.230	0.467	0.007	0.172	0.003	2518	19	2466	29	2571	31	4.08
15	139.1	123.2	1.12	119.2	5.0	0.110	0.333	0.005	0.110	0.002	1820	18	1850	23	1791	39	-3.29
16	132.1	135.8	0.98	133.4	5.9	0.130	0.352	0.005	0.122	0.003	1958	19	1941	25	1980	36	1.97
17	240	31.7	7.73	39.2	10.0	0.170	0.464	0.005	0.157	0.002	2434	15	2455	23	2417	26	-1.57
18	248	152	1.72	145.6	6.0	0.120	0.360	0.006	0.122	0.002	1976	17	1979	28	1980	31	0.05
19	90.6	81.5	1.12	86.3	5.7	0.170	0.357	0.006	0.117	0.003	1923	26	1965	26	1872	54	-4.97
20	222	145	1.53	145	6.3	0.120	0.369	0.005	0.123	0.003	2017	17	2022	25	1986	39	-1.81
23	119	81	1.64	77	6.1	0.150	0.361	0.006	0.123	0.003	1981	23	1986	29	1974	52	-0.61
25	31.7	43.9	0.74	45.4	7.1	0.340	0.372	0.009	0.137	0.006	2101	44	2043	42	2147	75	4.84
27	266.5	145.3	1.81	141.8	6.4	0.095	0.360	0.005	0.129	0.002	2029	13	1981	24	2074	27	4.48
29	291	175.9	1.59	180	6.3	0.120	0.375	0.005	0.122	0.002	2017	16	2052	23	1975	31	-3.90
30	194.6	77.9	2.46	97.2	11.4	0.180	0.486	0.006	0.171	0.002	2554	15	2549	28	2563	23	0.55
32	67	55.7	1.23	57.7	6.8	0.200	0.382	0.007	0.130	0.004	2083	28	2089	34	2077	55	-0.58
33	55.5	26.9	2.14	29	6.7	0.190	0.376	0.006	0.130	0.004	2058	25	2057	28	2068	54	0.53
34	65.5	47.1	1.36	36.5	3.5	0.150	0.266	0.005	0.096	0.004	1511	33	1516	28	1502	78	-0.93
35	176.3	95.5	1.80	101.7	6.2	0.130	0.355	0.005	0.128	0.003	1998	18	1958	24	2049	36	4.44
36	139.2	96.9	1.45	83.9	5.6	0.140	0.337	0.005	0.120	0.003	1904	22	1872	26	1942	45	3.60
37	59.5	63.9	0.91	69.8	6.1	0.210	0.352	0.007	0.128	0.004	1982	30	1941	34	2039	58	4.81
39	109.7	221.5	0.49	297	11.6	0.240	0.490	0.007	0.173	0.004	2563	19	2567	31	2577	35	0.39
40	127.4	61	2.11	61.8	6.7	0.130	0.379	0.005	0.130	0.002	2071	17	2068	23	2087	32	0.91
42	97.1	72.1	1.31	69.9	6.1	0.180	0.355	0.008	0.126	0.004	1982	25	1953	37	2013	49	2.98
43	72.7	46.9	1.57	46	6.0	0.130	0.352	0.006	0.126	0.003	1973	20	1944	27	2021	45	3.81
45	113.1	35.1	3.27	42.9	10.6	0.200	0.471	0.008	0.167	0.003	2486	18	2485	33	2511	32	1.04
46	78.4	58.9	1.33	57.5	5.8	0.160	0.352	0.007	0.122	0.003	1936	24	1941	32	1954	48	0.67
47	77.9	59.5	1.30	58.5	6.1	0.170	0.357	0.006	0.125	0.003	1978	25	1975	31	2008	44	1.64
48	128.6	107.1	1.20	74.9	3.4	0.098	0.264	0.004	0.095	0.003	1501	22	1510	22	1510	56	0.00
49	322	195.7	1.64	147.7	3.4	0.065	0.267	0.003	0.095	0.002	1512	15	1523	16	1519	35	-0.26
51	34.6	26.17	1.32	25.1	5.5	0.240	0.346	0.008	0.119	0.005	1886	37	1911	40	1891	83	-1.06
53	20.09	11.15	1.81	9.68	5.5	0.290	0.337	0.011	0.122	0.007	1906	43	1868	55	1950	110	4.21
54	65.9	73	0.90	65.3	5.1	0.180	0.327	0.007	0.117	0.005	1830	30	1819	32	1861	73	2.26
55	63.1	30.5	2.04	26.3	4.6	0.160	0.309	0.005	0.109	0.004	1728	29	1733	27	1729	66	-0.23
56	95.1	108.4	0.87	110.8	6.3	0.180	0.368	0.006	0.127	0.004	2013	25	2017	28	2028	51	0.54
58	48.1	30.2	1.56	28.8	6.1	0.210	0.367	0.007	0.122	0.005	1991	28	2019	34	1958	72	-3.12
61	227	79.4	2.90	54.1	3.2	0.075	0.262	0.004	0.091	0.002	1464	18	1500	19	1438	43	-4.31
62	78.7	67.4	1.18	58.8	4.8	0.160	0.319	0.006	0.111	0.004	1781	27	1782	28	1782	56	0.00
64	60.7	64.4	0.95	52.1	4.3	0.150	0.302	0.006	0.104	0.004	1677	28	1699	29	1666	62	-1.98

Basal diamictite lower package

Spot #	Compositional Data				Isotope Ratios						Apparent Ages (Ma)						Discordance
	U (ppm)	Th (ppm)	U Th	Pb (ppm)	207Pb 235U	±207Pb 235U	206Pb 238U	±206Pb 238U	207Pb 206Pb	±207Pb 206Pb	207Pb 235U	±207Pb 235U	206Pb 238U	±206Pb 238U	207Pb 206Pb	±207Pb 206Pb	(%)
65	57	75	0.8	98.6	13.4	0.320	0.528	0.010	0.185	0.004	2702	23	2727	40	2701	33	-0.96
67	51.2	61.3	0.8	57.2	5.3	0.180	0.343	0.007	0.114	0.004	1857	30	1898	32	1824	71	-4.06
69	143	34	4.2	31.5	5.4	0.130	0.349	0.007	0.115	0.003	1883	21	1932	35	1861	43	-3.82
70	128	241	0.5	188	4.6	0.150	0.304	0.008	0.111	0.003	1738	26	1708	41	1786	52	4.37
71	295	132	2.3	136.9	10.2	0.290	0.461	0.011	0.157	0.004	2448	26	2444	46	2424	44	-0.83
72	180.5	94	2.0	89.7	5.4	0.150	0.344	0.006	0.114	0.003	1876	24	1903	28	1854	44	-2.64
80	32.1	20.6	1.6	21.7	8.3	0.330	0.427	0.010	0.144	0.006	2246	37	2287	45	2249	76	-1.69
81	111	101.1	1.1	93.5	5.9	0.280	0.364	0.007	0.119	0.004	1942	37	2000	35	1919	68	-4.22
83	302	350	0.9	375	9.6	0.250	0.466	0.009	0.155	0.003	2394	25	2461	40	2392	31	-2.88
91	210	121.3	1.7	104	5.3	0.130	0.340	0.006	0.116	0.003	1867	22	1885	27	1882	38	-0.16
92	181.4	83.7	2.1	64.8	4.0	0.084	0.296	0.004	0.100	0.002	1636	17	1671	22	1607	43	-3.98
93	104	47.1	2.2	51.6	12.4	0.260	0.521	0.009	0.175	0.003	2632	19	2698	38	2599	31	-3.81
99	329	244.2	1.3	231.6	6.0	0.110	0.351	0.006	0.124	0.002	1976	16	1939	28	1999	33	3.00
101	320	195	1.6	169	5.8	0.093	0.352	0.005	0.119	0.002	1944	14	1945	22	1931	27	-0.73
102	36.2	39.9	0.9	34.9	5.4	0.260	0.339	0.010	0.114	0.006	1863	43	1876	47	1790	100	-4.80

Basal diamictite lower package

Spot #	Compositional Data				Isotope Ratios						Apparent Ages (Ma)						Discordance
	U (ppm)	Th (ppm)	U Th	Pb (ppm)	207Pb 235U	±207Pb 235U	206Pb 238U	±206Pb 238U	207Pb 206Pb	±207Pb 206Pb	207Pb 235U	±207Pb 235U	206Pb 238U	±206Pb 238U	207Pb 206Pb	±207Pb 206Pb	(%)
11	820	294	3.10	119	11.9	2.5	0.53	0.110	0.1607	0.003	2353	99	2430	300	2454	28	0.98
19	246	195	1.31	185	6.5	0.11	0.37	0.007	0.1262	0.002	2039	16	2009	32	2042	25	1.62
28	225	273	0.87	269	6.6	0.1	0.37	0.006	0.1282	0.002	2052	14	2039	26	2063	29	1.16
35	806	298	2.67	308	6.9	0.17	0.38	0.010	0.132	0.002	2088	20	2089	43	2118	23	1.37
45	221.6	239	0.92	215.7	5.2	0.092	0.33	0.005	0.1148	0.002	1847	15	1829	26	1871	29	2.24
49	294	302	0.98	281	6.3	0.16	0.36	0.009	0.1292	0.002	2024	24	1995	40	2077	28	3.95
55	320	191	1.68	172.9	5.5	0.088	0.35	0.005	0.1184	0.002	1905	13	1921	22	1926	22	0.26
59	167	105	1.80	95	5.7	0.12	0.35	0.006	0.1214	0.002	1925	18	1929	27	1965	32	1.83
60	352	196	1.69	180	6.4	0.13	0.37	0.007	0.1279	0.002	2025	18	2038	34	2061	26	1.12
63	1108	965	1.13	715	3.3	0.052	0.26	0.004	0.0957	0.002	1489	12	1484	22	1524	26	2.62
65	105	150	0.70	158	7.4	0.29	0.39	0.010	0.1393	0.004	2145	33	2142	42	2191	48	2.24
69	808	175	4.53	217.8	10.5	0.19	0.46	0.008	0.1689	0.002	2478	15	2437	35	2543	17	4.17
70	138.7	50.2	2.70	51.5	6.5	0.15	0.37	0.008	0.1276	0.002	2035	20	2039	36	2052	33	0.63
71	335	174	1.82	168	6.6	0.13	0.38	0.006	0.1277	0.002	2057	17	2085	29	2057	28	-1.36
73	289	476	0.60	382	4.3	0.066	0.29	0.004	0.1067	0.002	1683	13	1657	22	1734	28	4.44
74	237	118.6	2.00	141.5	10.0	0.16	0.45	0.008	0.1634	0.002	2433	15	2398	33	2484	22	3.46
76	298	200	1.51	167.6	4.6	0.12	0.31	0.007	0.1095	0.002	1744	20	1724	35	1779	30	3.09
78	287	282	1.02	247	6.1	0.1	0.36	0.007	0.125	0.002	1987	14	1973	30	2019	26	2.28
90	48.5	22.3	2.25	26.9	10.6	0.49	0.46	0.019	0.1692	0.005	2473	41	2416	80	2525	53	4.32
91	36.7	23	3.90	35.9	17.6	1.9	0.61	0.069	0.23	0.017	2920	110	3020	290	2982	89	-1.27
98	422	383	1.30	442	11.0	0.15	0.48	0.007	0.1664	0.002	2524	13	2528	32	2516	22	-0.48
136	284	149	1.69	57.7	1.6	0.047	0.16	0.004	0.0712	0.002	961	18	941	20	928	56	-1.40
137	301	400	0.89	300	5.1	0.15	0.32	0.009	0.1151	0.006	1839	22	1801	42	1838	51	2.01
142	270	226	1.16	191	4.9	0.088	0.31	0.006	0.113	0.002	1801	15	1762	27	1843	28	4.40
3	88.6	62.9	1.42	66.7	5.9	0.22	0.34	0.007	0.1229	0.004	1948	33	1903	32	1975	67	3.65
4	382	384	1.13	374	6.1	0.097	0.36	0.004	0.1237	0.002	1989	14	1963	21	2005	23	2.09
6	89.6	87.6	1.03	82.7	5.7	0.13	0.34	0.005	0.1204	0.003	1922	19	1888	23	1940	45	2.68
9	261	77.4	3.22	79.5	6.3	0.1	0.36	0.004	0.1257	0.002	2018	14	1976	17	2036	28	2.95
10	64.9	87.6	0.73	79.6	5.1	0.14	0.33	0.006	0.1119	0.003	1823	23	1829	27	1814	48	-0.83
13	102.5	85	1.19	82.2	5.7	0.14	0.34	0.005	0.1199	0.003	1923	21	1884	25	1944	42	3.09
14	329	256	1.31	221	4.4	0.12	0.30	0.007	0.1059	0.002	1707	24	1679	35	1723	27	2.55
15	68	36.4	1.87	35.3	5.6	0.18	0.34	0.007	0.1203	0.004	1923	27	1866	32	1947	53	4.16
21	700	359	1.97	296	4.1	0.077	0.29	0.004	0.1033	0.001	1661	15	1616	20	1683	23	3.98
25	236	63	4.60	68	10.3	0.18	0.46	0.006	0.1625	0.002	2466	16	2420	28	2477	23	2.30
28	92.8	30	4.99	40.2	10.7	0.24	0.46	0.007	0.1658	0.004	2489	21	2429	31	2502	36	2.92
29	86.1	28.7	3.15	37.1	10.0	0.24	0.44	0.007	0.1612	0.004	2429	22	2352	32	2452	40	4.08
31	169.7	140.5	1.22	129.6	5.1	0.11	0.32	0.005	0.1137	0.002	1827	18	1774	26	1846	37	3.90
33	93	133.3	0.69	144.3	6.4	0.16	0.36	0.006	0.1272	0.003	2031	22	1978	27	2042	44	3.13
35	85.8	97.9	0.89	89.5	5.1	0.14	0.32	0.006	0.1141	0.003	1834	23	1782	28	1853	53	3.83
36	249.1	150.4	1.66	161.8	7.3	0.19	0.38	0.007	0.1361	0.003	2149	23	2078	31	2168	38	4.15
37	58.6	47.2	1.22	41.1	4.4	0.17	0.30	0.007	0.1055	0.004	1700	33	1669	33	1692	74	1.36
38	92.1	75.7	1.20	79.1	6.2	0.2	0.35	0.009	0.1247	0.004	2004	31	1948	42	2025	59	3.80
40	206	89.2	2.27	93.7	7.7	0.18	0.39	0.006	0.1369	0.003	2188	21	2143	29	2181	34	1.74
43	212.5	212.1	1.00	185.3	4.4	0.09	0.30	0.005	0.106	0.002	1719	16	1691	24	1724	38	1.91
45	259	141	1.84	180	9.8	0.22	0.45	0.007	0.1557	0.003	2412	21	2379	29	2407	37	1.16
48	66	34.7	1.93	17.9	1.7	0.1	0.16	0.004	0.0765	0.005	976	39	946	20	990	120	4.44
49	54.7	43	1.28	46.8	6.2	0.2	0.35	0.008	0.1266	0.004	1999	29	1950	37	2038	58	4.32
54	32.1	46.4	0.69	43.6	4.9	0.22	0.32	0.007	0.1126	0.006	1792	38	1794	34	1767	91	-1.53
55	228	175.8	1.29	187.4	6.4	0.12	0.37	0.006	0.1271	0.002	2026	17	2013	27	2052	30	1.90
56	236	139.7	1.68	179.1	10.7	0.14	0.47	0.005	0.1679	0.002	2498	13	2462	22	2531	21	2.73
58	400	36.1	10.97	44.7	10.3	0.17	0.46	0.007	0.1612	0.002	2459	15	2453	29	2464	22	0.45
59	133.1	47.7	2.80	35.9	3.3	0.1	0.25	0.005	0.0939	0.003	1483	24	1458	25	1495	59	2.47
60	331	29.3	11.37	36.6	9.7	0.13	0.44	0.005	0.1601	0.002	2406	13	2341	20	2453	21	4.57
61	125.9	101	1.44	104	5.7	0.24	0.35	0.010	0.1179	0.004	1922	36	1921	49	1904	62	-0.89
76	464	120.9	3.82	86.5	3.6	0.095	0.26	0.004	0.0951	0.002	1538	21	1511	22	1518	45	0.46
78	562	193.9	2.89	271.3	15.0	0.2	0.54	0.006	0.1951	0.002	2812	13	2801	24	2782	18	-0.68
79	160	72.6	2.13	47.7	3.1	0.11	0.24	0.004	0.0887	0.003	1411	26	1402	20	1375	63	-1.96
80	142.9	89.3	1.63	87.5	6.2	0.15	0.36	0.005	0.124	0.003	1996	21	1963	25	2002	44	1.95
81	307	80.5	3.65	81	7.1	0.12	0.39	0.004	0.1299	0.002	2119	15	2118	20	2091	30	-1.29
83	353	194.3	1.79	194.7	6.8	0.098	0.38	0.005	0.1285	0.002	2084	13	2076	22	2074	25	-0.10
84	121.4	159.2	0.75	161.5	6.8	0.16	0.38	0.006	0.1284	0.003	2082	21	2070	26	2069	38	-0.05
85	240	151	1.56	140	6.9	0.39	0.39	0.018	0.1281	0.004	2086	43	2100	78	2066	50	-1.65
86	149	104.1	1.37	97.2	5.7	0.14	0.36	0.006	0.1162	0.003	1937	23	1965	26	1885	46	-4.24
88	201.1	146.4	1.36	159.6	7.0	0.18	0.38	0.006	0.1345	0.003	2111	23	2054	27	2156	37	4.73
89	228	297	0.88	271	5.6	0.13	0.35	0.006	0.1162	0.002	1907	19	1916	29	1886	35	-1.59
90	216.5	232	0.93	213.1	5.5	0.089	0.34	0.004	0.1175	0.002	1890	14	1869	20	1908	30	2.04
91	69.8	73.6	0.95	70.4	5.3	0.18	0.34	0.005	0.1138	0.004	1867	28	1895	26	1837	58	-3.16
92	477	507	0.99	469	6.4	0.13	0.37	0.006	0.1265	0.002	2032	19	2027	28	2043	24	0.78
94	240.1	288	0.83	268.1	5.3	0.12	0.34	0.007	0.1153	0.002	1868	19	1867	32	1873	35	0.32
96	94.2	54.8	1.71	40.2	3.4	0.14	0.26	0.005	0.0956	0.004	1501	31	1496	26	1506	74	0.66
97	189	78.6	2.36	52	2.9	0.082	0.24	0.004	0.0877	0.003	1387	21	1407	19	1365	53	-3.08
98	147	195	0.74	196.1	6.5	0.19	0.37	0.007	0.129	0.003	2035	26	2018	33	2071	43	2.56
99	424	306	1.37	330	7.4	0.12	0.39	0.005	0.1383	0.002	2158	14	2130	22	2199	25	3.14
100	159.7	133.5	1.19	143.4	6.2	0.18	0.37	0.006	0.1229	0.003	2000	26	2018	27	1984	48	-1.71
102	367	156.2	2.38	191.9	13.4	0.24	0.51	0.007	0.189	0.003	2703	18	2671	29	2728	25	2.09
103	333	174.3	1.86	177.2	6.1	0.11	0.37	0.004	0.1208	0.002	1983	15	2013	20	1964	28	-2.49
106	467	511	0.99	441	5.1	0.1	0.33	0.004	0.1136	0.002	1835	17	1830	21	1851	27	1.13
107	347	423	0.82	414	5.4	0.11	0.34	0.004	0.1153	0.002	1885	17	1896	17	1872	38	-1.28
108	83	84.8	0.98	86.4	5.5	0.18	0.34	0.006	0.1163	0.004	1886	29	1891	29	1885	60	-0.32
109	312.8	391	0.80	366.4	5.8	0.097	0.34	0.004	0.1228	0.002	1946	15	1907	21	1994	30	4.36
112	107.2	65	1.64	51.2	3.3	0.12	0.26	0.004	0.0941	0.004	1480	29	1479	22	1465	72	-0.96
113	183.8	154.5	1.17	155.5	5.4	0.11	0.34	0.004	0.1139	0.002	1872	17	1901	18	1847	36	-2.92
114	140.4	138.9	1.00	129.8	4.9	0.12	0.32	0.004	0.1119	0.003	1802	20	1793	20	1820	45	1.48
115	203	105	1.98	104.2	5.8	0.12	0.36	0.004	0.1179	0.003	1953	18	1987	21	1909	39	-4.09
116	184	140	1.35	111.3	3.7	0.1	0.27	0.004	0.0977	0.003	1559	22	1550	19	1563	54	0.83
117	517	573	0.90	531	5.2	0.081	0.33	0.004	0.1157	0.002	1848	14	1820	18	1883	27	3.35
118	160.3	116.6	1.37	83.5	3.0	0.12	0.24	0.004	0.0915	0.004	1401	30	1365	22	1433	76	4.75
119	392	436	0.96	379	5.8	0.19	0.35	0.008	0.1196	0.002	1938	31	1914	36	1954	38	2.05
120	184.3	99.1	1.78	91	4.7	0.11	0.31	0.005	0.1105	0.002	1752	20	1721	25	1795	39	4.12
122	121.6	80	1.51	84.7	6.1	0.15	0.36	0.005	0.1233	0.003	1992	21	1976	24	1990	45	0.70

Basal diamictite upper package

Spot #	Compositional Data				Isotope Ratios						Apparent Ages (Ma)						Discordance
	U (ppm)	Th (ppm)	U Th	Pb (ppm)	207Pb 235U	±207Pb 235U	206Pb 238U	±206Pb 238U	207Pb 206Pb	±207Pb 206Pb	207Pb 235U	±207Pb 235U	206Pb 238U	±206Pb 238U	207Pb 206Pb	±207Pb 206Pb	(%)
11	227	166.3	1.359	109.6	2.797	0.092	0.2325	0.0049	0.0867	0.0027	1350	25	1346	25	1317	63	-2.20
15	163	82.7	1.85	111	6.93	0.33	0.384	0.021	0.1304	0.0061	2104	45	2087	96	2080	80	-0.34
16	95.5	108.6	0.891	86.6	4.58	0.16	0.3022	0.0077	0.1093	0.004	1734	29	1699	38	1757	64	3.30
18	222	91.7	2.408	100.6	6.27	0.28	0.361	0.012	0.1268	0.0054	2005	39	1984	58	2029	77	2.22
20	126.4	95.2	1.321	55.4	2.347	0.098	0.2097	0.0054	0.081	0.0032	1218	30	1225	29	1169	79	-4.79
24	135.8	103.8	1.289	89.2	4.35	0.18	0.3019	0.0091	0.1052	0.0045	1694	34	1698	45	1684	81	-0.83
26	125	195	0.635	183	4.97	0.19	0.322	0.011	0.1104	0.0043	1805	33	1795	52	1778	70	-0.96
29	79.9	64.1	1.231	66.9	6	0.23	0.347	0.012	0.1254	0.0048	1963	35	1915	55	1998	72	4.15
30	295	66.1	4.49	43.9	2.782	0.086	0.2269	0.006	0.0883	0.0023	1349	23	1316	32	1369	51	3.87
31	171.5	205	0.845	189.1	5.24	0.19	0.3329	0.009	0.1127	0.0039	1847	30	1848	43	1824	63	-1.32
32	88.9	58.1	1.525	56.2	5.3	0.23	0.329	0.011	0.1184	0.0047	1849	35	1827	51	1879	70	2.77
37	223	179	1.49	157	5.54	0.25	0.337	0.011	0.1177	0.004	1893	40	1867	51	1888	62	1.11
38	32.2	28.4	1.136	26.5	5.87	0.27	0.356	0.013	0.1233	0.0061	1947	42	1952	61	1920	95	-1.67
39	484	304.6	1.583	160.4	1.845	0.066	0.1752	0.0042	0.0753	0.0025	1054	23	1040	23	1054	67	1.33
41	99	59.8	1.634	61.9	6.81	0.21	0.3763	0.0074	0.1301	0.004	2075	27	2061	36	2067	54	0.29
46	120.2	69.1	2.22	65.4	5.87	0.17	0.353	0.0078	0.1189	0.0036	1948	26	1946	37	1910	55	-1.88
49	501	493	1.011	346	3.241	0.084	0.2545	0.0054	0.0907	0.0022	1462	20	1460	28	1420	47	-2.82
53	145.1	111.1	1.297	100.9	5.61	0.13	0.3448	0.0053	0.1156	0.003	1914	20	1908	25	1872	47	-1.92
56	78.6	78.5	1.008	28.7	1.194	0.099	0.122	0.0036	0.0674	0.0053	775	46	741	21	710	170	-4.37
57	107.5	51.9	2.07	50.7	6.35	0.22	0.3677	0.0082	0.1226	0.004	2015	30	2016	38	1976	57	-2.02
59	91.6	69.1	1.339	68.2	6.41	0.25	0.3678	0.0079	0.1223	0.0048	2026	35	2023	39	1961	75	-3.16
62	368	234.6	1.556	152.9	2.97	0.1	0.2428	0.0059	0.0883	0.0028	1396	27	1399	31	1369	65	-2.19
66	120.7	112.2	1.082	108.3	6.37	0.2	0.3679	0.0074	0.1236	0.0033	2018	28	2017	35	1993	50	-1.20
68	53.2	73.1	0.727	24.7	1.215	0.09	0.1252	0.0044	0.0714	0.0055	780	41	759	25	760	160	0.13
70	250	130	2.21	91	3.06	0.11	0.2476	0.0088	0.091	0.0044	1415	28	1423	46	1406	95	-1.21
74	169	347	0.514	147	1.366	0.083	0.1425	0.0039	0.0702	0.0041	873	38	858	22	860	130	0.23
78	231.1	184.1	1.27	198.8	6.12	0.17	0.3591	0.0073	0.1246	0.0028	1982	25	1980	36	2013	43	1.64
87	210	102.6	2.054	135.7	9.03	0.27	0.437	0.01	0.1549	0.0043	2337	28	2332	45	2381	47	2.06
89	271	150.3	1.798	166.1	6.38	0.22	0.378	0.011	0.1267	0.0036	2020	30	2063	51	2031	52	-1.58
93	157	68.6	2.229	67.2	4.4	0.2	0.3052	0.0094	0.1105	0.0047	1706	38	1714	47	1784	75	3.92
97	219	133	1.669	148.6	6.06	0.16	0.3591	0.0076	0.1267	0.0032	1986	25	1976	36	2037	43	2.99
102	199.2	143.1	1.383	88.8	2.314	0.084	0.2077	0.0042	0.0824	0.0032	1211	26	1216	22	1202	78	-1.16
104	172.4	151.8	1.176	157.5	5.94	0.15	0.3556	0.0059	0.1215	0.0029	1961	21	1959	28	1960	44	0.05
109	322	333	0.927	383	8.03	0.2	0.415	0.011	0.1404	0.0033	2232	22	2235	52	2226	42	-0.40
113	148.4	81	2.25	54.1	3.08	0.12	0.2466	0.006	0.0901	0.0036	1422	30	1419	31	1391	77	-2.01
114	245	211.7	1.152	221.8	6.2	0.13	0.3633	0.0066	0.1214	0.0029	2002	19	1995	31	1963	44	-1.63
119	205.2	283.6	0.717	275.9	5.43	0.14	0.3335	0.0074	0.1141	0.0032	1885	22	1853	36	1845	51	-0.43
122	192.6	180	1.103	234	12.18	0.31	0.489	0.013	0.1757	0.0042	2618	25	2558	57	2603	41	1.73
124	215.5	154.5	1.38	150	5.55	0.13	0.344	0.0065	0.1134	0.0027	1903	21	1903	31	1837	44	-3.59
125	255	81.2	3.89	78.5	5.11	0.2	0.32	0.01	0.1134	0.0037	1826	33	1784	51	1840	56	3.04
129	206.9	91.3	2.247	47.7	1.949	0.094	0.1831	0.0053	0.0752	0.0037	1099	36	1088	30	1047	97	-3.92
131	225	97.5	2.15	52.8	1.885	0.083	0.1741	0.0042	0.0751	0.0034	1068	31	1033	23	1020	98	-1.27
132	108.3	57	1.995	61.6	7.03	0.24	0.3853	0.0094	0.1281	0.004	2100	30	2096	44	2040	57	-2.75
133	416	48.8	8.52	33	3.18	0.12	0.2485	0.0066	0.0899	0.0032	1444	30	1429	34	1412	65	-1.20
134	380	96.1	4.01	103	5.84	0.2	0.3531	0.0077	0.1167	0.0031	1947	30	1947	36	1892	49	-2.91
135	79.5	98.8	0.825	103.2	5.84	0.29	0.336	0.012	0.1185	0.0056	1939	42	1865	55	1897	86	1.69
138	99.4	83.4	1.18	67	5.49	0.27	0.336	0.011	0.1174	0.0056	1886	40	1862	51	1875	88	0.69
145	80.3	36.8	2.174	26.4	3.29	0.2	0.2546	0.0075	0.0928	0.0051	1460	48	1458	38	1420	100	-2.68
150	119.3	133	0.912	111.5	4.83	0.23	0.306	0.01	0.1116	0.0053	1774	39	1719	52	1792	80	4.07
151	325	154.6	2.094	98	2.94	0.13	0.2348	0.006	0.0897	0.0039	1383	32	1358	31	1382	85	1.74
152	185	88	2.154	56	2.895	0.096	0.2311	0.006	0.09	0.0034	1385	27	1338	31	1392	70	3.88
158	350	439	0.787	392	6.16	0.18	0.3637	0.0099	0.1215	0.0032	1999	24	1997	47	1975	49	-1.11
161	243	93.9	2.59	127.9	12.95	0.31	0.508	0.011	0.1806	0.004	2669	23	2645	45	2646	36	0.04
164	158.5	195	0.815	106.2	2.32	0.15	0.2001	0.0073	0.0824	0.0052	1202	46	1174	39	1190	130	1.34
165	275	148.7	1.826	126.9	5.02	0.15	0.3209	0.0083	0.1133	0.0037	1816	26	1792	41	1832	60	2.18
167	413	217	1.841	242	6.86	0.14	0.3843	0.0078	0.1284	0.0022	2088	18	2093	36	2064	31	-1.41
170	412	284	1.445	259	5.52	0.14	0.3429	0.007	0.1165	0.0028	1899	21	1899	34	1888	44	-0.58
172	93.9	118.1	0.809	123.7	6.32	0.24	0.365	0.01	0.124	0.0049	2010	33	2011	47	1989	75	-1.11
178	142	215	0.671	197	5.58	0.21	0.3476	0.0089	0.1152	0.0041	1907	31	1920	43	1873	67	-2.51
181	383	333.9	1.122	336	5.63	0.17	0.3439	0.0089	0.1182	0.0033	1914	25	1903	43	1912	50	0.47
182	230	236	1.047	225	5.42	0.13	0.3385	0.0073	0.114	0.0025	1880	20	1876	35	1851	38	-1.35
183	61.1	94.9	0.675	92.3	5.56	0.22	0.3413	0.0081	0.1156	0.0044	1895	35	1889	39	1859	72	-1.61
184	197	175	1.173	170	5.56	0.16	0.334	0.01	0.1199	0.0037	1902	25	1852	48	1936	55	4.34
185	156	99.1	1.59	108.5	5.65	0.34	0.334	0.012	0.119	0.0061	1897	51	1854	57	1908	97	2.83
186	119.4	59.7	2.13	41.9	2.54	0.13	0.2081	0.005	0.0869	0.0049	1277	40	1218	27	1280	110	4.84
187	186.9	79.9	2.332	66.3	2.94	0.13	0.2317	0.008	0.0873	0.0036	1382	34	1341	41	1343	86	0.15
190	14.71	11.56	1.29	19.1	20.49	0.97	0.616	0.023	0.231	0.0097	3084	47	3075	89	3041	69	-1.12
202	88.8	94.1	0.925	101.9	6.22	0.25	0.3511	0.0099	0.1228	0.0049	1994	35	1943	49	1953	74	0.51
204	264	226	1.176	237	6.91	0.23	0.3851	0.0095	0.1258	0.0036	2091	31	2096	44	2023	49	-3.61
208	202.9	67.5	3.071	73.8	6.59	0.17	0.3745	0.0081	0.1211	0.0034	2052	24	2048	38	1951	49	-4.97
211	177	141.7	1.248	72.3	1.97	0.11	0.1799	0.0058	0.0764	0.0044	1092	39	1065	32	1030	120	-3.40
213	174	50	3.48	52.2	6.75	0.22	0.3792	0.0088	0.1222	0.0036	2070	28	2070	41	1973	55	-4.92
216	204	33.6	6.21	43.6	5.32	0.19	0.3229	0.0074	0.1136	0.0035	1860	30	1801	36	1846	54	2.44
217	384	301	1.219	286	5.99	0.14	0.3569	0.0066	0.1168	0.0021	1970	21	1965	31	1895	33	-3.69
219	171	192	0.918	157	5.03	0.15	0.3261	0.0079	0.1096	0.0037	1819	26	1816	39	1754	64	-3.53
221	226	451	0.548	203	1.762	0.082	0.1681	0.0041	0.073	0.0034	1031	31	1001	23	980	99	-2.14
225	207	294	0.716	189	3.09	0.11	0.2434	0.0062	0.0899	0.0038	1423	28	1403	32	1379	79	-1.74
230	184	212	0.891	234	5.7	0.29	0.333	0.015	0.1187	0.0048	1927	43	1851	71	1926	71	3.89
234	100.3	57.9	1.731	77.7	14.72	0.71	0.534	0.021	0.1956	0.0073	2783	46	2749	87	2771	61	0.79
241	218.3	110.2	1.997	123.9	6.27	0.21	0.3543	0.0091	0.126	0.0038	2005	29	1952	43	2019	54	3.32
245	81.8	103.8	0.788	930	54	21	0.77	0.19	0.349	0.056	3320	320	3280	520	3360	240	2.38
246	246	191	1.327	172.9	4.97	0.15	0.3245	0.0067	0.1114	0.0031	1807	25	1809	33	1799	50	-0.56
263	87.9	53.9	1.64	40.7	2.94	0.16	0.2454	0.0082	0.0901	0.0048	1387	41	1412	42	1390	100	-1.58
265	405.2	506	0.796	467	5.65	0.19	0.347	0.011	0.1226	0.0038	1918	29	1915	53	1992	61	3.87
271	144.8	153.1	0.938	130.1	4.28	0.14	0.2972	0.007	0.1073	0.0042	1680	27	1680	36	1720	73	2.33
272	156.4	96.9	1.616	54.1	1.86	0.11	0.1784	0.0067	0.0774	0.0051	1055	40	1057	37	1070	130	1.21
274	222.5	145.4	1.527	155.3	6.6	0.23	0.3749	0.0093	0.13	0.0048	2051	31	2050	43	2069	66	0.92
275	86	128.7	0.664	129.1	5.53	0.25	0.353	0.013	0.1164	0.0053	1892	39	1943	63	1874	79	-3.68
278	133.2	58.2	2.39	89.5	8.12	0.31	0.411	0.013	0.147	0.0052	2229	35	2212	61	2278	60	2.90
280	561	128.8	4.307	111.5	3.53	0.1	0.2684	0.0076	0.0957	0.0029	1531	25	1530	38	1512	57	-1.19
288	370	398	0.924	392	5.1	0.17	0.3219	0.0093	0.1152	0.0041	1836	30	1797	45	1863	66	3.54
291	147.5	57.3	2.601	56.9	4.99	0.16	0.3262	0.0076	0.1106	0.0039	1811	26	1817	37	1773	63	-2.48
293	68.5	100.7	0.697	35.8	1.14	0.14	0.1125	0.0044	0.0681	0.0077	730	69	686	25	670	250	-2.39

lower KPS

Spot #	Compositional Data				Isotope Ratios						Apparent Ages (Ma)						Discordance
	U	Th	U	Pb	207Pb	±207Pb	206Pb	±206Pb	207Pb	±207Pb	207Pb	±207Pb	206Pb	±206Pb	207Pb	±207Pb	(%)
	(ppm)	(ppm)	Th	(ppm)	235U	235U	238U	238U	206Pb	206Pb	235U	235U	238U	238U	206Pb	206Pb	
1	89.2	102.3	0.883	102.1	10.16	0.19	0.47	0.01	0.17	0.003	2444	18	2461	34	2501	28	1.60
2	32.6	23.5	1.396	21.2	5.94	0.18	0.37	0.01	0.12	0.005	1962	29	2008	45	1966	70	-2.14
3	173.2	145.9	1.195	114.1	5.84	0.14	0.35	0.01	0.13	0.003	1951	21	1951	36	2016	40	3.22
6	37	39	1.19	34.1	6.87	0.28	0.39	0.01	0.14	0.006	2086	37	2116	65	2135	72	0.89
7	53.9	25.8	2.53	16.6	5.51	0.26	0.34	0.01	0.12	0.004	1886	40	1887	63	1960	61	3.72
9	52.2	39.6	1.379	28.6	4.66	0.2	0.32	0.01	0.11	0.004	1756	36	1799	45	1761	74	-2.16
11	218	276	0.809	219	5.27	0.12	0.33	0.01	0.12	0.002	1858	19	1853	32	1920	35	3.49
14	189.8	72.2	2.656	68.6	10.56	0.35	0.47	0.01	0.17	0.005	2477	31	2485	62	2524	48	1.55
15	30.8	35.7	0.864	10.54	0.989	0.083	0.11	0.00	0.07	0.006	683	42	685	23	660	180	-3.79
17	148.7	46.7	3.24	40.3	5.62	0.2	0.36	0.01	0.12	0.004	1914	30	1974	44	1891	61	-4.39
18	212	189	1.73	45.4	8.67	0.38	0.43	0.02	0.15	0.003	2289	42	2289	75	2351	39	2.64
19	67.9	45.8	1.499	40.2	5.99	0.16	0.37	0.01	0.12	0.004	1969	24	2005	32	1983	56	-1.11
20	377	35.7	12.13	16.74	4.72	0.1	0.32	0.01	0.11	0.002	1766	18	1770	28	1815	36	2.48
21	778	82	10.71	74.4	10.78	0.27	0.47	0.01	0.17	0.002	2501	24	2500	49	2546	21	1.81
22	573	316.3	1.821	264.8	4.928	0.094	0.32	0.01	0.11	0.002	1804	16	1782	31	1872	32	4.81
28	131.4	145.1	0.901	154.5	6.11	0.19	0.36	0.01	0.12	0.003	1987	27	1973	48	2021	47	2.38
29	41.9	33.5	1.229	34.8	6.06	0.18	0.36	0.01	0.12	0.004	1975	27	1979	42	1981	58	0.10
31	114.1	75.9	1.554	91.8	10.71	0.34	0.47	0.01	0.17	0.004	2487	29	2483	54	2504	36	0.84
32	147.1	126.5	1.153	127.1	6.63	0.19	0.38	0.01	0.13	0.003	2054	26	2072	47	2039	47	-1.62
33	56.2	22.1	2.591	36.3	19.47	0.5	0.60	0.01	0.23	0.006	3056	25	3054	57	3067	40	0.42
34	395	42.9	9.06	38.2	5.31	0.15	0.34	0.01	0.11	0.003	1864	24	1873	41	1852	45	-1.13
35	100.5	82.6	1.288	74.6	5.45	0.18	0.34	0.01	0.12	0.004	1885	28	1871	43	1898	57	1.42
36	229.9	63.1	3.75	36.7	2.68	0.072	0.23	0.01	0.09	0.002	1321	21	1320	27	1313	48	-0.53
37	172	128.4	1.337	133.8	6.07	0.19	0.36	0.01	0.12	0.004	1980	27	1970	52	1993	53	1.15
38	346.4	444	0.777	398	4.89	0.19	0.32	0.01	0.11	0.004	1793	33	1761	55	1831	61	3.82
39	101.8	67.3	1.565	65.9	5.76	0.18	0.35	0.01	0.12	0.003	1929	28	1914	43	1941	46	1.39
40	155.7	66.8	2.3	99.5	16.69	0.31	0.57	0.01	0.21	0.004	2913	18	2881	47	2928	31	1.61
41	110.7	162.1	0.649	154.9	6.25	0.14	0.37	0.01	0.12	0.003	2008	19	2012	36	1992	44	-1.00
42	192	320	0.599	304	5.86	0.17	0.35	0.01	0.12	0.003	1950	24	1922	40	1973	49	2.58
43	134.8	64	2.059	64.3	6.17	0.19	0.36	0.01	0.12	0.003	1992	26	1997	41	1979	47	-0.91
45	302	272	1.135	224	4.89	0.11	0.32	0.01	0.11	0.002	1799	18	1788	28	1784	33	-0.22
46	157	90	1.692	107.9	11.73	0.22	0.49	0.01	0.17	0.003	2578	18	2572	36	2565	28	-0.27
48	137.3	85.2	1.615	83.2	6.56	0.17	0.37	0.01	0.13	0.003	2048	23	2041	35	2038	41	-0.15
50	244	125.3	2.037	106.2	7.4	0.13	0.40	0.01	0.14	0.002	2157	16	2159	32	2155	26	-0.19
51	176.3	181.1	0.98	163.1	6.2	0.16	0.36	0.01	0.13	0.003	2000	22	1961	40	2042	37	3.97
52	54.4	26.3	2.125	34.1	17.54	0.63	0.58	0.02	0.22	0.007	2956	35	2956	66	2953	51	-0.10
53	160.3	86.6	1.856	99.5	12.45	0.3	0.50	0.01	0.18	0.003	2634	22	2606	46	2657	31	1.92
55	96.9	63.8	1.538	62.5	5.69	0.16	0.35	0.01	0.12	0.003	1922	24	1922	37	1925	49	0.16
56	79.4	41.4	1.904	48.8	11.09	0.3	0.48	0.01	0.17	0.005	2529	26	2512	54	2539	45	1.06
57	92.9	42.5	2.208	51.4	10.58	0.23	0.47	0.01	0.16	0.004	2486	21	2487	45	2487	43	0.00
59	128	25	8.3	22.6	5.55	0.21	0.34	0.01	0.12	0.004	1896	32	1898	39	1896	56	-0.11
60	70.2	132	0.563	116.1	6.69	0.23	0.38	0.01	0.13	0.004	2062	32	2060	47	2061	60	0.05
62	332	185	1.798	226.6	12.19	0.36	0.50	0.01	0.18	0.004	2611	28	2609	62	2605	35	-0.15
64	222	84.4	2.577	98.9	11.16	0.22	0.48	0.01	0.17	0.003	2534	19	2538	43	2522	33	-0.63
65	110.2	206	0.534	191.5	6.05	0.16	0.36	0.01	0.12	0.003	1976	23	1995	38	1950	46	-2.31
66	82.1	82.9	1.034	91.3	11.14	0.38	0.48	0.02	0.17	0.005	2522	32	2521	70	2507	52	-0.56
67	90.5	64.3	1.419	61.2	6.21	0.18	0.37	0.01	0.12	0.004	2003	26	2023	39	1955	53	-3.48
68	70.6	49.8	1.447	62.8	12.89	0.41	0.51	0.01	0.18	0.005	2664	30	2667	53	2648	48	-0.72
71	143.4	130.2	1.154	101.5	6.86	0.28	0.37	0.01	0.13	0.004	2084	37	2036	63	2118	50	3.87
73	120.5	147.2	0.829	165.3	10.49	0.25	0.46	0.01	0.16	0.003	2473	22	2431	36	2481	35	2.02
74	58.6	44.7	1.29	42.3	6.1	0.21	0.36	0.01	0.12	0.004	1980	30	1982	35	1945	65	-1.90
75	131	108	1.409	127	12.47	0.28	0.51	0.01	0.18	0.003	2634	21	2636	45	2595	31	-1.58
76	120	64.8	1.884	86	11.38	0.26	0.49	0.01	0.17	0.004	2549	21	2548	44	2496	37	-2.08
77	129.5	111.6	1.153	151.4	16.94	0.32	0.57	0.01	0.21	0.004	2930	19	2883	41	2898	31	0.52
79	140	90	1.713	81	5.98	0.21	0.35	0.01	0.12	0.004	1964	29	1940	52	1941	58	0.05
80	109.4	50.3	2.193	52.1	7.96	0.28	0.41	0.01	0.14	0.003	2220	33	2217	50	2159	44	-2.69
81	117.4	62.5	1.969	55.6	5.85	0.12	0.34	0.01	0.12	0.002	1949	18	1884	26	1935	37	2.64
83	47.1	24	1.983	21	4.9	0.18	0.32	0.01	0.11	0.005	1794	31	1792	44	1727	86	-3.76
84	133.2	128.7	1.04	128.5	6.25	0.12	0.37	0.01	0.12	0.003	2010	18	2010	34	1927	40	-4.31
85	99.9	85.8	1.166	86.1	6.07	0.16	0.35	0.01	0.12	0.004	1981	23	1947	38	1942	54	-0.26
87	316	215.9	1.451	125.4	2.608	0.064	0.22	0.00	0.08	0.002	1300	19	1255	21	1275	39	1.57
91	81.8	24.6	3.32	30.1	8.93	0.33	0.44	0.02	0.14	0.005	2323	34	2325	69	2234	66	-4.07
92	128	44.5	2.947	28.4	2.607	0.088	0.22	0.01	0.08	0.003	1299	24	1273	31	1231	62	-3.41
96	88.7	31.4	2.847	45	14.65	0.41	0.53	0.02	0.19	0.006	2785	27	2732	68	2729	48	-0.11
98	215	290	0.738	245.7	5.47	0.16	0.33	0.01	0.11	0.003	1891	25	1827	40	1850	52	1.24
99	162	74.6	2.195	65	5.86	0.18	0.34	0.01	0.12	0.003	1948	26	1880	42	1908	48	1.47
102	167	78.5	2.19	51	3.52	0.11	0.26	0.01	0.09	0.003	1528	24	1474	34	1484	55	0.67
104	118.2	14.05	8.58	19	10.29	0.28	0.46	0.01	0.15	0.004	2455	25	2458	41	2351	41	-4.55
105	121.8	44.9	2.693	43.1	6.03	0.15	0.35	0.01	0.12	0.003	1972	22	1949	31	1900	41	-2.58
109	188.8	117.4	1.564	120.5	6.77	0.2	0.38	0.01	0.13	0.004	2077	26	2094	43	2054	48	-1.95
111	176.5	250.3	0.701	214.5	4.54	0.18	0.31	0.01	0.11	0.004	1732	32	1728	44	1740	63	0.69
112	311.9	125	2.533	114.6	6.24	0.14	0.36	0.01	0.12	0.003	2006	20	2003	37	2015	37	0.60
114	228	24.4	9.92	26.7	9.5	0.25	0.44	0.01	0.16	0.003	2386	25	2343	50	2434	29	3.74
115	228	169.2	1.331	182.2	7.53	0.22	0.41	0.01	0.14	0.003	2169	27	2188	49	2171	41	-0.78
117	363	82.2	4.32	85.6	7	0.21	0.39	0.01	0.13	0.003	2104	27	2104	46	2125	38	0.99
119	101.3	51.6	1.97	45.8	9.26	0.31	0.44	0.01	0.16	0.004	2353	31	2349	62	2395	43	1.92
120	234.7	190.2	1.21	187.9	5.84	0.27	0.35	0.01	0.12	0.005	1945	39	1949	61	1973	67	1.22
122	128.2	105.4	1.24	103	6.36	0.23	0.38	0.01	0.13	0.004	2019	32	2050	53	2028	54	-1.08
124	223.2	59.8	3.81	61.4	6.49	0.2	0.39	0.01	0.13	0.004	2036	28	2094	51	2021	52	-3.61
125	266.9	121.7	2.167	124.8	7.43	0.24	0.40	0.01	0.14	0.004	2161	28	2166	57	2197	42	1.41
127	108	68.7	1.515	67.8	6.44	0.26	0.38	0.02	0.12	0.004	2025	36	2088	67	2007	64	-4.04
128	313	105.2	2.959	114.5	5.82	0.2	0.36	0.01	0.12	0.003	1947	29	1970	52	1954	49	-0.82
131	189.4	189	1.001	175.1	6.64	0.18	0.38	0.01	0.13	0.003	2059	24	2089	50	2072	38	-0.82
132	171	118.6	1.443	104.9	5.42	0.3	0.34	0.02	0.12	0.004	1872	48	1875	74	1910	64	1.83
133	119.7	85.3	1.393	83.6	6.2	0.21	0.37	0.01	0.13	0.004	1996	29	2001	48	2054	60	2.58
134	140.1	78.2	1.779	51.7	2.84	0.11	0.24	0.01	0.09	0.003	1362	29	1363	28	1387	67	1.73
135	74	56.5	1.29	64.6	6.91	0.22	0.40	0.01	0.13	0.004	2093	28	2146	55	2067	61	-3.82
138	149.7	59.3	2.464	64.6	7.35	0.24	0.40	0.01	0.14	0.004	2149	29	2142	48	2187	51	2.06
139	147	139	1.034	116.2	5.84	0.26	0.35	0.01	0.12	0.005	1946	38	1943	56	1967	76	1.22
141	219.4	164	1.343	177.5	6.94	0.21	0.39	0.01	0.13	0.003	2105	29	2103	45	2073	45	-1.45

Middle diamictite

Spot #	Compositional Data				Isotope Ratios						Apparent Ages (Ma)						Discordance
	U (ppm)	Th (ppm)	U Th	Pb (ppm)	207Pb 235U	±207Pb 235U	206Pb 238U	±206Pb 238U	207Pb 206Pb	±207Pb 206Pb	207Pb 235U	±207Pb 235U	206Pb 238U	±206Pb 238U	207Pb 206Pb	±207Pb 206Pb	(%)
142	159	91	1.733	115.4	11.19	0.31	0.48	0.02	0.17	0.006	2536	26	2518	68	2511	63	-0.28
144	120.8	95.1	1.277	96.1	5.99	0.22	0.36	0.01	0.12	0.005	1966	32	1979	49	1925	70	-2.81
145	101.3	78.6	1.268	78.9	5.91	0.19	0.35	0.01	0.12	0.004	1956	27	1947	37	1926	52	-1.09
148	153.9	83.6	1.842	109.9	11.17	0.28	0.49	0.01	0.17	0.004	2534	23	2551	56	2508	37	-1.71
149	133.4	77.6	1.702	83.8	6.86	0.20	0.38	0.01	0.13	0.004	2092	26	2095	41	2066	52	-1.40
150	36.63	31.33	1.171	41.9	10.02	0.38	0.46	0.01	0.16	0.006	2433	37	2433	59	2418	66	-0.62
151	119.1	171.1	0.697	159.3	5.89	0.20	0.35	0.01	0.12	0.004	1953	29	1950	42	1958	65	0.41
152	143.5	109.3	1.336	120	10.69	0.41	0.47	0.02	0.16	0.004	2493	38	2489	64	2482	45	-0.28
154	69.9	227.7	0.309	184	14.42	0.84	0.53	0.02	0.20	0.009	2764	56	2742	98	2781	72	1.40
155	170.9	125.2	1.36	122.9	5.94	0.18	0.36	0.01	0.12	0.004	1962	26	1984	45	1934	57	-2.59
156	246	246	1.41	110	1.823	0.09	0.18	0.01	0.08	0.003	1048	33	1051	37	1066	78	1.41
158	184.9	108.2	1.71	137.1	10.71	0.41	0.47	0.02	0.17	0.005	2495	34	2467	66	2501	56	1.36
161	184	102	1.882	105	6.97	0.43	0.39	0.02	0.13	0.006	2093	56	2122	92	2069	84	-2.56
163	150	120.4	1.217	139.7	10.29	0.39	0.47	0.02	0.16	0.005	2462	36	2465	73	2462	50	-0.12
164	282	176	1.88	85	2.52	0.17	0.22	0.02	0.09	0.003	1258	48	1265	83	1320	63	4.17
165	368.5	283.1	1.311	252.3	5.87	0.21	0.35	0.01	0.12	0.004	1949	31	1908	50	2005	53	4.84
166	83.6	41.6	2.053	54.4	10.11	0.40	0.47	0.02	0.16	0.005	2433	37	2479	65	2407	58	-2.99
167	142.2	91.8	1.558	90.1	6.4	0.22	0.37	0.01	0.13	0.004	2030	32	2033	54	2052	58	0.93
168	89.4	139.5	0.644	128	5.84	0.18	0.36	0.01	0.12	0.004	1945	27	1961	41	1950	61	-0.56
169	193.6	166.7	1.172	157.4	5.57	0.19	0.35	0.01	0.12	0.004	1903	30	1938	52	1897	52	-2.16
170	93.3	109.5	0.861	108.8	5.47	0.23	0.35	0.01	0.11	0.004	1883	35	1931	47	1848	71	-4.49
171	207	190	1.187	143	5.6	0.21	0.35	0.01	0.12	0.003	1903	33	1906	60	1928	41	1.14
174	213	212	1.034	189	5.67	0.17	0.35	0.01	0.12	0.003	1920	25	1921	40	1924	46	0.16
175	53.6	58.7	0.936	76	13.05	0.44	0.54	0.02	0.18	0.006	2673	32	2757	71	2628	55	-4.91
178	79.2	82.5	1.002	79.2	7.24	0.28	0.40	0.01	0.13	0.004	2135	33	2170	54	2107	53	-2.99
180	258	225	1.171	204	5.58	0.15	0.34	0.01	0.12	0.003	1906	23	1907	51	1934	42	1.40
181	320	186	2.12	67.3	26.2	2.40	0.70	0.06	0.27	0.005	3270	86	3330	220	3312	29	-0.54
182	141.9	105.3	1.35	83.7	4.14	0.17	0.29	0.01	0.10	0.004	1656	33	1623	32	1682	71	3.51
185	82.3	74.5	1.111	59.6	4.99	0.23	0.33	0.01	0.11	0.004	1802	37	1840	71	1771	59	-3.90
188	290	151.9	1.912	144.2	5.95	0.17	0.36	0.01	0.12	0.003	1965	25	1977	39	1942	46	-1.80
190	156	214	0.722	188	6.35	0.19	0.36	0.01	0.13	0.004	2019	27	1970	41	2054	50	4.09
192	78.9	62.3	1.267	58.2	5.96	0.22	0.35	0.01	0.12	0.004	1958	32	1916	53	1990	55	3.72
194	162.7	61.1	2.689	62	6.92	0.21	0.38	0.01	0.13	0.003	2094	26	2090	48	2077	44	-0.63
196	260	509	0.513	525	10.49	0.37	0.46	0.02	0.16	0.004	2473	32	2433	69	2485	40	2.09
198	254	105	2.05	72.9	7.46	0.31	0.40	0.02	0.14	0.004	2155	39	2143	72	2158	47	0.70
199	92.3	266	0.35	231	5.53	0.21	0.34	0.01	0.12	0.005	1895	33	1871	47	1900	73	1.53
200	469	195	2.516	154.6	6.15	0.25	0.35	0.01	0.13	0.003	1985	34	1933	62	2023	44	4.45
201	232.3	104.3	2.247	106	7.89	0.24	0.41	0.01	0.14	0.004	2211	28	2206	45	2194	51	-0.55
203	153.2	110.6	1.365	103.5	6.45	0.14	0.37	0.01	0.12	0.003	2035	20	2036	36	2021	42	-0.74
207	98.6	68	1.448	64.5	6.58	0.26	0.38	0.01	0.13	0.005	2053	38	2052	60	2015	64	-1.84
212	96	75	1.313	76	6.6	0.20	0.38	0.01	0.13	0.004	2051	27	2055	47	2024	56	-1.53
213	59.3	43.1	1.389	53.9	12.45	0.39	0.49	0.01	0.18	0.005	2631	28	2571	49	2657	47	3.24
217	153.3	277	0.55	234.3	5.41	0.21	0.34	0.01	0.12	0.004	1886	35	1882	44	1896	60	0.74
218	128.3	107.2	1.207	118.9	10.79	0.27	0.46	0.01	0.17	0.004	2500	24	2453	45	2545	37	3.61
221	191	37.1	5.28	38.5	8.81	0.29	0.43	0.01	0.15	0.004	2313	30	2316	63	2311	44	-0.22
226	178	160	1.121	152	7.37	0.21	0.40	0.01	0.14	0.004	2155	26	2154	43	2161	46	0.32
227	320	494	1.09	172	9.4	1.10	0.44	0.05	0.15	0.004	2250	110	2290	200	2359	45	2.92
229	104.7	89.8	1.183	84	6.1	0.19	0.37	0.01	0.12	0.004	1982	27	2029	50	1944	61	-4.37
230	196.3	147.2	1.336	145.6	6.73	0.25	0.39	0.01	0.13	0.004	2069	33	2097	51	2044	56	-2.59
233	117.2	52.4	2.299	53.7	6.12	0.21	0.37	0.01	0.12	0.004	1983	30	2008	49	1957	51	-2.61
235	420	133.9	3.158	132.5	6.59	0.21	0.39	0.01	0.12	0.003	2052	28	2097	50	2011	50	-4.28
236	180.9	186.5	0.973	222.4	11.32	0.36	0.49	0.02	0.17	0.005	2547	29	2548	67	2545	47	-0.12
238	182.9	90.6	2.094	78.5	4.79	0.18	0.32	0.01	0.11	0.003	1773	33	1801	49	1755	54	-2.62
239	204	142	1.85	54.8	2.81	0.13	0.24	0.01	0.09	0.003	1361	38	1357	63	1426	62	4.84
240	103	95.3	1.117	90.1	6.77	0.44	0.38	0.02	0.13	0.007	2066	58	2072	98	2060	100	-0.58
241	320	277	1.122	252	6.29	0.30	0.36	0.02	0.13	0.003	2006	41	1975	72	2043	46	3.33
242	259	119	2.374	93.3	5.76	0.24	0.34	0.01	0.12	0.004	1928	37	1886	67	1984	51	4.94
243	315	159.6	1.975	158.4	6.58	0.18	0.38	0.01	0.13	0.003	2050	24	2066	43	2024	36	-2.08
246	273	270	1.018	349	13.13	0.48	0.52	0.02	0.18	0.005	2681	35	2679	69	2684	42	0.19
247	29.3	15.2	2.04	23.6	17.39	0.69	0.58	0.02	0.22	0.010	2945	39	2940	85	2962	68	0.74
249	528	105	6.65	116	6.56	0.18	0.37	0.01	0.13	0.003	2049	24	2043	49	2064	39	1.02
252	199.7	99.1	2.029	109.2	7.73	0.20	0.41	0.01	0.14	0.004	2204	23	2202	51	2199	48	-0.14
255	182.6	189	0.993	183	6.79	0.23	0.37	0.01	0.13	0.004	2077	31	2033	50	2121	57	4.15
260	191.1	131.2	1.533	132.6	6.77	0.22	0.37	0.01	0.13	0.004	2076	28	2032	49	2134	53	4.78
262	70.2	54.9	1.293	79.7	16.77	0.65	0.56	0.02	0.22	0.008	2913	36	2854	79	2961	56	3.61
263	91.1	43.9	2.22	43.1	7	0.23	0.39	0.01	0.13	0.004	2109	28	2129	44	2096	52	-1.57
264	87.5	42.2	2.075	38.3	6.35	0.24	0.37	0.01	0.13	0.005	2017	33	2014	47	2033	62	0.93
266	258	196	1.298	173.1	6.22	0.21	0.37	0.01	0.12	0.003	2004	29	2002	58	2006	46	0.20
270	344	193	1.764	213	7.91	0.26	0.41	0.01	0.14	0.003	2219	32	2204	52	2229	38	1.12
271	90.8	47.7	2	61.6	12.91	0.77	0.52	0.03	0.18	0.007	2663	55	2690	110	2646	69	-1.66
272	190	179	1.079	156.6	6.27	0.27	0.36	0.01	0.13	0.004	2009	38	1961	61	2057	49	4.67
273	225.5	174.1	1.35	187.9	7.53	0.24	0.40	0.01	0.14	0.004	2171	28	2184	50	2160	48	-1.11
274	534	336	1.568	295	5.51	0.21	0.34	0.01	0.12	0.003	1892	33	1888	53	1886	50	-0.11
275	250.6	147.7	1.702	146	6.11	0.20	0.36	0.01	0.12	0.003	1987	28	1975	54	2008	48	1.64
276	508	101.5	5.07	97.9	7.28	0.22	0.39	0.01	0.14	0.003	2141	28	2109	51	2173	40	2.95
279	217	271	0.812	207.2	16.23	0.69	0.56	0.03	0.22	0.007	2903	47	2860	130	2945	50	2.89
283	104.4	69.8	1.495	98.5	13.01	0.56	0.52	0.02	0.18	0.007	2670	40	2698	81	2646	62	-1.97
284	209.7	269.7	0.794	279	6.53	0.27	0.37	0.01	0.13	0.005	2043	36	2034	60	2026	60	-0.39
285	694	459	1.522	188.4	1.8	0.10	0.18	0.01	0.08	0.003	1038	38	1056	53	1042	71	-1.34
287	444	127	3.87	71.7	2.28	0.10	0.20	0.01	0.08	0.002	1197	32	1193	47	1184	56	-0.76
289	202	223	0.938	208	5.29	0.16	0.34	0.01	0.11	0.003	1860	26	1881	39	1844	45	-2.01

Middle diamictite

	Compositional Data				Isotope Ratios						Apparent Ages (Ma)						Discordance
	U	Th	U	Pb	207Pb	±207Pb	206Pb	±206Pb	207Pb	±207Pb	207Pb	±207Pb	206Pb	±206Pb	207Pb	±207Pb	(%)
Spot #	(ppm)	(ppm)	Th	(ppm)	235U	235U	238U	238U	206Pb	206Pb	235U	235U	238U	238U	206Pb	206Pb	
1	478	202.2	2.363	134.3	2.97	0.08	0.24	0.004	0.09	0.002	1394	20	1399	21	1350	40	-3.63
2	740	351	2	204	2.87	0.11	0.24	0.009	0.09	0.002	1364	27	1370	45	1415	47	3.18
3	141.5	38.36	3.721	25.2	2.99	0.11	0.24	0.005	0.09	0.004	1397	29	1384	30	1364	79	-1.47
4	1497	287	5.261	181.9	2.82	0.06	0.24	0.004	0.09	0.001	1359	15	1365	23	1357	28	-0.59
8	275	429	0.653	361	5.23	0.17	0.33	0.009	0.12	0.003	1850	27	1849	44	1890	42	2.17
10	639	249.1	2.61	136.6	2.65	0.08	0.23	0.006	0.09	0.003	1311	23	1315	32	1346	60	2.30
11	143.6	64.2	2.289	39.8	2.82	0.08	0.24	0.005	0.09	0.003	1358	22	1360	24	1297	62	-4.86
12	203.9	89.1	2.34	47.8	2.70	0.14	0.23	0.006	0.09	0.004	1320	39	1319	32	1339	98	1.49
17	83	137.8	0.608	155	9.71	0.31	0.45	0.012	0.15	0.005	2406	30	2411	51	2336	54	-3.21
20	153	88	1.735	56	2.79	0.11	0.23	0.006	0.09	0.003	1349	32	1350	28	1315	73	-2.66
21	947	112.9	9.61	68.7	2.75	0.05	0.23	0.004	0.08	0.001	1343	14	1342	20	1293	29	-3.79
26	225	288	0.778	245	4.59	0.10	0.31	0.005	0.11	0.002	1745	19	1745	23	1736	37	-0.52
28	257	212	1.227	274	12.62	0.35	0.51	0.012	0.18	0.005	2646	26	2648	51	2682	41	1.27
30	934	388	2.443	292	3.20	0.08	0.25	0.005	0.09	0.002	1449	20	1449	26	1490	32	2.75
36	65.8	32.5	2.024	35.6	7.21	0.21	0.39	0.008	0.14	0.004	2128	26	2126	38	2172	48	2.12
37	369	196	1.929	135.1	2.84	0.08	0.23	0.004	0.09	0.002	1359	20	1355	21	1426	46	4.98
39	105.3	60.4	1.736	46.4	3.32	0.14	0.26	0.006	0.09	0.004	1476	33	1498	32	1450	79	-3.31
51	92.4	82.2	1.149	95.6	9.43	0.25	0.45	0.010	0.15	0.005	2375	25	2374	45	2330	55	-1.89
3	74.8	43.3	1.729	34.8	4.20	0.16	0.29	0.005	0.11	0.004	1663	31	1639	24	1682	77	2.56
4	166.9	109.6	1.495	105.4	5.66	0.16	0.34	0.005	0.12	0.003	1924	26	1897	22	1953	52	2.87
8	337	136.2	2.446	94.1	2.70	0.05	0.23	0.002	0.09	0.002	1326	14	1316	12	1320	38	0.30
9	71.7	107.3	0.655	102.2	5.15	0.16	0.33	0.005	0.11	0.003	1836	26	1834	25	1818	53	-0.88
10	78.8	43.8	1.768	29.2	2.77	0.11	0.23	0.004	0.09	0.004	1335	30	1333	23	1301	84	-2.46
13	110	72.5	1.532	68	5.76	0.14	0.35	0.006	0.12	0.003	1942	21	1938	30	1942	48	0.21
14	231	42.7	5.14	30.2	2.90	0.07	0.24	0.003	0.09	0.002	1379	18	1375	15	1367	44	-0.59
16	198.6	152.3	1.29	109.9	3.22	0.08	0.25	0.004	0.09	0.002	1456	18	1450	18	1432	44	-1.26
17	332	114.3	2.7	76.3	2.94	0.07	0.24	0.004	0.09	0.002	1389	18	1393	22	1381	40	-0.87
18	186.5	84	2.2	56.3	2.76	0.08	0.23	0.003	0.09	0.002	1338	20	1326	16	1336	48	0.75
21	179.6	140.1	1.309	142.8	6.29	0.16	0.36	0.006	0.13	0.003	2011	22	1965	26	2055	34	4.38
22	85.6	57.9	1.496	36.6	2.79	0.10	0.23	0.005	0.09	0.004	1354	25	1349	24	1311	77	-2.90
23	271.2	395	0.683	263.6	2.71	0.06	0.23	0.002	0.09	0.002	1327	16	1313	13	1336	38	1.72
24	406	164	2.497	120	2.97	0.07	0.24	0.004	0.09	0.002	1396	18	1388	21	1384	34	-0.29
25	92.6	70.9	1.315	67.3	5.78	0.15	0.35	0.005	0.12	0.003	1935	22	1912	25	1949	43	1.90
26	239	97.8	2.446	106.9	6.45	0.12	0.37	0.005	0.13	0.002	2036	16	2018	24	2042	29	1.18
28	197.8	112.1	1.754	69.9	2.78	0.09	0.23	0.004	0.09	0.003	1343	26	1323	20	1371	60	3.50
30	82.8	54.1	1.526	43.1	4.28	0.12	0.29	0.005	0.11	0.003	1682	24	1640	22	1699	57	3.47
31	304	224	1.342	192	4.41	0.08	0.30	0.003	0.11	0.002	1711	16	1676	17	1748	33	4.12
32	89.8	76.3	1.194	70.1	5.36	0.19	0.34	0.006	0.12	0.004	1873	29	1868	27	1867	57	-0.05
34	174.4	88.6	1.93	91.1	6.51	0.15	0.37	0.006	0.13	0.003	2042	21	2037	28	2044	38	0.34
35	158.7	58.1	2.692	37.6	2.58	0.08	0.22	0.003	0.08	0.003	1291	23	1296	16	1264	63	-2.53
36	447	164	2.64	43.5	2.68	0.09	0.23	0.005	0.09	0.002	1316	24	1320	28	1293	48	-2.09
39	119.4	50.9	2.303	33.1	2.84	0.09	0.23	0.004	0.09	0.003	1362	23	1339	21	1367	56	2.05
40	187.8	95.5	1.944	114.1	10.43	0.18	0.45	0.006	0.17	0.002	2470	16	2415	25	2504	25	3.55
42	202.5	74.9	2.732	52.2	2.80	0.07	0.23	0.003	0.09	0.002	1350	19	1332	17	1365	50	2.42
43	87.5	51.9	1.753	35.8	2.69	0.11	0.22	0.004	0.09	0.004	1315	29	1292	22	1322	79	2.27
45	301	106.2	2.744	72.7	2.73	0.08	0.23	0.006	0.09	0.002	1330	22	1319	33	1346	44	2.01
46	251	110.3	2.259	78.7	2.96	0.07	0.24	0.004	0.09	0.002	1395	18	1390	20	1385	41	-0.36
47	85.6	76.8	1.15	75.2	5.75	0.16	0.34	0.007	0.12	0.004	1934	25	1897	35	1958	56	3.12
48	227.8	140.5	1.614	132.9	5.96	0.15	0.35	0.006	0.13	0.003	1967	23	1925	28	2019	43	4.66
49	533	472	1.157	379	4.83	0.08	0.31	0.003	0.11	0.002	1789	13	1752	16	1824	28	3.95
52	191	171	1.082	162.1	6.42	0.14	0.37	0.005	0.12	0.003	2030	20	2041	24	2005	39	-1.80
53	132.3	70.2	1.873	55.9	4.44	0.12	0.31	0.006	0.10	0.003	1714	23	1741	27	1676	51	-3.88
54	94.4	101.7	0.932	88.8	4.67	0.20	0.32	0.006	0.11	0.005	1747	34	1770	28	1732	77	-2.19
55	156	255	0.637	239	5.90	0.16	0.36	0.005	0.12	0.003	1956	23	1991	25	1917	48	-3.86
56	387	380	1.028	326	5.14	0.10	0.33	0.003	0.11	0.002	1842	17	1829	16	1850	36	1.14
58	374.2	264.2	1.403	228.4	5.48	0.12	0.33	0.005	0.12	0.002	1893	18	1851	23	1927	29	3.94
59	256	77.5	3.25	52.4	3.00	0.09	0.24	0.003	0.09	0.002	1402	21	1389	15	1395	51	0.43
60	518	206	2.492	129	2.88	0.06	0.23	0.003	0.09	0.002	1373	14	1346	13	1395	32	3.51
61	187.9	140	1.331	116.5	4.54	0.11	0.31	0.004	0.10	0.002	1739	19	1750	19	1703	44	-2.76
62	228.8	90.1	2.6	57.8	2.70	0.07	0.23	0.004	0.09	0.002	1326	20	1313	19	1335	52	1.65
63	174.5	110	1.99	99	5.09	0.13	0.33	0.005	0.11	0.003	1829	21	1829	26	1817	41	-0.66
66	144.1	93	1.71	47.1	2.87	0.11	0.23	0.006	0.09	0.003	1362	29	1358	29	1359	74	0.07
68	245.7	83.1	2.971	56.2	2.92	0.06	0.24	0.003	0.09	0.002	1388	15	1372	16	1390	38	1.29
69	83.8	42.9	1.969	45	6.24	0.16	0.36	0.006	0.12	0.003	2003	22	1992	28	1994	48	0.10
72	319	225	1.423	248	8.86	0.14	0.44	0.005	0.15	0.002	2321	15	2347	24	2292	26	-2.40
73	46.1	8.6	9.7	8.7	3.29	0.24	0.25	0.010	0.10	0.006	1455	60	1425	54	1450	130	1.72
74	233.9	42	5.68	38.7	5.59	0.11	0.34	0.005	0.12	0.002	1910	17	1907	23	1891	31	-0.85
75	168.5	146.5	1.146	127	5.62	0.21	0.34	0.008	0.12	0.004	1913	33	1899	36	1918	65	0.99
76	241	103.9	2.336	73.4	3.57	0.09	0.27	0.004	0.10	0.003	1544	21	1546	18	1524	48	-1.44
77	310	222	1.388	207	6.41	0.12	0.37	0.005	0.12	0.002	2030	17	2030	21	2018	29	-0.59
78	57.5	52.4	1.088	47.8	5.40	0.17	0.34	0.006	0.11	0.004	1877	26	1904	28	1820	56	-4.62
80	265.5	107.4	2.485	69.3	3.04	0.08	0.25	0.003	0.09	0.002	1413	19	1427	16	1368	50	-4.31
84	338	140	2.31	116.5	5.27	0.10	0.34	0.004	0.11	0.002	1862	16	1872	20	1829	26	-2.35
85	549	207	3.22	133.9	2.76	0.05	0.23	0.003	0.08	0.002	1345	14	1360	13	1305	37	-4.21
86	91.6	50.8	1.842	43.6	5.02	0.16	0.33	0.007	0.11	0.003	1817	28	1836	34	1783	55	-2.97
87	160.9	73.7	2.2	70.1	6.35	0.15	0.36	0.005	0.13	0.003	2021	21	1998	24	2040	44	2.06
90	411.5	187.6	2.18	116.4	2.72	0.07	0.23	0.004	0.09	0.002	1338	19	1325	20	1348	49	1.71
91	251.7	123.4	2.035	105.4	4.43	0.13	0.30	0.005	0.10	0.003	1713	24	1711	25	1698	49	-0.77
92	241.5	224	1.094	203.2	5.93	0.12	0.36	0.005	0.12	0.003	1966	19	1967	23	1962	38	-0.25
93	309.7	448	0.702	365	5.19	0.11	0.33	0.005	0.12	0.002	1850	18	1816	22	1879	36	3.35

Upper diamictite